ISSN 1980-9743

Soils and Rocks

Volume 34, N. 3

2011

Soils and Rocks

Soils and Rocks

An International Journal of Geotechnical and Geoenvironmental Engineering

Volume 34, N. 3
September-December 2011

Soils and Rocks is an International Journal of Geotechnical and Geoenvironmental Engineering published by

ABMS - Brazilian Association for Soil Mechanics and Geotechnical Engineering
Av. Prof. Almeida Prado, 532, – Prédio 11 – Térreo
Cidade Universitária, 05508-901 São Paulo, SP
Brazil

SPG – Portuguese Geotechnical Society
LNEC, Avenida do Brasil, 101
1700-066 Lisboa
Portugal

Issue Date: *December 2011*

Issue: *350 copies and 2150 online-distributed copies*

Manuscript Submission: *For review criteria and manuscript submission information, see Instructions for Authors at the end.*

SOILS and ROCKS

An International Journal of Geotechnical and Geoenvironmental Engineering

Editor André Pacheco de Assis - University of Brasilia, Brazil

Co-editor Ricardo Oliveira - COBA, Portugal

Soils and Rocks publishes papers in English in the broad fields of Geotechnical Engineering, Engineering Geology and Geo-environmental Engineering. The Journal is published in April, August and December. Subscription price is US$ 90.00 per year. The journal, with the name "Solos e Rochas", was first published in 1978 by the Graduate School of Engineering, Federal University of Rio de Janeiro (COPPE-UFRJ). In 1980 it became the official magazine of the Brazilian Association for Soil Mechanics and Geotechnical Engineering (ABMS), acquiring the national character that had been the intention of its founders. In 1986 it also became the official Journal of the Brazilian Association for Engineering Geology and the Environment (ABGE) and in 1999 became the Latin American Geotechnical Journal, following the support of Latin-American representatives gathered for the Pan-American Conference of Guadalajara (1996). In 2007 the journal acquired the status of an international journal under the name of Soils and Rocks, published by the Brazilian Association for Soil Mechanics and Geotechnical Engineering (ABMS), Brazilian Association for Engineering Geology and the Environment (ABGE) and Portuguese Geotechnical Society (SPG). In 2010, ABGE decided to publish its own journal and left the partnership.

Soils and Rocks

1978,	1 (1, 2)
1979,	1 (3), 2 (1,2)
1980-1983,	3-6 (1, 2, 3)
1984,	7 (single number)
1985-1987,	8-10 (1, 2, 3)
1988-1990,	11-13 (single number)
1991-1992,	14-15 (1, 2)
1993,	16 (1, 2, 3, 4)
1994-2010,	17-33 (1, 2, 3)
2011,	**34 (1, 2, 3,**

ISSN 1980-9743 CDU 624.131.1

ISSN 1980-9743

SOILS and ROCKS
An International Journal of Geotechnical and Geoenvironmental Engineering

Publication of
ABMS - Brazilian Association for Soil Mechanics and Geotechnical Engineering
SPG - Portuguese Geotechnical Society
Volume 34, N. 3, September-December 2011

Table of Contents

Articles

Acquired Knowledge on the Behavior of Deep Foundations Vertically and Horizontally Loaded in the Soil of Brasília

R.P. Cunha

Abstract. This paper presents and discusses a limited set of results from an extensive testing program which has been carried out since 1995 at the University of Brasília Experimental Research site. This site is underlain by the typical tropical, unsaturated and collapsible soil deposit of the Federal District, which has been thoroughly studied via an on going program of laboratory and *in situ* geotechnical tests. In this specific location, several isolated deep foundations were constructed and vertically and horizontally loaded with distinct soil moisture conditions. These foundations, and the soil deposit, do represent typical conditions that occur in other areas of the region, and have therefore been simulated under semi controlled conditions. Since 1995, a large number of research theses were involved with this particular theme, and for the first time some of their main results have been condensed and discussed in the same publication within a logical framework. The knowledge in terms of the observed site behavior, its hypothetical explanation, and some theoretically or empirically derived design variables are shown herein. General conclusions in terms of the vertical and horizontal design values are given together with experimental observations on attained displacements under distinct load levels. The influence of specific external factors on the results is studied; for instance the dissimilar behavior of piles constructed with different methods, or the influence of the weather seasons on the bearing capacity values. From this overall set of data one can have an insight into the complex physical mechanisms involved with the performance, and the difficult simulation, of deep foundations founded in tropical "non-classical" soils. It is a collection of results with value for researchers and practitioners at both regional and national levels.

Keywords: tropical soil, deep foundation, experimental load test, bearing capacity, displacement, acquired experience, design values.

1. Introduction

The pre-designed Brazilian capital Brasília, located in the Federal District of Brazil, was built in the early 60's to house the main Governmental administrative institutions and its public employees. After 50 years (celebration in 2010) it has grown, and is still expanding, considerably more than what was initially envisioned by its founders. The city borders and inner "sectors" have advanced through different (geological) zones of this same District, thus allowing the use of distinct techniques for deep foundation deployment and design during the last half century.

Given such conditions, one can conclude that foundation and *in situ* testing are two demanding research (and practical, in terms of design) topics at the Brazilian capital. Besides, given its distance from major Brazilian cities with already established foundation practice, together with the particular conditions of the regional tropical subsoil, design solutions for the area must be applied solely based on local expertise, not on foreign ones. This point is clearly exemplified, for instance, when one remembers the early stages of foundation construction in this city. At that time, most of the solutions incorporated the accumulated experience of "outside" engineering firms, which led later on to cracking problems in few buildings by the absolute unawareness of the collapsible conditions of the Brasília "porous clay".

Perhaps also because of that, more sound and research-based solutions and techniques have been and are since then under development (and scrutiny) by designers, contractors and researchers of the region. These latter under the support and investigative scope of the Research Group on Foundations, *In Situ* Testing and Retaining Structures, *i.e.* the "GPFees" Group (www.geotecnia.unb.br/gpfees) of the University of Brasília (UnB). As the name states, this group is composed by Professors, technicians and students of the Geotechnical Graduation Program of this university who are in charge, among other things, of the understanding of the problem and the development of sound based design solutions tied to questions related to these geotechnical construction works.

It can be said that the good academic-industry interaction has not only advanced the existing and the new foundation technologies of the city, but it also stimulated a pioneering use of high level *in situ* tests (such as the cone test CPT, the pressuremeter, the Marchetti Dilatometer, pile integrity tests, and others), as the design basis for the foundations constructed within the tropical soil of the region.

R.P. Cunha, Civil Engineer, PhD, Associate Professor, Departamento de Engenharia Civil e Ambiental, Universidade de Brasília, Brasília, DF, Brazil. e-mail: rpcunha@unb.br.
Submitted on April 14, 2010; Final Acceptance on September 8, 2010; Discussion open until April 30, 2012.

The behavior of such foundations founded in the local soil of Brasília is one of the most important research topics from this Group, also because of the lack of information on the complex (soil-structure) response that takes place around and below these foundations. This knowledge is fundamental to aid in understanding and further design, as well as furnishing information on the reliability of the existing theories and on the establishment of design criteria for new foundation techniques.

Once it was understood that the necessity of acquiring knowledge was intermingled with the lack of design criteria in the region, the University of Brasília decided in 1995 to launch a major research project in this area. This was initially done in order to enhance the knowledge of the behavior *in situ* of the distinct foundation types which were founded in the predominant subsoil of the Federal District[1]. At such occasion it was decided to carry out horizontal and vertical field loading tests on the different types of locally used deep foundations, and to understand the behavior and apply known (analytical, empirical, numerical) theories to simulate the results. These foundations were constructed at full scale size within the University of Brasília campus, specifically at the Experimental Site of the Geotechnical Graduate Program (Mota *et al.* 2009). A large effort was also undertaken in association with local engineering companies to characterize this site, by performing advanced *in situ* tests, standard and high level laboratory tests, and other experimental techniques.

This paper therefore conveys a limited, summarized fraction, of the gathered knowledge so far, with the focus on the behavior of deep foundations under vertical and horizontal load, the estimation of their bearing capacity both at horizontal and vertical directions, the assessment of their displacement at working loads, and the beneficial or detrimental influence of some external variables in their performance, such as their construction condition/type or the local weather seasons, among others.

The acquired experience to be discussed herein undoubtedly serves as a start point to design projects in the region, and in others of similar characteristics. It is of value to practitioners and researchers, and it was originally published (in Portuguese) within several Dissertations and Theses from members of this same research Group. Their work will be stated within the following sections (Perez, 1997, Jardim, 1998, Lima, 2001 and Mota, 2003) together with international publications (in English) that also served to consolidate in a logical sequence the main points of information of this paper.

2. Experimental Research Site

The Experimental Research Site of Foundations and *In Situ* Testing has already been portrayed in several publications. Its main characteristics will be presented herein, but the interested reader can review its detailed aspects published in Mota *et al.* (2009), Anjos (2006) and Cavalcante *et al.* (2006), among others.

This site is located in the city of Brasília, which was established 50 years ago in the highly elevated (close to 1000 m) plateau of the central area of Brazil, as depicted in Fig. 1. The city of Brasília was erected in a special unit of the Federation, called the "Federal District", a geometrically designed rectangular area of 5814 km^2. According to many, this city has the shape of an airplane, and being so, one can notice that the Experimental Site is located in its upper north "wing" section, within the university campus. Figure 1 also shows this location, which is complemented

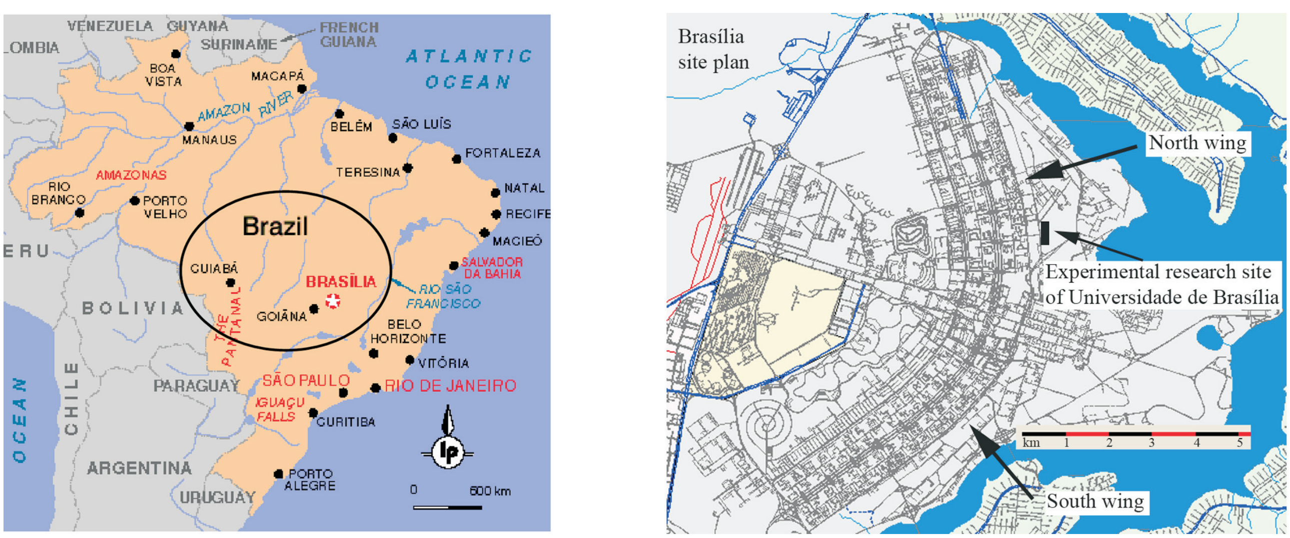

Figure 1 - Location of the city of Brasília and the Experimental Site.

1 Later on the research objectives also encompassed questions related to *in situ* tests, unsaturated soil conditions and others. It should be acknowledged that, before this time, research on foundations was undertaken in this same site, although in a more limited manner.

by Fig. 2 where a more detailed section of the site, close to the Civil & Environmental Engineering Dept., is presented.

Within the Federal District it is common the occurrence of extensive areas covered by weathered latosol of the tertiary-quaternary age. This soil has a variable thickness (in the range of 10 to 30^+ m), which depends on several factors as the topography, the vegetal cover, and the mother rock. In localized points of this area the top latosoil overlays a saprolitic/residual soil with a strong anisotropic mechanical behavior (Cunha & Camapum de Carvalho 1997) and high blow count resistance (N_{SPT}) from the Standard Penetration Test (SPT), which is originated from a weathered, folded and foliate slate typical of the region. Given its characteristics, this is the soil horizon which bears most of the (highly loaded) end bearing piles for high-rises in Brasília.

The superficial latosoil has a dark reddish coloration, and displays a much lower (N_{SPT}) penetration resistance and much higher permeability than the bottom saprolitic/residual soil. According to Araki (1997), the high porosity and weak particle cement bonding (iron and aluminum oxides) of this soil are originated from typical physic-chemical geological processes associated to the superficial soils of the Brazilian Central Plateau, whereas combined lixiviation and laterization processes have an important role due to well defined and extreme "wet" and "dry" seasons of the region (weather seasonality).

In the particular area occupied by the experimental research site the lateritic "porous clay", as it is known, has a thickness of ≈ 8 m, followed by a transition zone overlying the saprolitic/residual soil of slate, as depicted in Fig. 3.

The figure also presents the average (arithmetic mean) values of N_{SPT} blow counts (N_{avg}) and maximum torque measurements ($Tmax_{avg}$), plus respective coeff. of variations in percentage, for each meter depth at the site. This data comes from 5 SPT tests (SP1 to SP5) carried by Mota (2003) - situated in the layout figure to be shown later in this paper.

Table 1 presents the geotechnical characterization of the site, based on soil classification tests also carried out by Mota (2003) including grain size proportions both without and with a deflocculating agent. By breaking down the structure with this agent, the grain size curve of this soil shows a greater concentration of clay-size particles. In this table one can also notice the low unit weight, and high void ratio of this deposit.

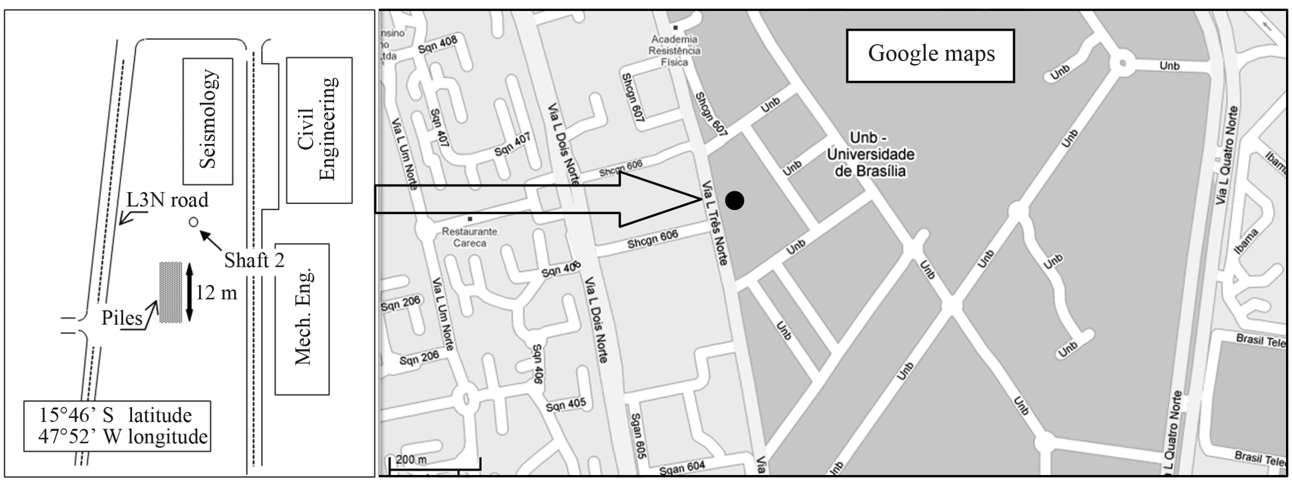

Figure 2 - Location map of the site within the University Campus.

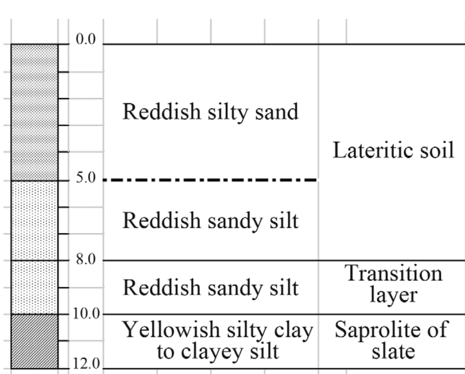

N_{avg}	CVar (N_{SPT}) (%)	$Tmax_{avg}$ (Nm)	CVar ($Tmax$) (%)
3.0	29.8	14	43.9
2.0	0.0	35	26.9
2.8	26.7	67	20.9
3.0	21.1	72	7.5
3.8	10.5	90	8.3
6.0	14.9	98	22.2
7.4	20.2	79	26.1
8.4	36.6	64	34.3
11.4	23.9	107	58.6
19.2	51.2	222	36.6
15.7	21.1	240	22,7
16.3	2.9	247	9.1

Figure 3 - Simplified geotechnical profile of the Research Site.

Table 1 - Typical Geotechnical values of the site (after Mota 2003).

Parameter	Depth (m)									
	1	2	3	4	5	6	7	8	9	10
γ_{dry} (kN/m^3)	10.2	10.4	11.5	11.5	12.0	12.0	12.8	13.9	13.8	13.3
γ_{nat} (kN/m^3)	13.3	13.7	14.7	14.5	15.0	14.4	15.4	18.0	17.8	17.5
γ_{sat} (kN/m^3)	16.5	16.5	17.1	17.0	17.5	17.3	17.8	18.6	18.8	18.5
G_s	2.7	2.7	2.7	2.7	2.7	2.6	2.7	2.7	2.8	2.8
e	1.6	1.6	1.3	1.3	1.2	1.1	1.1	0.9	1.0	1.1
n (%)	61.6	61.1	56.0	55.9	55.6	53.5	51.7	47.2	49.0	51.9
Gravel ND (%)	0.2	0.2	0.7	0.8	1.4	2.1	4.3	3.6	0.6	0.0
Sand ND (%)	56.2	56.2	53.2	53.0	49.2	34.9	30.1	42	10.2	1.4
Silt ND (%)	51.4	35.9	34.2	43.1	48.6	61.4	61.9	51.9	86.8	79.5
Clay ND[1] (%)	2.2	7.7	11.9	3.1	0.8	1.6	3.7	2.5	2.4	19.1
Gravel WD (%)	0.2	0.2	0.7	0.8	1.4	2.1	4.3	3.6	0.6	0.0
Sand WD (%)	41.5	41.5	41.6	33.7	31.6	25.7	22.7	33.8	10.2	3.4
Silt WD (%)	24.9	29.2	25.7	26.3	26.5	22.9	24.6	27.4	80.4	93.2
Clay WD[2] (%)	33.4	29.1	32.0	39.2	40.5	49.3	48.4	35.2	8.8	3.4
w_L (%)	38	36	39	41	45	44	46	43	44	46
w_P (%)	28	26	29	29	34	33	35	34	26	30
PI (%)	10	10	10	12	11	11	11	9	18	16

[1]Clay portion with no deflocculating agent; [2]Clay portion with deflocculating agent.
γ = unit weight, G_s = specific gravity, e = void ratio, n = porosity, w = Atterberg limits, PI = plasticity index.

All the pile load tests were carried out in a zone not larger than 30 x 30 m, within this typical profile. The first layout of piles, of distinct construction methods, was established in mid 1995 within a grid of around 4 x 12 m (see dotted rectangle of Fig. 2). Around this original grid, several other foundations combined with site and laboratory investigations (under distinct research theses) were carried out. Manually excavated shafts, as “shaft 2” from this same figure, were bored to obtain samples for further laboratory tests. Given its tropical nature, it is obvious that somewhat distinct geotechnical values were obtained from point to point in the site, but around the range specified by the typical results of Table 1.

Figure 4 shows quantitatively the typical precipitation rates of Brasília, by records measured during years 1999 to 2001 (Mota, 2003) in the INMET station of Brasília, located around 7 km from the site. As one clearly notices, there are two distinct weather periods, being the “dry” season related to months May to September. This aspect may influence pile behavior during load, as will be shown later on, and is referred as the “weather seasonality” effect.

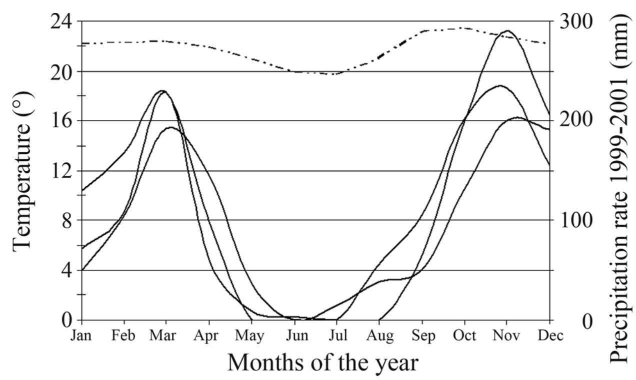

Figure 4 - Typical precipitation and temperature in Brasília (modified after Mota, 2003).

3. Experimental Study

3.1. Pile load tests

Horizontally and vertically loaded piles constructed with distinct methodologies and under different soil conditions have been tested during research at the Experimental Site. Figure 5 presents the location of such load tests, related to the previous aforementioned work from Perez (1997), Jardim (1998) and Mota (2003). This figure is linked to Fig. 2, and complements it in large detail.

The tests depicted in this figure are described in Table 2, where their general characteristics are given. Pile geometric conditions, as diameter and length (D and L), date of testing and loading type (slow or quick maintained), maximum attained load and displacement (P_{max} and Δ_{max}), as well as weather seasonality (wet or dry) are detailed for each test.

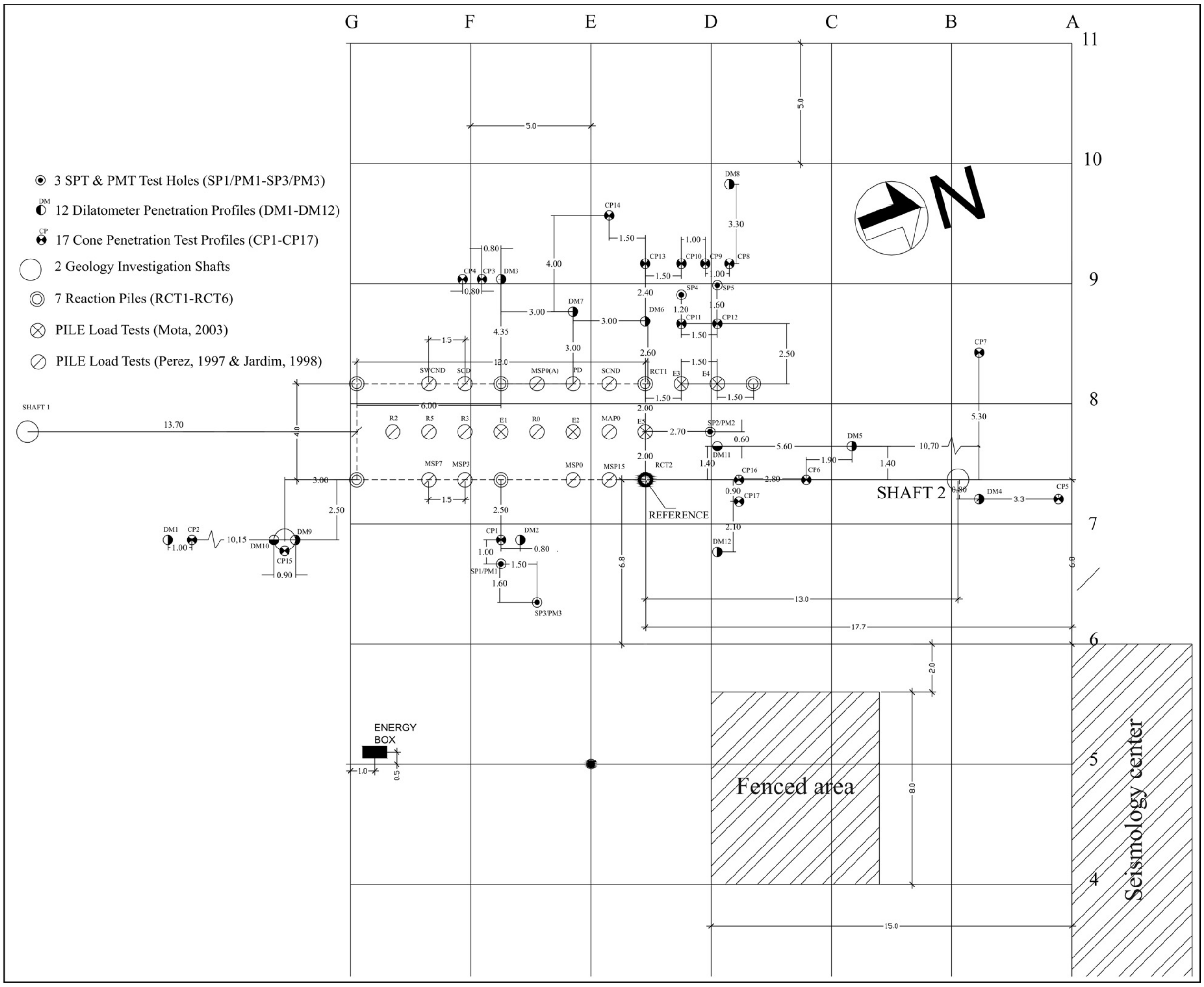

Figure 5 - Layout of some deep foundations and *in situ* tests of the Experimental Site (each square has 5 x 5 m).

All the tests were done in accordance to the recommendations put forward by the Brazilian NBR 12131 (ABNT, 2006) standard, and they consisted of (slow and quick, according to Table 2) maintained tests in two categories.

The loading tests were performed in loading intervals of 20% of the working load up to failure. The piles were subsequently unloaded in approximate 4 intervals. These load tests adopted a reaction frame and "reaction" piles few meters apart. Both the top foundation block and the reaction frame were monitored for tilting and vertical displacements, by using 0.01 mm precision dial gauges. A 1000 kN hydraulic jack was used in conjunction with a 1000 kN precision load cell.

The first testing category (Perez, 1997) consisted of vertically loaded piles with the soil in its natural moisture content, as follows:

a) Four mechanically screwed (or bored cast-in-place) piles: labeled as MSP0, MSP3, MSP7 and MSP15. They were constructed with concrete at different days after the soil excavation (0, 3, 7 and 15 days, according to above nomenclature, where "0" means just after excavation). A fifth pile labeled MSP0(A) was also constructed and field loaded. It was cast in place just after excavation, but it was composed by a concrete mixed with a special expander additive. All the bored (MSP) piles were excavated by using a continuous hollow flight auger, which was introduced into the soil by rotation. The hydraulic mechanical auger was assembled in the back part of a truck specially devised for this type of work. No soil was removed during auger introduction, and, after the final depth was reached, the auger was withdrawn leaving a freshly excavated hole. Cleaning of the base of the hole was not carried out, although care was taken to try stopping auger rotation on more "competent" strata. The designed reinforcing bars were then introduced and, in the MSP0 and MSP0(A) piles, the concrete was promptly poured by using the transportable service of a local concrete company. The MSP piles had a length of ≈ 8 m and diameter of ≈ 30 cm, and were loaded by slow maintained tests;

Table 2 - General characteristics of the pile load tests.

Nomenclature & pile type	*D* (m)	*L* (m)	Test date	Load type	Ref.	Observation
			Vertically Loaded Piles			
MAP0: Manually bored pile molded after excavation	0.28	7.9	Jun 1997	SML		P_{max} = 240 kN, Δ_{max} = 44.7 mm
MSP0(A): Bored pile molded after excavation with additive	0.30	8.4	Jun 1997	SML		P_{max} = 360 kN, Δ_{max} = 28.5 mm
MSP0: Bored pile molded after excavation	0.30	7.9	Jun 1997	SML		P_{max} = 320 kN, Δ_{max} = 28.5 mm
MSP3: Bored pile molded 3 days after excavation	0.30	8.0	May 1997	SML		P_{max} = 320 kN, Δ_{max} = 9.5 mm
MSP7: Bored pile molded 7 days after excavation	0.30	8.0	May 1997	SML		P_{max} = 320 kN, Δ_{max} = 29.6 mm
MSP15: Bored pile molded 15 days after excavation	0.30	8.0	May 1997	SML		P_{max} = 280 kN, Δ_{max} = 19.1 mm
R0: Root pile with no pressure	0.22	10.2	Jun 1997	QML		P_{max} = 330 kN, Δ_{max} = 26.1 mm
R2: Root pile with 200 kPa of injection pressure	0.22	10.1	May 1997	QML	Perez (1997)	P_{max} = 525 kN, Δ_{max} = 41.8 mm
R3: Root pile with 300 kPa of injection pressure	0.22	10.0	May 1997	QML		P_{max} = 360 kN, Δ_{max} = 27.7 mm
R5: Root pile with 500 kPa of injection pressure	0.22	10.0	May 1997	QML		P_{max} = 360 kN, Δ_{max} = 29.6 mm
SCD: "Strauss" cased type pile with compacted concrete	0.30	8.9	May 1997	SML		P_{max} = 400 kN, Δ_{max} = 8.7 mm
SCND: "Strauss" cased type pile without compaction	0.30	8.1	Jun 1997	SML		P_{max} = 280 kN, Δ_{max} = 20.7 mm
SWCND: "Strauss" uncased type pile without compaction	0.30	8.2	May 1997	SML QML		P_{max} = 300 kN, Δ_{max} = 9.7 mm
PD: Precast concrete driven hollow pile	0.33	8.4	Jun 1997	SML		P_{max} = 205 kN, Δ_{max} = 10.4 mm
E1: Bored instrumented floating pile	0.30	7.6	Feb 2000	SML		Wet Season
E2: Bored instrumented floating pile	0.30	7.2	Aug 2000	SML		Dry Season
E3: Bored instrumented floating pile	0.30	7.8	Oct 2001	SML	Mota (2003)	Wet Season
E4: Bored instrumented floating pile	0.30	7.3	Mar 2001	SML		Wet Season
E5: Bored instrumented floating pile	0.30	7.8	Jun 2000	SML		Dry Season
			Horizontally loaded piles			
RCT1: Bored pile used for reaction at vert. test	0.5	10.0	Sept 1997	QML		Nat. & "inundated" conditions. Max y_{0n} = 3.7, y_{0i} = 15.7 mm
RCT2: Bored pile used for reaction at vert. test	0.5	10.0	Sept 1997	QML		Nat. & "inundated" conditions. Max y_{0n} = 5.0, y_{0i} = 10.6 mm
R2: Root pile with 200 kPa of injection pressure	0.22	10.1	Sept 1997	QML		Nat. & "inundated" conditions. Max y_{0n} = 3.6, y_{0i} = 4.4 mm
R3: Root pile with 300 kPa of injection pressure	0.22	10.0	Sept 1997	QML	Jardim (1998)	"Inundated" conditions only. Max y_{0i} = 9.4 mm
R5: Root pile with 500 kPa of injection pressure	0.22	10.0	Sept 1997	QML		Natural conditions only. Max y_{0n} = 16.1 mm
PD: Precast concrete driven hollow pile	0.33	8.4	Sept 1997	QML		Nat. & "inundated" conditions. Max y_{0n} = 11.2, y_{0i} = 13.1 mm

b) One manually augered (or bored cast-in-place) pile, defined as MAP0, and casted just after soil excavation in a similar way as previously described for the MSP0 pile. In the former case, however, the excavation was done with a shell type auger that was hand augered in the field by adopting successive 1 m steel rods. The MAP0 pile had a final approximate length of 8 m and diameter of 28 cm. The same loading as before was used;

c) Three "Strauss" (Brazilian label) type piles defined as SWCND, SCD and SCND, they were also bored cast-in-place piles. The Strauss pile is a locally used deep foundation which has the execution process close, but not exact, to the one used for "Franki" piles. They were constructed by adopting a cylindrical metallic shell with a bottom valve bailer that was handled in the field by means of a hoist mounted on a tripod. This shell was continuously advanced as the bailer removed the soil softened by a bottom punching with auxiliary water. The hole was encased for two of the piles (SCD and SCND), and not encased for the third one (SWCND). The casing was punched into the hole as soon as the shell excavation stage finished. This operation, however, was done in steps, since the shell had to be lifted up to surface several times to be internally cleaned of its "entrapped" soil. At the end of the excavation, at the desired depths, the bottom of the hole was cleaned out, the fix rebars were introduced and fresh concrete was poured. For one of the piles (SCD) the concrete was compacted afterwards by using a 2.5 kN hammer falling onto it, whereas for the other piles (SCND, SWCND) the concrete was simply poured. All the piles had a final approximate length of 8 m and diameter of 30 cm. Same field loading as before;

d) One precast driven centrifuged (displacement) concrete pile labeled as PD, was dynamically inserted into the soil by using a 32 kN (free fall) drop hammer falling from a height of 30 cm. A wood cushion was used to soften the impact on the top of the pile, and it was mounted together with the hammer on the leads of a standard crawler crane. The precast (hollow, "SCAC" company type) pile had a final length of 8.4 m with an external and internal diameter of, respectively, 33 cm and 25 cm. Same loading as before;

e) Four injected type piles (cast-in-place with pressure, locally know as "root" pile - with very distinct construction aspects from the known "micropile" type). They were constructed by adopting distinct injection pressures (0, 200, 300 and 500 kPa) during the formation of the mortar shaft. They are defined herein as R0 for the pile without injection pressure (mortar just poured from surface), R2 for an injection mortar pressure of 200 kPa, R3 for an equivalent pressure of 300 kPa and R5 for a pressure of 500 kPa. These piles were executed with a specially devised drill rig which operated hydraulically. The soil was excavated by a continuous and static introduction of a rotating casing with pressurized water. The water "washed out" the generated mud in front of this casing, opening a small annular gap between the casing and the excavated hole. Once drilling was finished, the interior of the casing was cleaned up and the fix rebars were introduced. Mortar was then poured inside the casing until it was filled. The top of the casing was then connected to an air pressurizing system, and air pressure was applied to the inner fluid mortar. By simultaneously applying air pressure and lifting up the casing, it was possible to form the corrugated pile's shaft (for the piles with injection pressure). This operation was done in sequence, continuously filling up the remaining casing with fluid mortar, thus leading at the end to piles with an approximate length of 10 m and final average (nom.) dia. of $\approx$ 22 cm. They were loaded by quick maintained tests;

f) Five mechanically excavated and fully electronically instrumented piles (Mota, 2003), defined as E1 to E5. They were executed with similar conditions as those aforementioned bored piles, but loaded at specifically distinct weather seasons.

The second category of tests (Jardim, 1998) consisted of horizontal load tests on some of the piles mentioned before, which had been previously tested under vertical load (the only exceptions were for the reaction RCT1 and RCT2 piles). However, given the experience obtained during the previous stage, some modifications were introduced. The tests were done with fast loading intervals ("quick maintained load tests") with loading intervals of 10% of the working load up to failure, and with a compulsory stabilization time of 5 min (according to the NBR12131 standard). The obtained loading rate was in the range of 3.6 kN/min (three times faster than the rate of the previous stage). Similar loading equipment and instrumentation as described before were used for these tests, with the difference that a lower capacity (500 kN) hydraulic jack was adopted, and the piles were now tested against "each other" without reaction frames, as portrayed in Fig. 6. In this figure it is also noted that the soil served as a support for the loading equipment, *i.e.*, the hydraulic jack and its extension made of a metallic tube used to transmit the load from one pile to another. In order to avoid undesirable tilting during the field test, a cylindrical hinge was adopted between one end of the jack and the load cell for both (vertical and horizontal) cases. Rigid metallic plates were fixed to both tested piles by means of metallic rings, so that a constant distance was maintained between the load application point and the base of the trench, at the pile/soil interface. A constant distance was also maintained between the upper dial gauge, at the pile's head, and the load application point.

These loading tests were carried out in two phases, with the soil in its natural field water (moisture) content in the first phase and in its "inundated" conditions in the second phase. In order to "inundate" the soil a 60 cm deep trench was dug all around the piles, with a diameter of approximately 2 times each pile's diameter. The inundation took place after the horizontal loading tests with the soil in the natural moisture content conditions. Soil inundation

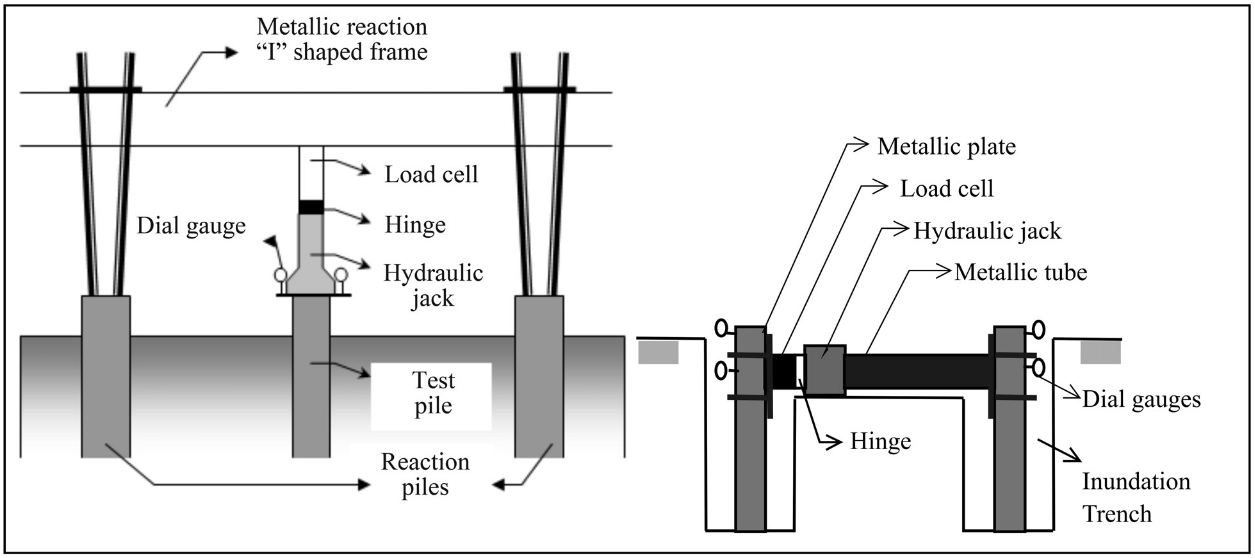

Figure 6 - Sketch of vertical and horizontal loading tests (modified after Jardim, 1998).

was achieved by filling the trenches with water and keeping the water level constant for about 48 h before the loading tests. This procedure tried to simulate the effects of a heavy rain on the soil deposit, given the known collapsibility characteristics of the Brasília porous clay. The following piles and loading sequence was adopted for the horizontal tests:

a) Reaction piles RCT1 and RCT2: They were tested against each other, with the soil initially at the natural moisture content condition, and later inundated;

b) Precast driven centrifuged concrete pile PD: Tested against the reaction piles, also with the soil in its natural and later in inundated conditions;

c) Root piles R2, R3 and R5: They were tested against each other, but in accordance to the following sequence: R2-R5 with the soil in its natural moisture content conditions, leading to the structural rupture of R5, followed by R2-R3 with the soil under "inundated" conditions, which also led to the structural rupture of R3.

All the tests were carried out at the final stage of the 1997 dry season, between August to October. Figures 6 and 7 respectively present the sketch on how the load tests were done and some of the load-deflection resulting curves. Notice that Δ is the vertical deflection on top of the pile and y_0 is the horizontal deflection at ground level. Maximum values of y_0 at either natural ("n") or inundated ("i") soil conditions attained during the tests are also given in Table 2.

3.2. Pile echo tests

Pile echo tests, or simply PET, have been carried out in some of the piles analyzed in this paper. This test uses the Pulse-Echo method for quick quality control of a large number of piles, in order to verify their integrity and length.

The pile top is struck with a lightweight handheld hammer. The reflected wave is captured and analyzed by the PET's digital accelerometer to provide information regarding the length and shape of the pile.

These tests were carried out in 2010 in order to check the geometrical information provided in Table 2, by using a recently acquired PET tester under an ongoing research project from the GPFees Group.

Although many of the piles could not be found anymore in 2010, given the alterations that the Experimental site suffered throughout the last years[2], those which could be tested confirmed the geometry expressed in aforementioned table, assembled with data from the original theses at this site.

4. Results and Discussion

The analyses are subdivided into major topics, as loading in the vertical direction, and its derived parameters, and loading in the horizontal direction. They are presented and discussed next.

4.1. Vertical direction

4.1.1. Construction methodology effect

This particular discussion has already been presented elsewhere (Cunha *et al.*, 2001) and is addressed here in its essence to enhance the final conclusions.

The vertical failure load was defined as the average value between the predictions of Brinch-Hansen (1963) and Mazurkiewicz (1972), since, according to Perez (1997), these methods yielded failure loads which were closer to the "physical failure" values (asymptote of the load-de-

2 The current Site is scheduled to be closed very soon, given the lack of space and university policy. A new area has been provided for this purpose within UnB campus.

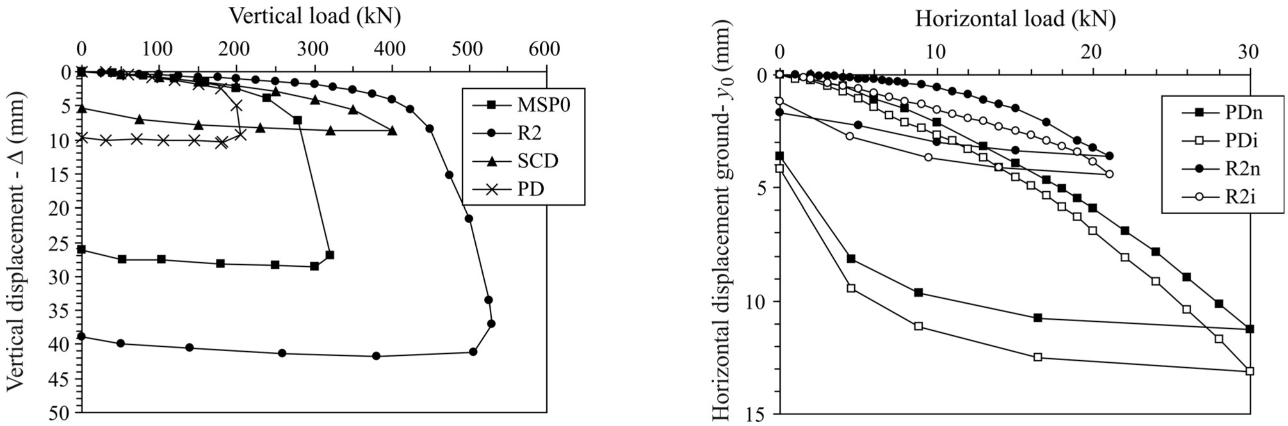

Figure 7 - Some of the obtained load-displacement curves (modified after Jardim, 1998).

flection curve) from each of the foundations. The only exception is for the Strauss piles, in which the NBR6122 (ABNT, 2010) standard method was adopted because it presents a procedure to define the failure load for continuously increasing testing curves, in which the maximum load is not clearly depicted. This feature was noticed for the Strauss piles.

Figure 8 presents a plot of the vertical failure load of all piles tested by Perez (1997). In regard to this figure some observations can be given:

• The mechanically bored pile with the expander additive (MSP0(A)) had a failure load 8.0% higher than the equivalent load of the pile without the additive (MSP0);

• The failure load of the mechanically bored piles (MSP) decreased with the time span between excavation and casting (from MSP3 onwards). The failure load has unexpectedly increased 8.5% from MSP0 to 3, perhaps due to unnoticed differences in nominal (“as built”) length/diameter of these piles;

• The failure load of the root piles has marginally increased with the increase of injection pressure (comparing R0 to R3 and R5). This load has considerably increased (as far as 55%) from R0 to R2, but has dropped sharply afterwards, which may be indicative of an “optimal” injection pressure of 200 kPa (in terms of bearing capacity) for this type of pile and soil characteristics. A possible explanation is derived from the simultaneous (and distinct) effects of collapse and increase of lateral stress on the failure load of the soil. It is postulated that such combined factors (stress/collapse) unequally affect the capacity and the rigidity of the soil when increasing the injection pressure inside the borehole. Thus, it seems that a “threshold” pressure of around 200 kPa exists, beyond which a major structural soil breakage starts to take place. These combined effects led to the marginal increase in the failure load of the piles from R0 to R5, predominantly due to the gradual increase of the level of lateral stress with the increase of injection pressure. Besides, with the increase of injection pressure there was a marginal increase in the final (“as built”) pile diameter. It appears, however, that beyond the “threshold” 200 kPa pressure, the influence of the collapse of the soil on the failure load surpasses the influence of any of the other factors (as the increase in lateral stress and pile diameter). This happened because, as hypothesized herein, the structure of the soil surrounding the hole was somehow destroyed. With this destruction the soil/pile interface partially lost its lateral friction. It has already been experimentally shown that the generalized collapse of the soil is extremely non beneficial, since it reduces the interface friction. The pile capacity was very close from R3 to R5, probably given the generalized collapse of the soil surrounding the borehole at such high pressure stages;

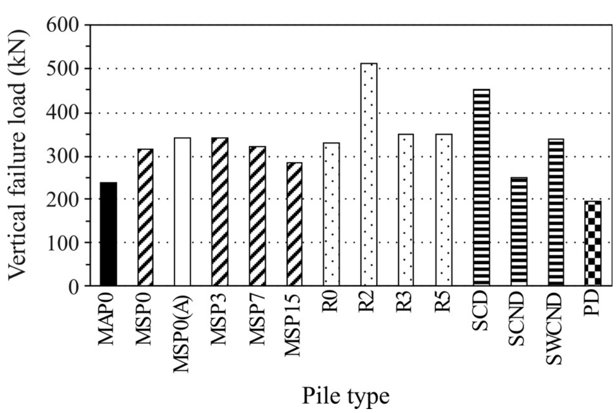

Figure 8 - Influence of construction method (after Cunha *et al.*, 2001).

• The pile with the compacted concrete SCD had the highest failure load for the Strauss type piles. It seems then that it was the “concrete driven” effect, not the use of casing during excavation, that caused a beneficial response on the bearing capacity of this type of pile. Besides, by constructing with casing (comparison SCND *vs.* SWCND), the capacity decreases, as most probably there is a reduction in lateral friction by the more regularly shaped shaft of the SCND pile;

• The dynamic insertion of the precast driven pile in this type of soil considerably affected its original structure, given its fragile nature. It was noted, for all compared piles, that the driven PD pile was the one with the lowest failure load. It shall be mentioned, however, that such observation is based solely on the single test of this type carried out in the site.

4.1.2. Weather seasonality effect

Mota (2003) carried out pile load tests in distinct seasons of the year, at both "wet" and "dry" periods in accordance to Fig. 4. These results are plotted in Fig. 9, where the seasonality aspect is indirectly evaluated by the comparison of bearing capacity against pile name (or weather season), using distinct estimation methodologies for pile failure values.

The tested piles have lengths of around 7.5 m as presented in Table 2. Their bases were located in the transition layer, where the N_{SPT} blow count is not high enough to turn them into end bearing type foundations. Moreover, as noticed by Mota (2003), the "active" zone of (considerable) suction variation is approximately comprised within the 3 initial meters of the soil profile, which represents almost 40% of the pile's average length.

So, it is reasonable to suspect that the piles were indeed subjected to the influence of the weather seasonality, *i.e.*, the suction variation of the active zone. This variation in the soil's suction must have caused a distinction in the lateral friction of the piles along the seasons of the year, thus allowing for the differences. Other causes may not be discarded, but the similar characteristics and close distance apart of the piles, as seen in Fig. 5, do point to this logical explanation.

4.1.3. Bearing capacity

The estimation of the bearing capacity of bored piles is usually undertaken in Brazil by empirical (N_{SPT} based) techniques, as the recognized original methods of Aoki & Velloso (1975) and Décourt & Quaresma (1978) (*i.e.*, criteria A). These methods were then chosen to evaluate the bearing capacity of the floating bored piles of Mota (2003), using the closest SPT values to each respective pile (according to Fig. 5). The methodologies were also tested with local correction factors proposed by Rodrigues *et al.* (1998) to be used in the Brasília porous clay (*i.e.*, criteria B).

Mota (2003) has compared in Fig. 10 the failure loads by each of the techniques against experimental pile load test results. The latter results come from Van der Veen (1953) estimation criteria, since, according to this author, this criteria leads to results in the conservative safe side, also close to the average values from all tested failure methods (expressed in Fig. 9).

Figure 10 allows the perception that, although the experimental data is markedly influenced by weather season effects, such trend is not found by the empirical estimations. This is so given the lack of sensitivity of the SPT test to suction variations at the Brasília porous clay, as already stated elsewhere (Cunha *et al.* 2007).

It is also noticed that the tested methods do tend, in general, to give results in the safe side. It also seems that Décourt and Quaresma (1978) method produces values that are closer to the load tests at each pile. Without local correction factors, this method estimates an average value (for all piles) lower than the average experimental data. By using correction factors, the average estimated value approaches the experimental one, but on the unsafe side.

4.1.4. Average lateral friction values

All five bored piles from Mota (2003) where instrumented, but only one of them yielded results which could be interpreted, due to problems in the glue used (as usual, found after experiments). Therefore, Fig. 11 presents the lateral measured friction values of pile E1, during its loading stage till failure (according to aforementioned criteria) at 270 kN and Δ_{max} of 16.1 mm.

As noticed, the lateral friction seems to be fully mobilized in depths 0 to 3.4 and 5.4 to 7.4 m, at the ultimate load

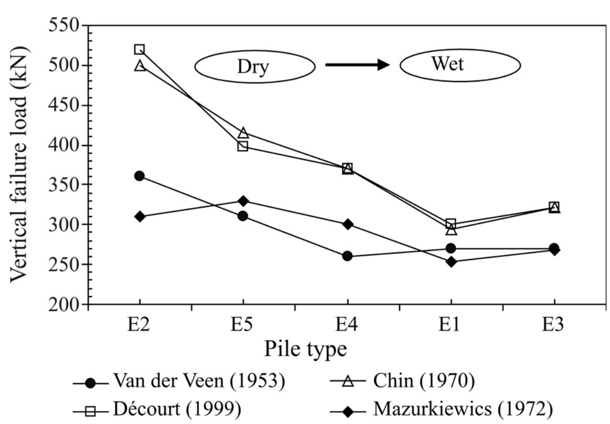

Figure 9 - Influence of weather seasonality (after Mota, 2003).

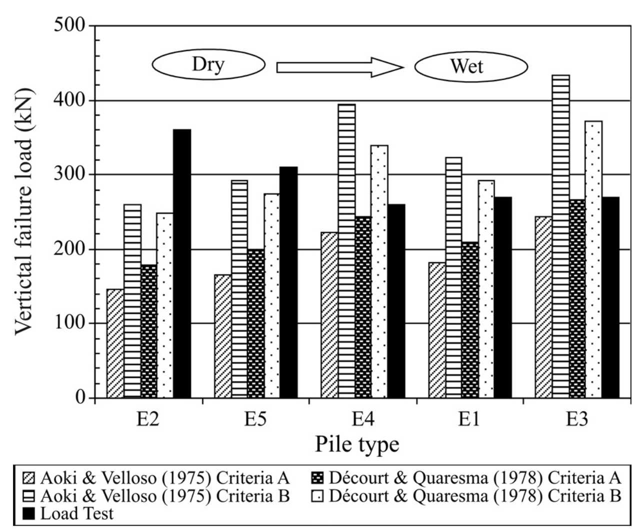

Figure 10 - SPT estimation methods (after Mota, 2003).

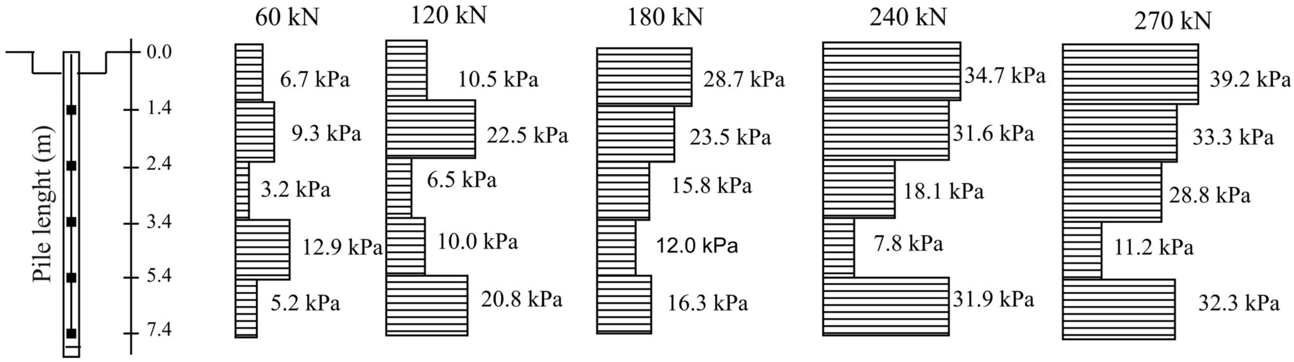

Figure 11 - Results of vertical lateral friction stress during E1 load test (after Mota, 2003).

or displacement level (~ 5% dia.). This aspect is better depicted by comparing the results at the last two loading stages. Nevertheless, for depths 3.4 to 5.4 m the applied level of displacement wasn't enough to generate maximum friction values. Besides, for depths beyond 5.4 m, there is a clear perception that the lateral friction is of higher magnitude than values at shallower depths. By comparing that with data from Fig. 3, one also notices that, below 5 m the maximum SPT torque increases (in general) as well and the profile changes from silty sand to sandy silt, perhaps explaining the differences.

Albuquerque *et al.* (2001) observed in several load tests with bored piles with dia 0.45 m and length 12 m, at the Campinas Univ. Research Site (residual soil from diabase), that the lateral friction was fully mobilized for average pile head displacements of around 5 mm (~ 1% of dia). Their ultimate friction values were in the range of 40 kPa, close to herein values.

The results of Fig. 11 do also tend to agree with numerical simulations (on distinct piles) carried out by Cunha & Kuklík (2003) in the Brasília porous clay. The values seem to be in the same magnitude of the expected (predictions) by these authors.

It is necessary to emphasize, however, that such observations are quite limited by the reduced amount of data and lack of (well instrumented in this site) experimental piles which could corroborate with the given trend.

Load cell results[3] at the base of this particular pile have also shown that from the load applied at its top only 0.5% effectively reached its tip at ultimate stage (in average less than 1% throughout load test). This aspect is aligned with the normal design assumption of bored piles in Brasília as behaving as fully "floating" piles. Off course, one can argued that mobilization at pile base do take place but at a rather higher level of displacement. Anyway, this wouldn't be feasible from a design point of view.

4.1.5. Young's Modulus of the soil

This item has also been presented elsewhere (Cunha *et al.*, 2001) and it is included here to enhance the understanding of the key (behavioral) aspects of deep foundations founded in this particular tropical soil.

The vertical Young's Modulus of the soil surrounding each of the piles was determined with a unique point of the load-settlement field curve, *i.e.*, the point in which the load was half the value of the bearing capacity value. By using this (working) load and its associated settlement it was possible to numerically backanalyze a unique, average, Young modulus by adopting a program denominated DEFPIG (Deformation Analysis of Pile Groups, Poulos 1990). This software determines the deformations and load distribution within a group of piles and isolated piles subjected to general loading. It was specifically written for piles designed under the "conventional approach", by considering a group of identical elastic piles having axial and lateral stiffness that are constant with depth. It also allows for the eventual slippage between the piles and the surrounding soil. The stress distributions are computed from the theory of elasticity, more specifically from Mindlin's solutions for an isotropic, homogeneous, linear elastic medium.

Hence, Fig. 12 presents a plot of the Young modulus of the soil around each of the piles. In regard to this figure the some observations can be given:

• The mechanically bored pile with the expander additive (MSP0(A)) had a Young modulus of the soil around its shaft much higher than the equivalent modulus of the pile without additive (MSP)). This means that this former pile has settled much less than the latter one, at similar loading conditions. This fact may be physically interpreted by a possible higher lateral pressure (than the normal MSP case) exerted by the soil around the MSP0(A)) pile's shaft, rather than an eventual rearrangement of the soil structure (with

3 Mota (2003) states that the load cell was probably not well aligned, or "fully" supported, at the base of the excavation. This may have some impact on the results.

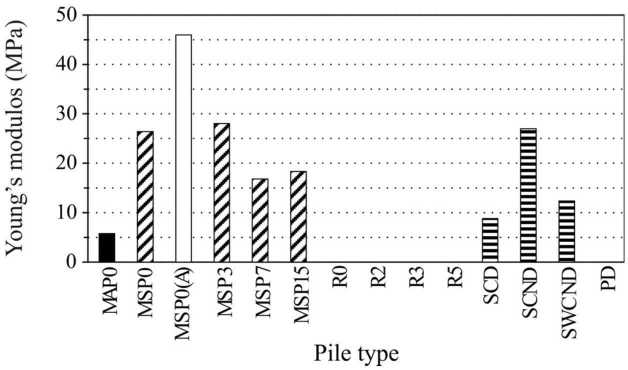

Figure 12 - Backanalyzed Young Modulus (after Cunha *et al.*, 2001).

stiffness increase). The phenomena, however, is still subjected to other arguments;

• The manually augered pile (MAP0) had a Young modulus of the soil around its shaft much lower than the equivalent modulus of the mechanically bored pile (MSP0);

• Similar trend as before in Fig. 8 (for vertical failure) are observed for the mechanically bored piles, *i.e.*, the Young modulus of the soil around the piles decreased with the increase of the time span between excavation and casting (from MSP3 onwards). Hence the piles settled more with the increase of time span between excavation and casting;

• Some of the piles (as the root "R" and the precast driven PD piles) could not be backanalyzed by the program, since the obtained moduli were unrealistically high. This was related to the nature of these piles, rather than to the program itself. These piles had very low settlements (around ±1 mm, at working loads), which were of the same magnitude of their (estimated) structural elastic compression. This particular feature has hampered the backanalysis, since it was done on the basis of an assumed structural Young modulus for each of the piles. Hence, small differences in the assessment of the elastic compression of the piles (by the program) yielded large estimations on the value of the Young modulus of the soil;

• The Strauss pile with the compacted concrete SCD had the lowest Young modulus for the soil around its shaft (hence the highest settlement at working load) in comparison to the others Strauss type piles. This feature is exactly the opposite of what has been found in terms of capacity, and may be indicative of the fact that, for this type of tropical collapsible soil, the concrete "compaction effect" is beneficial solely in terms of failure load. Besides, by constructing without compacting the concrete (comparison SCND *vs.* SWCND), the use of casing seems to be preferable, as it considerably reduces the settlement at working loads (as one notices in this figure with the higher Young modulus). The causes for this and the former observed aspect are difficult to explain, but perhaps are intrinsically related to some features of the soil as the stress increase and relaxation, or dynamic effect during pile construction. More research is necessary to better understand this point.

4.2. Horizontal direction

4.2.1. Displacements

The main purpose of the horizontal load tests was the definition of the failure loads. Nevertheless, it is interesting to compare the results of the relative displacements (horizontal y_0 value at soil/pile interface divided by the diameter) from the tests.

Table 3 presents the main characteristics observed and computed for each of the tests, for the soil at both inundated and natural water content conditions. From this table some features are found:

Table 3 - Specific characteristics from horizontal load tests.

Pile type	Maximum load (kN)	y_{0max}/D (%)	Failure load (kN)	Work load (kN)	y_{0work}/D (%)
RCT1 n	75	0.7	90*	45	0.2
RCT1 i	82.5	3.1	90*	45	0.4
RCT2 n	75	1.0	90*	45	0.2
RCT2 i	82.5	2.1	90*	45	0.6
R2 n	21	1.6	30*	15	0.7
R2 i	21	2.0	30*	15	1.1
R3 i	21	4.3+	30*	15	1.8
R5 n	21	7.3+	30*	15	2.3
PD n	30	3.4	50**	25	2.6
PD i	30	4.0	50**	25	2.9

(*) Van der Veen (1953) criteria; (**) NBR 6122 (2010) criteria; (+) structural failure (Jardim. 1998).
n = natural. i = inundated conditions. Working load for Safety Factor of 2.0.

• The maximum relative displacements attained throughout the tests were under 10%. Besides, by considering a working load of half the estimated failure value, one concludes that equivalent relative displacements at working conditions do not surpass an approximate value of 3%. Indeed, the few tests in which a structural failure of the shaft took place were pushed to displacements as high as ~ 7% of the pile diameter, which corroborates to the low magnitudes at the working conditions;

• The relative displacement of the piles at working conditions with inundated soil was, in general, much higher (double and above) of equivalent values for the soil at natural conditions. The only exception is the precast PD pile, perhaps because during its dynamic insertion it has considerably affected the original structure of the soil around its shaft (as mentioned before), hence mobilizing an annulus of soil already disturbed in any of the testing cases. This observation seems to agree with the fact that the relative displacements of the PD pile were the highest ones of this table;

• Failure loads estimated for similar piles with soil at inundated or natural water content conditions were indeed very close numerically. In part, this is related to the simplifications and adjustment problems of the extrapolation method employed by Jardim (1998) to derive the failure loads. By observing Fig. 7 one notices that physical failure was not reached by most of the tested piles (examples for R2 and PD), and indeed some sort of extrapolation criteria, or idealization, had to be used to define the ultimate value. Another reason relates the volume of soil mobilized during failure. Notice that, in this case (distinctively from the vertical direction) a large volume of soil is encompassed during horizontal compression, rather than a thin annulus at the pile/soil interface (more prone to be influenced by soil inundation). Given this aspect, the next comparison will focus solely on the results at natural water content conditions.

4.2.2. Bearing capacity

The horizontal failure load was estimated by the classical theory of Broms (1964 a,b) for long, or slender, piles in which the failure takes place with a plastic hinge in the pile shaft, *i.e.*, it primarily depends on the structural yield moment of the pile itself.

The distinct graphic solutions for unrestrained piles at both cohesive and cohesionless soils were adopted, since this particular soil has cohesive-frictional characteristics. So, in order to furnish the methodology with soil resistance values, the CK0D triaxial results presented in Cunha *et al.* (1999) for soil samples at natural water content conditions were adopted. Given the fact that horizontal behavior is more dependent on superficial soil layers, only the test results for the undisturbed sample of 3 m of depth was used. This refers to a drained cohesion of 11 kPa and a drained friction angle of 27.9°.

The yield moments of the piles are those presented by Lima (2001), calculated respectively with the structural resistances of both concrete and steel reinforcement used during construction of the piles.

In order to use this methodology an assumption had to be made by Lima (2001) to employ the cohesion resistance factor within the graphical solution. As it is well known, Broms' methods are valid for cohesive (undrained) and cohesionless (drained behavior) materials. Hence, the use of the friction angle was straightforward with the graphics, but this was not so with the cohesion value. Since the solution was developed for the undrained cohesion, rather than the drained one, it was assumed by this author that one could furnish this latter value within the graphical solution to obtain the failure load caused by the cohesive part of the effective shearing resistance of the soil. This is so given the fact that the soil at the experimental site does not behave in an undrained mode, as there is no water level there.

With aforementioned simplification, open to criticism, the method was tested against the experimental failure load results expressed in Table 3. Figure 13 shows the comparison using each adopted parcel of the soil's resistance.

As clearly noticed, both ways of calculating do lead to reasonably close results, being therefore sufficiently acceptable for practical use. The larger differences between experimental to estimated values relate to the precast driven pile, perhaps, again, because the soil is more disturbed around this pile (compared to other foundations) as commented before. If this is the case, it certainly relates to a soil characteristic more distinct to the undisturbed material tested at the triaxial tests. Nevertheless other aspects can also be raised to explain the differences, as aforementioned questions related to the extrapolation of the failure load.

4.2.3. Coefficient of subgrade reaction

The use of the "beam on elastic foundation" theory for horizontally loaded pile problems requires the specification of a soil modulus which represents the linear, or proportional, relationship between the horizontal pile

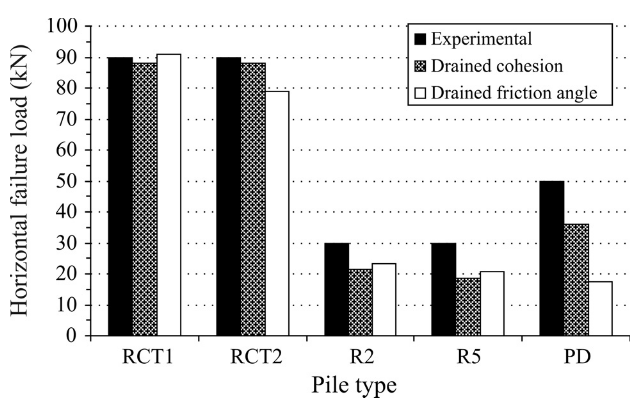

Figure 13 - Horizontal failure load – soil at natural conditions (modified after Lima. 2001).

displacement and the respective soil reaction. This modulus is defined for each distinct section of the pile along its depth, and is termed the "modulus of subgrade reaction" of the soil (K). It can be then used to simulate "Winkler" springs during the analysis of laterally loaded piles, as presented by Reese and Matlock (1956) in their classical paper.

The K coefficient is related to the total width of the pile's shaft, and has a dimension FL^{-2} (kN/m^2). If we introduce the lateral subgrade reaction modulus K_h for a pile of unit width, we obtain:

$$K = K_h \times D \tag{1}$$

where D is the diameter of the pile and K_h has a FL^{-3} (kN/m^3) dimension.

The subgrade reaction moduli (K and K_h) have distinct values, or variation, for distinct soil types, and hence, two different cases can be considered. The first case assumes K constant with depth, and the second case assumes a linear variation of K with depth. The latter according to the following equation:

$$K = \eta_h \times \text{ depth} \tag{2}$$

where η_h represents the rate of increase of the subgrade reaction modulus, or the "coefficient of horizontal subgrade reaction" of the soil, in units of FL^{-3} (kN/m^3).

In general, for sandy soils and for soft clays the subgrade reaction modulus increases linearly with depth. This idealized hypothesis is in accordance with the (drained) characteristics of the tropical unsaturated soil deposit of the experimental site. Therefore, only the coefficient of subgrade reaction modulus was backcalculated here.

The backanalysis was, however, simplified by assuming a constant structural Young's modulus of the pile during the loading process (25 GPa for root piles and 20 GPa for all others). Thus, it does not follow the more advanced analytical technique put forward by Reese *et al.* (1998), by not taking into account the (unknown) variable stiffness of the piles.

In order to obtain η_h it was necessary to use the relationship between the horizontal applied load and the pile/soil displacement at the soil surface (y_0) as given by Matlock & Reese (1961):

$$y_0 = 2.435 \times H \times \frac{T^3}{EI} \tag{3}$$

$$T = \sqrt[5]{\frac{EI}{\eta_h}} \tag{4}$$

where E is the structural Young's modulus of the pile; I = structural moment of inertia and H = horizontal load.

However, in most of the cases the horizontal load is not applied at the pile/soil interface, but at some other point on the pile. It will then generate a displacement y_t at the pile head that can be calculated by Kocsis (1971) equations. These equations relate the displacement at any level of the pile head above the ground (as measured during load tests) to the displacement at the pile/soil interface y_0, taking on account the pile head rotation (function of T, EI and H), the horizontal load (H), the pile characteristics (I and E), and η_h.

Therefore, in order to obtain the backanalyzed coefficients at each (calculated and plotted as in Fig. 7) y_0 displacement level a spreadsheet was developed to interactively solve the general formula for each experimental pair of known values of top head displacement and horizontal load (details in Jardim, 1998).

The results for the (reaction) bored, the root and the (precast) driven concrete piles, with the soil at both natural water content and inundated conditions, are shown in Fig. 14. The moduli were backanalyzed up to the maximum displacement values of the load tests, as expressed in Table 3.

From this figure it is noticed that:

• As expected, the moduli have considerably decreased at an asymptotic rate with the increase of the displacement level. Besides, when comparing R2 and R5 at natural soil conditions, one also notices that the moduli decreased with the increase of the injection pressure beyond 200 kPa, perhaps related to aforementioned structural aspects of this soil;

• Based on the previous statement, Cintra (1981) has respectively suggested y_0 design intervals of 4-8 mm for the soil at natural conditions, and 12-18 mm for the inundated case. Nevertheless, based on the working load levels of herein cases, Jardim (1998) suggested the use of the design intervals 4-10 and 6-12 mm to respectively represent the soil at the natural water content and at inundated conditions. These intervals do already encompass the working displacement levels of the piles depicted in Table 3;

• Based on the aforementioned intervals it was possible to obtain average backanalyzed moduli for practical use, as presented in Table 4. It shall be noticed that the injection (R2n) pile case was discarded in the averaging, given the very distinct result of this load test in comparison to others of this same pile type. This table do serve, therefore, as a start point for designing similar foundations on this same soil, when using the described theoretical methodology of this item;

Table 4 - Suggested avg. reaction moduli at working loads (after Jardim 1998).

Pile type	η_h (MN/m^3)	
	Natural conditions	Inundated conditions
Bored	16	7
Root	19.5	14
Precast	7	5.5

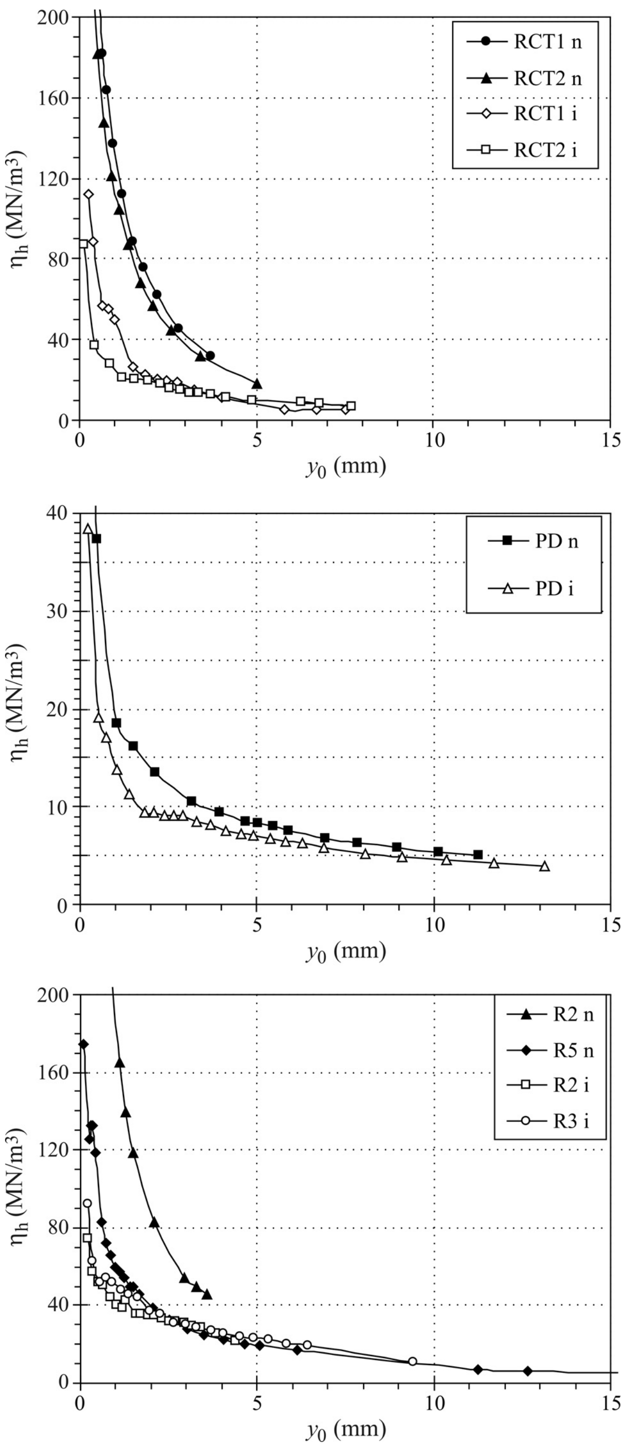

Figure 14 - Backanalyzed coeff. of subgrade reaction (after Jardim 1998).

• The moduli for the inundated condition are lower than those from the soil at natural conditions, at same pile and displacement levels. This reflects the higher displacements attained at such former test conditions, as noticed before. An average decrease of around 50, 30 and 20% was noticed in relation to the moduli at natural soil conditions, respectively for the bored, the root and the precast pile type;

• The backanalyzed moduli from the driven precast pile were the lowest from all load tests, again reflecting the fact that the dynamic insertion considerably affected the soil's original structure, given its fragile nature.

5. Conclusions

This paper emphasized the main results obtained from load tests on several large scale deep foundations located at the Experimental Research Site of the Geotechnical Graduation Program of the University of Brasília. Typical foundations adopted in this city, and the Federal District as well, were vertically and horizontally loaded, yielding loading displacement curves that were interpreted according to recognized empirical and theoretical methods from the soil mechanics.

Experimental data acquired from the load tests, as the displacement levels at failure and working conditions, or the lateral friction mobilized at the pile shaft, were also presented and discussed. Empirical or theoretical methods currently employed to respectively derive the ultimate vertical and horizontal capacity of loaded piles have been explored together with backanalyzed elastic moduli, also for both considered directions.

The analyses have also allowed a reasonable insight into some of the most relevant variables that affect the behavior of the deep foundations once vertically or horizontally loaded on tropical soils. The influences of several external aspects, as the construction methodology or the weather seasonality, have been addressed in the paper, but in a limited manner. Although some of the results come from research theses which have been finished more than a decade ago, they have been assembled for the first time in a comprehensive manner, allowing a perspective of some of the key aspects when designing pile foundations on the collapsible tropical soil of Brasília.

Although the results are restricted to the conditions of the analyses, based on a limited set of data, they allow preliminary generalizations of the overall behavior. Moreover, they do highlight the fact that the phenomena involved with such processes are rather complex. In this regard, this paper has provided a better understanding of some of the features which are involved by the loading mechanisms of isolated piles on tropical soils. It shall be noticed, however, that some comments have been hypothesized in order to explain the results, and do need further research for a more grounded appreciation in the future.

Therefore, from the trends observed with the data and analyses, some general conclusions can be drawn:

• Manually augered piles are not recommended as foundation solution to replace mechanically excavated ones, with exception to perhaps low level constructions or lightly loaded structures;

• The use of an expander additive mixed in the fresh concrete increases the vertical failure load and decreases the vertical settlement of bored piles, and shall be adopted whenever possible;

• Bored piles should be preferably cast-in-place between 0 to a maximum of 3 days after the soil excavation, since there is a tendency of decrease of vertical bearing capacity, and of increase on the vertical settlement, with increasing time spans between hole excavation and concreting after the 3rd. day;

• The vertical bearing capacity of root piles does increase with the level of pressure, but up to a value of around 200 kPa. This pressure appears to be a "threshold" value beyond which a major structural breakage, or collapse, takes place in the soil surrounding the borehole. Hence, such pile types should be limited to low injection pressures, specially on the collapsible layers of this deposit, close to surface;

• The dynamic insertion of some pile types, as the precast driven, should be avoided in this type of material, given its fragile nature at the collapsible layers. This effect influences the results of both the vertical and the horizontal capacity values;

• Suction effects, or weather seasonality, do influence the vertical capacity of floating bored piles founded in this soil, and should be taken into account specially for short length piles;

• The traditional Décourt and Quaresma (1978) method can in principle be safely used in design for vertically loaded bored piles, with N_{SPT} results at any time of the year;

• Bored piles do seem to behave as floating ones in this particular deposit, with very low vertical bearing capacity values at the base. Perhaps the base pressure could be more effectively mobilized at higher displacement levels, *i.e.*, in a range above the usual admissible values. Ultimate lateral shaft values below 40 kPa mobilized at vertical head displacements of around 5% of the pile diameter can be used as a design starting value - to be further verified *in situ* given the (already cited) constraints of herein data;

• Horizontal displacements attained on loaded bored piles increase at both working and failure conditions when the soil is inundated. As noticed for the root piles, the injection pressure beyond a certain level also increases this displacement;

• The bearing capacity estimated for bored, root or precast driven piles horizontally loaded in this soil, via the traditional extrapolation or the norm criteria, do not change considerably with subsoil conditions (*i.e.* inundation or not);

• The traditional Broms (1964a,b) method can in principle be safely used in design for horizontally loaded bored, root and precast driven piles in this soil. Nevertheless, in the case of the precast driven, the methodology seems to be very conservative;

• The coefficient of subgrade reaction decreases with the level of horizontal displacement of the pile. Hence, to be suitable for practical purposes, this modulus should be chosen at the corresponding design range that the pile is expected to displace in its life;

• Similar to the vertical case, the dynamic insertion of some pile types, as the precast driven, should be avoided in this soil. This technique has caused the driven pile to have the lowest values of horizontal subgrade reaction at the working loads.

This paper is a collection of the contribution of many theses from the Geotechnical Graduation Program of the University of Brasília. Given the small number of foundations, the limited spatial size of the studied area within the geographical context of the Federal District, and the multitude of external factors that could affect the results, it is evident that more studies are still necessary (and are underway).

Therefore, it shall be emphasized that the conclusions drawn herein have to be considered of limited range and applicability. Nevertheless, these results, together with the experience acquired during the exercise, can be of high interest for researchers and foundation designers of this region and abroad. In many aspects, the presented data of this paper can be readily used in practical design of equivalent foundations on similar soil deposits as the one studied herein, or, at least, be used as a start point for the project in "non classical" tropical soil types.

Acknowledgments

The author would like to express his gratitude to the engineering contractors Embre, Sonda, WRJ, Gerdau, Infrasolos, Soltec, Meksol, Sarkis Mix, Engemix and the Brazilian institutions DER-DF, FAP-DF, Finatec and Furnas-GO for all the support during the implementation of the Experimental Research Site.

This research was also possible due to the numerous scholarships provided by the Governmental sponsorship organizations CAPES and CNPq, by funds of the Geot. Grad. Program as well as to the hard work of some of its Professors, Technicians and Students, in particular Engs. E. Perez, N. Jardim, M. Lima and N. Mota.

Grant provided by MCT/CNPq 14/2009 Research fund proposal, to buy the PET equipment, is also acknowledged and valued.

Finally, the authors appreciates the English review of the paper done by Prof. Patrick Stewart from BCIT, Canada.

References

ABNT (2006) Estacas – Prova de Carga Estática – Método de Ensaio, NBR 12131, 8 pp.

ABNT (2010) Projeto e Execução de Fundações, NBR 6122, 91 pp.

Albuquerque, P.J.R.; Massad, F.; Carvalho, D. & Ferreira, M.A.M. (2001) Comportamento à Compressão de Estacas Escavadas, Hélice Contínua e Hélice Tipo Ômega, em Solo Residual de Diabásio (Compressive Behavior of Bored Piles, CFA Piles and Omega Piles in Residual Diabase Soil). Unicamp Univ. Publication, Campinas, 198 pp.

Anjos, G.J.M. (2006) Estudo do Comportamento de Fundações Escavadas em Solos Tropicais. D.Sc. Thesis, Dept. of Civil and Env. Engineering, University of Brasília. Pub. G.TD-033/06, 341 pp.

Aoki, N. & Velloso, D.A. (1975) An approximate method to estimate the bearing capacity of piles. Proc. V Panamerican Conference on Soil Mechanics and Foundation Engineering, Buenos Aires, v. 5, pp. 373-388.

Araki, M.S. (1997) Aspectos Relativos às Propriedades dos Solos Porosos Colapsíveis do Distrito Federal. M.Sc. Dissertation, Dept. of Civil and Env. Engineering, University of Brasília, Pub. G.DM-040A/97, 121 pp.

Brinch Hansen, J. (1963) Hyperbolic stress strain response: Cohesive soils. Journal Soil Mechanics and Foundation Division, ASCE, v. 89:SM4, p. 241-242.

Broms, B.B. (1964a) Lateral resistence of piles in cohesive soils. Journal of the Soil Mechanics and Foundations Division, ASCE, v. 90:2, p. 27-63.

Broms, B.B. (1964b) Lateral resistence of piles in cohensionless soils. Journal of the Soil Mechanics and Foundations Division, ASCE, v. 90:3, p. 123-156.

Cavalcante, E.H.; Giacheti, H.L.; Danziger, F.A.B.; Coutinho, R.Q.; Souza, A.; Kormann, A.C.M.; Belicanta, A.; Pinto, C.S.; Costa Branco, C.J.M.; Ferreira, C.V.; Carvalho, D.; Marinho, F.A.M.; Cintra, J.C.A.; Dourado, K.C.A.; Moraes, L.S.; Albuquerque Filho, L.H.; Almeida, M.S.S.; Gutierrez, N.H.M.; Albuquerque, P.J.R.; Chamecki, P.R.; Cunha, R.P.; Teixeira, R.S.; Menezes, S.M. & Lacerda, W.A. (2006) Campos experimentais de fundações. Proc. XIII Braz. Cong. of Soil Mechanics and Geot. Engineering, Volume of Experimental Site Workshop, Curitiba, pp. 1-165.

Cintra, J.C.A. (1981) Uma Análise de Provas de Carga Lateral em Estacas e Comparação com os Métodos da Teoria de Reação Horizontal do Solo. M.Sc. Dissertation, São Carlos School of Engineering, University of São Paulo, São Carlos, 150 pp.

Cintra, J.C.A. & Toshiaki, T. (1988) Instrumentação de Modelos de Estacas com "Strain Gauges". Publication 049/88. University of São Paulo, São Carlos.

Cunha, R.P. & Camapum de Carvalho, J. (1997) Analysis of the behaviour of a drilled pier foundation in a weathered, foliated and folded slate. Proc. XIV International Conference on Soil Mechanics and Foundation Engineering, Hamburg, pp. 785-786.

Cunha, R.P. & Kuklík, P. (2003) Numerical evaluation of pile foundations in tropical soils of the Federal District of Brazil by means of a semi-analytical mathematical procedure. Solos e Rochas, v. 26:2, p. 167-182.

Cunha, R.P.; Assis, A.P.; Marques, F.E.R. & Santos, C.R.B. (2007) Influência do estado de tensão de um túnel e da sazonalidade em ensaios de campo em argila colapsível do Brasil. Luso-Brazilian Journal Geotecnia, n. 110, p. 157-182.

Cunha, R.P.; Jardim, N.A. & Pereira, J.H.F. (1999) *In situ* characterization of a tropical porous clay via dilatometer tests. Proc. Geo-Congress 99 on Behavorial Characteristics of Residual Soils, ASCE Geotechnical Special Publication 92, Charlotte, pp. 113-122.

Cunha, R.P.; Pereira, J.H.F.; Soares, J.M.; Mota, N.M.B. & Poulos, H.G. (2001) Backanalyses of field loading tests on deep foundations in a tropical clay. Proc. XV International Conference on Soil Mechanics and Geotechnical Engineering – XV ICSMGE, Istanbul, v. 2, pp. 869-872.

Décourt, L. & Quaresma, A.R. (1978) Capacidade de carga a partir de valores de SPT. Proc. VI Brazilian Cong. of Soil Mech. and Geot. Engineering, Rio de Janeiro, pp. 45-53.

Jardim, N. (1998) Metodologia de Previsão de Capacidade de Carga Vertical e Horizontal com o Dilatômetro de Marchetti. M.Sc. Dissertation, Dept. of Civil and Env. Engineering, University of Brasília, 141 pp.

Kocsis, P. (1971) Discussion of lateral load tests on piles – Arkansas River Project. Journal of the Soil Mechanics and Foundations, ASCE, n. 97:SM6, p. 932-935.

Lima, M.J. (2001) Avaliação de Metodologias de Projeto para Estacas Carregadas Horizontalmente Assentes em Argila Porosa Colapsível. M.Sc. Dissertation, Dept. of Civil and Env. Engineering. University of Brasília. Pub. G.DM-084/01, 99 pp.

Matlock, H. & Reese, L.C. (1961) Foundation analysis of offshore pile supported structures. Proc. 5th International Conference on Soil Mechanics and Foundations Engineering, Paris, v. 2, pp. 91-97.

Mazurkiewicz, B.K. (1972) Test Loading of Piles According to Polish Regulations. Royal Society and Academy of Engineering Sciences. Communication on Pile Research, Report no. 35, Stockholm, 20 pp.

Mota, N.M.B. (2003) Ensaios Avançados de Campo na Argila Porosa Não Saturada de Brasília: Interpretação e Aplicação em Projetos de Fundação. Ph.D. Thesis. Dept. of Civil and Env. Engineering, University of Brasília. Pub. G.TD-013A/03, 336 pp.

Mota, N.M.B.; Cunha, R.P.; Anjos, G.J.M. & Albuquerque Filho, L.H. (2009) Capítulo 15 intitulado Campo experimental de fundações e ensaios de campo (Chapter 15 titled Experimental site of foundations and *in situ* testing). Celebration Book on the 20 years of the Geotechnical Graduation Program of the UnB, Brasília, pp. 325-345.

Perez, E.N.P. (1997) O Uso da Teoria da Elasticidade na Determinação do Módulo de Young do Solo Adjacente a Estacas Carregadas Verticalmente na Argila Porosa de Brasília. M.Sc. Dissertation, Dept. of Civil and Env. Engineering. University of Brasília, 146 pp.

Poulos, H.G. (1990) DEFPIG User's Guide. Centre for Geot. Research, Univ. of Sydney, Sydney, 55 pp.

Reese, L.C. & Matlock, H. (1956) Non-dimensional solutions for laterally loaded piles with modulus assume proportional to depth. Proc. 8th Texas Conference on Soil Mechanics and Foundations Engineering, The University of Texas, Austin, 41 pp.

Reese, L.C.; Isenhower, W.M. & Wang, S.T. (1998) Developments in horizontal capacity estimation of bored piles. Proc. International Symposium on Bored and Auger Piles III, Ghent, pp. 23-34.

Rodrigues, A.A.; Camapum de Carvalho, J.; Cortopassi, R.S. & Silva, C.M. (1998) Avaliação da adaptabilidade de métodos de previsão de capacidade de carga a diferentes tipos de estacas. Proc. XI Brazilian Cong. of Soil Mech. and Geot. Engineering, Brasília, v. 3, pp. 1591-1598.

Van der Veen, C. (1953) The bearing capacity of a pile. Proc. 3rd International Conference on Soil Mechanics and Foundation Engineering, Switzerland, v. 2, pp. 84-90.

Understanding the Mechanism of Static Soil-Structure Interaction - A Case Study

G. Savaris, P.H. Hallak, P.C.A. Maia

Abstract. During the construction of a building, a transfer of loads occurs from the columns which tend to settle more to those that tend to settle less. This observable fact can be attributed to the mechanism called static soil-structure interaction (SSI). In order to understand this mechanism, which is often not considered in designs, an experimental campaign and a numerical simulation were carried out on a building which had its settlements monitored from the start of its construction. For this purpose, linear tridimensional numerical models were constructed for each floor and numerical analysis was performed, using the finite elements method. In this analysis, numerical models corresponding to the execution of each floor were used, considering the settlements measured at each stage of the construction. Results show a change in reaction forces which occurs when settlements are introduced into the model. It was also possible to verify that the spring coefficients of the foundations change along the ground surface, which suggests that they are related to the structural stiffness and with the foundation adopted. Furthermore, the analysis of the susceptibility of the structure to settlements presents results which could justify a greater influence of settlements during the first stages of the construction, with lower stiffness of the structure associated with greater load variation in columns.

Keywords: FEM analysis, static soil-structure interaction, settlements, soil-foundation spring coefficient, structural stiffness.

1. Introduction

Traditionally, building projects have been drawn up presuming that the supports on the ground are non-displaceable, resulting in a set of loads (vertical, horizontal reactions and flexural moments) which are passed to the foundation engineer who, considering the results obtained in the field trials, designs the foundations.

In reality, the performance of a building is governed by the interaction between the superstructure, infrastructure and foundation soil, in a mechanism denominated static soil-structure interaction (SSI). Through this mechanism, during the construction of a building, a transfer of loads occurs from the columns which tend to settle more to those that tend to settle less. Load transfer between the columns causes a trend towards uniformity of settlements, resulting in smaller displacements than those estimated. This effect may be found when settlements of foundations are monitored during construction, and throughout the lifetime of the building.

Nonetheless, monitoring building during construction, observing the behaviour of the foundations as they are being loaded, in addition to serving as a certification of quality of the projects and execution of the construction, is also a great contribution to the study of the mechanism of interaction between the structure and the soil.

Following this trend of monitoring buildings during their construction, this work intends to present the results obtained with the numerical analysis of a construction which had its settlements monitored from the beginning. Actually, the main focus is concentrated on observing the interaction between the structure and the foundations, by measuring their displacements during the construction of the building. The effects of this mechanism is analysed as regards certain important aspects such as the load variation in columns, the spring foundation coefficients and the stiffness of the structure.

Furthermore, this work contributes to the formation of a database about the static SSI and makes this mechanism an important tool that should not be underestimated or misunderstood in building design. Through this study, we expect to help future research into the development of methodologies for analysing the soil-structure interaction in building projects.

In the next section the mechanism of the soil-structure interaction and its observed consequences in a number of cases are presented. After that, a review of some models found in the literature is presented as well as the description of the building. Finally, the results and conclusions are presented.

G. Savaris, Master in Civil Engineering, Departamento de Engenharia, Civil, Universidade Estadual do Norte Fluminense Darcy Ribeiro, Av. Alberto Lamego 2000, 28013-600 Campos dos Goytacazes, RJ, Brazil. e-mail: gustavo.savaris@yahoo.com.br.
P.H. Hallak, Associated Professor, Departamento de Mecânica Aplicada e Computational, Faculdade de Engenharia, Universidade Federal de Juiz de Fora, Rua José Lourenço Kelmer sn, Cidade Universitária, 36036-900 Juiz de Fora, MG, Brazil. e-mail: patricia.hallak@ufjf.edu.br.
P.C.A. Maia, Associated Professor, Departamento de Engenharia of Civil, Centro de Ciência e Tecnologia, Universidade Estadual do Norte Fluminense Darcy Ribeiro, Av. Alberto Lamego 2000, 28013-600 Campos dos Goytacazes, RJ, Brazil. e-mail: maia@uenf.br.
Submitted on April 28, 2010; Final Acceptance on March 10, 2011; Discussion open until April 30, 2012.

2. Static Soil-Structure Interaction (SSI) Mechanism

The static soil-structure interaction mechanism can be observed, for example, by the static analysis of a system composed of a beam supported by three columns, subjected to a uniformly distributed load, as presented in Fig. 1(a). In this case, the load acting on the central column, determined by conventional static analysis, corresponds to twice the load on the lateral columns. Due to the higher load, the foundation of the central column tends to suffer greater displacements; however, depending on the magnitude of the beam rigidity, this displacement is restricted, causing transfer of loads to the lateral columns. Consequently, the displacement of the central column is less than expected, while the displacement of the lateral columns will be greater.

In addition to the effects of rigidity of the structure on the foundation displacements, these displacements will also influence the deformation of the structure. This can be observed when we compare the deformation of elements of the structure in Fig. 1. In a linear analysis we observe that the final conditions of deformation of a structure consist of the sum of the deformations of the elements, due to the loads and redistributions, and they can be obtained only by an interactive analysis of the soil-foundation-structure system.

Thus, the study of settlements may be used as a tool for the analysis of the static soil-structure interaction mechanisms. For this purpose, an initial prediction of the settlements is made, considering the isolated foundations, and the settlements of the building are monitored during its construction and over its lifetime.

The performance of any building can be evaluated by means of two models of analysis: in the first model (Fig. 2(a)) the foundations are designed and the settlements estimated considering only the loading coming from the structure and in the second model (Fig. 2(b)) the stiffness of the structure is considered in the estimate of settlements. It can be verified that the deformation of settlements becomes smaller due to the influence of the interaction of the soil and structure, with the central supports tending to settle less than predicted and the peripheral supports settling more.

The impediment of settlements caused by the rigidity of the structure alters the maximum and minimum settlements, and consequently the differential settlements. Nevertheless, the total mean estimated settlements do not alter

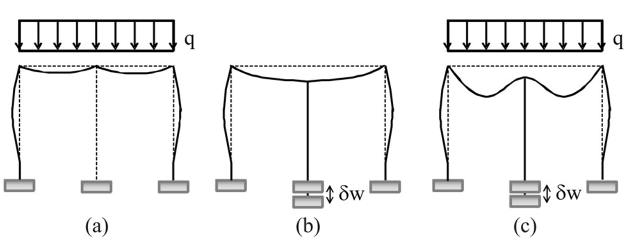

Figure 1 - Soil-structure interaction model.

significantly. Thus, the angular distortions caused by the differential settlements are minimized, making it feasible to use foundations solutions that would not be possible to achieve by conventional studies (Gusmão & Calado, 2002).

The redistribution of forces on elements of the structure is a consequence of greater uniformity of the settlements. According to Goshy (1978), this occurs with greater intensity on the lower floors of buildings, where the open framed structure with panels behaves in the same way as vertical planes, similarly to a deep beam. Thus, the lower parts of the structure are more susceptible to flexural deformations, as shown in Fig. 3.

According to Gusmão & Calado Jr. (2002), the variation in the flexural moments, and torsional and cutting forces, are negligible, in comparison with the axial forces. Redistribution of load on the columns generates the transfer of load from the supports that tend to settle more to those that tend to settle less. These increases in load are signifi-

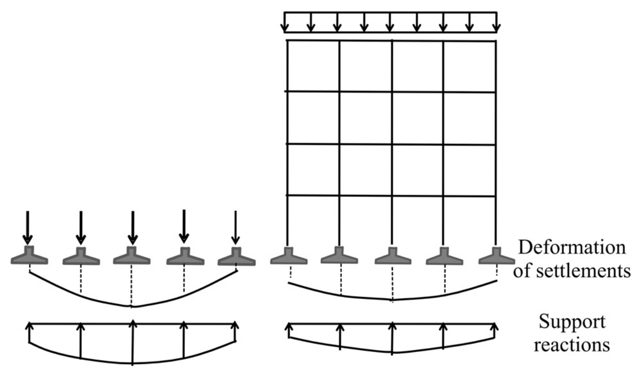

Figure 2 - Effect of SSI on settlements and support reactions (adapted from Gusmão (1994)).

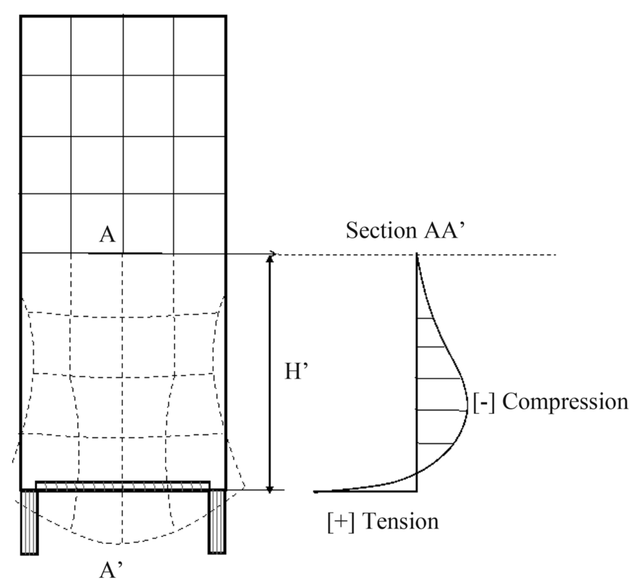

Figure 3 - Analogy with the Deep Beam (H' → is the influence height).

cant, and can attain variations of up to 30% in the load foreseen in the rigid model (Gusmão (2006) and Gusmão & Calado Jr. (2002)). These increases in loads can cause pathologies in the structural elements, such as cracking of beams and concrete slabs, and crushing of columns.

Determining the loads acting on the columns of buildings has been performed in two ways: by measuring the deformation of the columns, using defined concepts of strength of material for load determination, or by estimation or measurement of settlements, using computer programs for structural analysis, in which the settlements measured are applied as prescribed displacements on the supports.

In modelling the structure, some simplifications are generally made, directly related to the consequences on the final product built. Some of these simplified hypotheses and their respective consequences have been reported by Gusmão (1994) and are presented in Table 1. Thus, we observe the need for considering the interaction between the soil and the structure in designing buildings, with the goal, above all, of minimizing pathologies.

3. Proposed Models for the Static SSI Evaluation

A review of the main methods for static soil structure analysis is presented in Table 2. It should be noted that all methodologies aim to simplify the problem by transforming the superstructure into an equivalent stiffness element. A more rigorous method allows for the superstructure and the foundation working together as a whole body.

All methodologies have some limitations as regards their numerical performance and the available computational capacity. Moreover, all methods are based on the elasticity theory, which can narrow their applicability for cases with large deformation of the superstructure or the foundation.

It is important to note that, in these methodologies, the calculation of settlements is usually done using theoretical models based on the literature. However, optionally, one can use settlements measured *in situ*, which allow a better definition of the spring foundation coefficient. This was the option adopted in the present work, in accordance with the methodology proposed by Iwamoto (2000) and Crespo (2004).

Illustrations of each model are as follows: Fig. 4 shows the equivalent beam proposed by Meyerhof (1953); Fig. 5(a) is a representation of the model proposed by Chamecki (1954) and used by Poulos (1975), Iwamoto (2000) and Crespo (2004); Fig. 5(b) is a representation of the model adopted by Colares (2006) and Mota *et al.* (2007); and, finally, Fig. 5(c) is the model adopted by Almeida (2003) and Ribeiro (2005)

The methodology adopted in this work uses the finite element method of a discretised building in order to investigate its structural behaviour. The numerical model does not consider the foundation and soil directly, but by introducing the measured settlements of all columns and for each stage of construction. This procedure is similar to that adopted by Gonçalves (2004) and Gonçalves *et al.* (2007).

4. Description of the Building Analysed and Computational Modelling

The study was carried out in a residential building, called Edifício Classic, located in the city of Campos dos Goytacazes - RJ, Brazil. In Fig. 6 a photo of the building is presented, in the final stages. Following the trend towards verticalization of buildings in the city, this building has 12 floors, constructed above the surface of the ground. The ground level has a social entrance and the garages, which are also extended to the following two floors. After this, there are nine floors with four residential units each, and the top-floor apartment, with a party area, machinery rooms and elevated reservoir.

Table 1 - Consequences of the hypotheses of projects with regard to SSI (Gusmão, 1994).

Calculation hypotheses	Consequence
Supports considered fixed	Redistribution of loads and forces on structural elements, especially beams and columns. Load relief on most loaded columns and overload on less loaded columns. There may be damage to structural elements.
Supports may settle in a manner independent of one another	The connection between structural elements gives the structure a rigidity that restricts differential settlements. The measured deformation of settlements is less than that conventionally estimated. There is a tendency towards uniformity of settlements.
The loading of the building only occurs at the end of construction	As the structure is being constructed there will be an increase in its load and in the absolute settlements. There is, however, an increase in the rigidity of the structure, which causes a trend towards uniformization of the settlements. There is a limit height, corresponding to the first five floors, beyond which there is practically no further increase in rigidity for the purposes of uniformity of settlements.

Table 2 - Methodologies normally used for static soil structure analysis (adapted from Aoki & Cintra (2004) and Savaris (2008)).

Model	Meyerhof (1953)	Iwamoto (2000); Crespo (2004); Chamecki (1954); Poulos (1975)	Colares (2006); Mota *et al.* (2007)	Almeida (2003); Ribeiro (2005)
Model conception	The structure is replaced by a beam with equivalent stiffness	The superstructure and the foundation are considered as a separated body in balance. The elements of the foundation are considered as part of the fixed soil mass	The superstructure and the foundation are isolated and in equilibrium The foundation elements is part of the superstructure	It is considered as a single body in balance. The global system is formed by the structure and the mass of soil and the edge is limited by the fixed soil mass
Type of method for the solution to the problem	Analytical method	Displacement method	Finite element method	Finite element method and/or boundary method
Methodology for computing the stiffness of the structure	The stiffness of the equivalent beam is equal to the sum of the flexural stiffness of bars which compose the building and the masonry panel	The equivalent stiffness is determined as the force necessary to displace a point of the top surface of the foundation in one unit of length	The equivalent stiffness in each support is determined by dividing each reaction of the structure by its respective settlements	Numerically determined
Disadvantage	Large quantity of numerical operations and simplified computation of the stiffness of the structure	Each combination for one foundation element with one type of soil presents a different equivalent stiffness value		Large quantity of data associated with high number of numerical operations

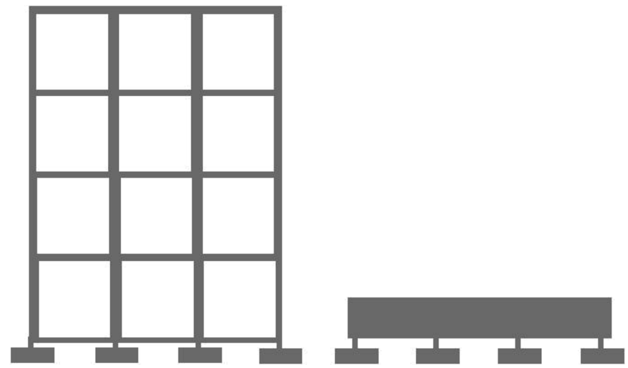

(a) Set of superstructure and foundation

(b) Equivalent beam and foundation

Figure 4 - Beam with equivalent stiffness proposed by Meyerhof (1953).

4.1. Features of the Structure and of the Monitoring System

The building structure is formed by columns, board beams, ramps and stairs of conventional reinforced concrete, smooth concrete decks and two prestressed reinforced concrete transition beams, using a non-adherent prestressed system with greased single cables. The building has 35 columns in the first three floors, starting with the foundations, and for each floor 18 columns follow, with the transition of three columns occurring on prestressed beams. Closure of the building and internal divisions was done with brickwork using ceramic bricks with holes, and for closing the stairs, concrete blocks were used.

Figure 7 shows important details of the position of the foundations and the numbering of the columns. The columns in the central region (columns 1 to 20) have deep foundations and continue along the typical floor, whereas the columns in the external region (columns 21 to 37) are supported on footing foundation and end on the 2nd or 3rd floor. Also in Fig. 7 it is possible to see the foundation loads obtained by conventional design, which means considering fixed supports, range between 300 kN and 5200 kN.

The footing foundation is seated at 1.80 m from the surface of the ground, on a compacted layer of soil, improved by the mixture of sand and cement. The piles were made by continuously monitored helical equipment, 400 mm in diameter, and a mean depth of 12.5 m, reinforced in the first three metres.

In Fig. 7 it is also possible to see the network of the hydraulic system for monitoring the settlements of all columns, which is based on the communicant pipe principle, similar to the Terzaghi system. In this work, interconnected silicon pipes, with water outlets in the base of all columns and in the reference mark, were adopted. This scheme made it possible to observe the level of water in all columns and in the reference mark simultaneously.

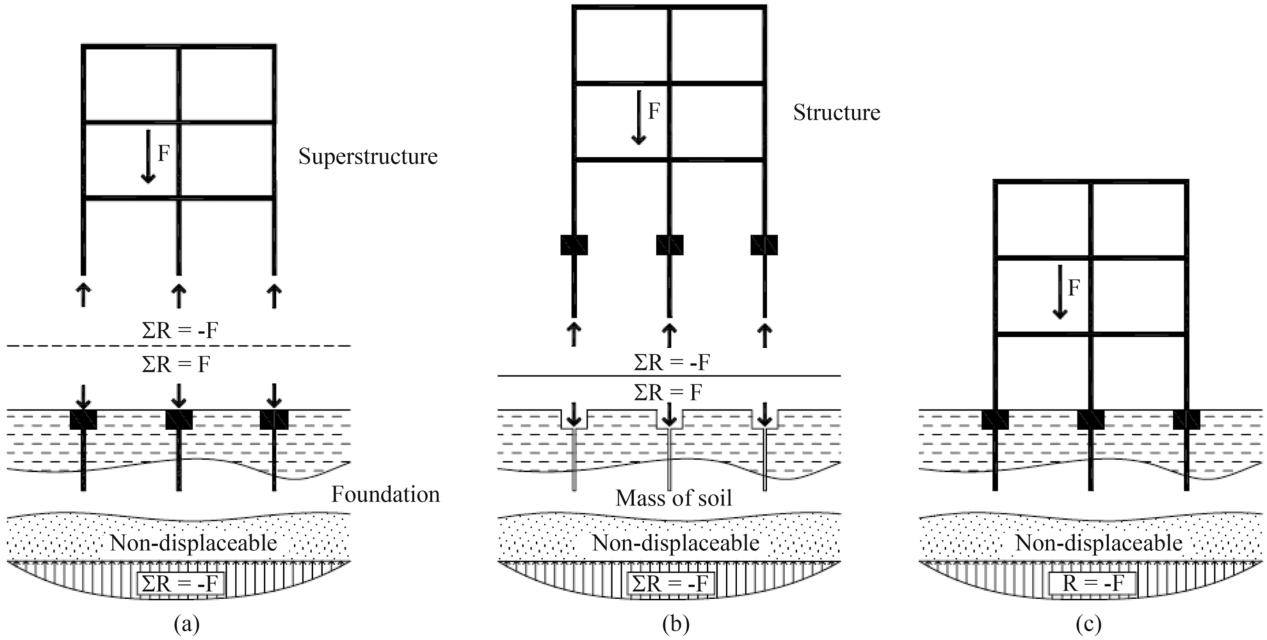

Figure 5 - Models for soil-structure interaction analysis (adapted from Mota *et al.*, 2007).

Figure 6 - Front Elevation of Edifício Classic.

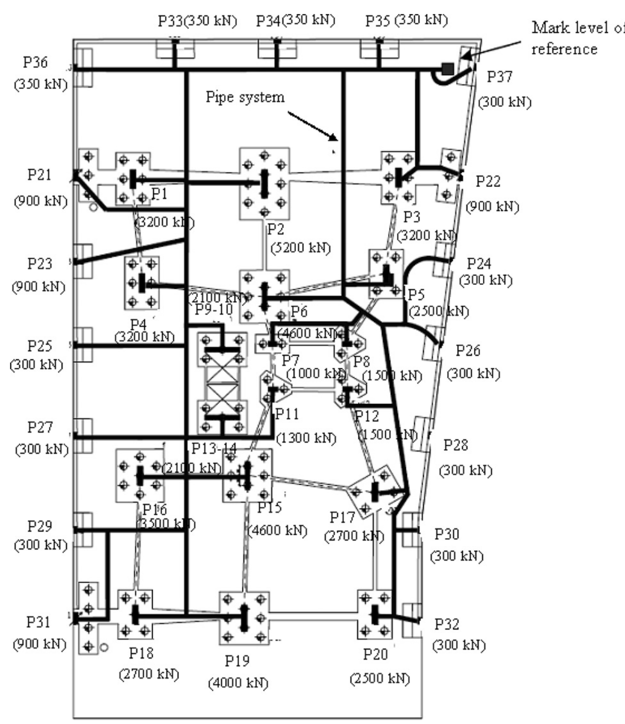

Figure 7 - Sketches of the foundations, location of columns with respective design loads, level reference mark, pipe network and project loads.

The reference mark level was installed in a region that did not suffer any influence from the foundation elements. It was made up of a deep foundation with 10 m of length to which a graduated calibrated metallic bar was coupled. On the edge of the tubulation network, located on each column and on the reference mark, glass tubes were installed. On the reference mark the glass tube was fixed on the lateral of the graduated bar. The position of the level of water in relation to the top of the reference mark level was determined by the distance of the meniscus to the graduation of the metallic bar, as shown in Fig. 8.

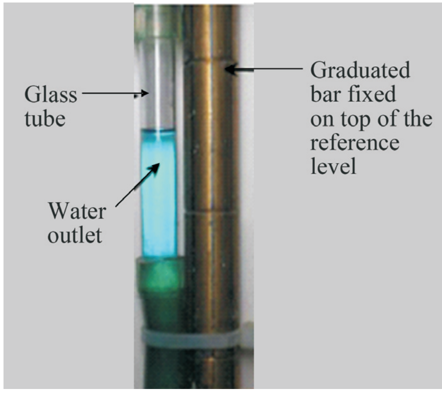

Figure 8 - Metal post and water outlet on the reference mark.

On columns, the glass tube was fixed on their reference level. The position of the reference level in relation to the reference level in the column is determined by the distance from the meniscus to the orifice of the metallic bars.

To circumvent the difficulties of reading the water levels and ensure greater accuracy, a digital process was adopted as a tool for determining the position of the meniscus. After obtaining a photograph of the meniscus in the field, the image was treated and examined in the laboratory using an image manipulation program.

Although we give only this short explanation about the monitoring system, readers are invited to consult the original dissertation of Savaris (2008) should they wish to obtain more details about the settlement measuring system used in the study.

4.2. Modelling of the structure

The Edifício Classic structure was modelled as finite elements, allowing a static numerical and linear analysis to be made, using a computer program for structural analysis. The beams and columns were modelled as uniaxial bar elements, defined by two nodes located on the line that passes through the centre of gravity of the section. These elements have tension, compression, torsion and flexural capacities. The elements have six degrees of freedom in each node, three being rotations and three translations. On the columns, the eccentricities of the beams were disregarded, except for the columns of the lift shaft, in which rigid bar elements were inserted. These rigid bars transfer the load from the beams directly onto the axes of the columns.

The concrete slabs were considered as plate elements, defined by four nodes, with six degrees of freedom in each node, three being rotations and three translations. These were discretised in quadrangular elements according to the tracing of the prestressing cables.

The structural analysis took into consideration the construction process of the building through the development of twelve tridimensional models, corresponding to the execution of each of the concrete slabs of the building. Only the stages of construction in which the settlements of all the columns were monitored were considered.

As the measurements of the settlements had been made at points located at the bottom extremity of the ground floor columns, the tridimensional models did not take into consideration the elements of foundation and soil. In fact, this information was introduced by means of measured settlements.

By follow-up of the construction schedule, data was obtained on the execution of the brickwork on each floor, presented in Table 3, with the loads being entered because of the brickwork in the models with reference to the respective stages of the construction process. The wall was considered to have a thickness of 12 cm for the internal divi-

Table 3 - Important construction data.

Model	Date	Time of construction (days)	Stage of construction
I	15/08/2005	0	Execution of slab 1
II	22/09/2005	37	Execution of slab 2
III	27/10/2005	73	Execution of slab 3
IV	25/11/2005	101	Execution of slab 4 and masonry on slab 1
V	14/12/2005	120	Execution of slab 5
VI	29/12/2005	135	Execution of slab 6
VII	14/01/2006	151	Execution of slab 7 and masonry on slab 2
VIII	31/01/2006	167	Execution of slab 8 and masonry on slab 3
IX	17/02/2006	184	Execution of slab 9 and masonry on slab 4
X	16/03/2006	211	Execution of slab 10 and masonry on slab 5
XI	15/04/2006	240	Execution of slab 11 and masonry on slab 6
XII	17/07/2006	331	Execution of slab 12 and masonry on slab 7
XIII*	04/10/2006	413	Completed structure and masonry on slab 10
XIV*	02/07/2007	681	Final stage of the construction.

*For these stages there is no numerical model.

sions executed with ceramic bricks, and 15 cm for the stair walls, constructed with mortar blocks.

The weight of the structure itself was automatically calculated by the computer program from the dimensions of the elements and the physical properties of the materials. The accidental loadings were disregarded in the analyses. The specifications of the materials used in the construction were obtained from the architectural and structural projects, and, occasionally for the materials with non-specified properties, the recommendations in the Brazilian Standards NBR 6118 (ABNT, 2003) and NBR 6120 (ABNT, 1980) were adopted, as presented in Table 4. In this table fck is the characteristic compressive resistance of the concrete, fptk is the characteristic tension of rupture to traction of the prestressed steel and fpyk is the characteristic leakage resistance of the prestressed steel.

The prestressing performed in the concrete slabs and transition beams was considered as a set of Equivalent Concentrated Loads, as presented by Menegatti (2004). This methodology was proposed for considering prestressing in prestressed concrete elements. It aims to contribute to the optimization of the task of modelling the structure, due to the simplicity of obtaining the forces and the ease of application in commercial programs for structural analysis.

5. Performance of the Structure and the Influence of Settlements on the Analysis

This work intends to understand the mechanism of the interaction between the structure under construction and the foundation, referred to here as the static SSI mechanism. This mechanism represents the static action and reaction between both parts of a building, considering the experimental settlements obtained for each stage of construction. To accomplish this, a study about the variation of loads on the supports during the time of construction is first presented. Next, following certain tendencies which use spring coefficients in order to represent the soil reaction in the structures, we present an analysis of this parameter over the time of construction. Finally, an analysis of the influence of the stiffness of the structure on the behaviour of the settlements is presented.

Table 4 - Physical parameters of construction materials used.

Material	Property	Adopted value
Reinforced concrete	Specific weight (kN/m^3)	25
	Poisson coefficient	0.2
	fck(MPa)	30
	Elasticity modulus (GPa)	30.67
Pre-stressed cable	Diameter (mm)	15.2
	fptk(MPa)	1900
	fpyk(MPa)	1710
Ceramic masonry	Specific weight (kN/m^3)	18
Blocks of cement	Specific weight (kN/m^3)	22

5.1. Variation of loads in columns

With the aim of quantifying the load variation on columns, considering the settlements or not, two hypotheses for the supports were considered in the analysis. In the first hypothesis the supports were considered as fixed, to obtain the reactions on the supports as is done traditionally in structural building projects. In the second hypothesis, the settlements measured at each stage were imposed, as prescribed displacements on the supports, to obtain the effects of the settlements on the reactions of the supports. By superimposing the effects of the weight of the structure itself and brickwork, prestressing and the settlements, the effects of the static SSI in the loads on columns were then analysed.

In order to quantify the influence of settlements on the loads, a redistribution coefficient of loads factor (*FR*) was employed. This factor is defined as:

$$FR = \left(\frac{R_\delta - R}{R} \right) \times 100 \quad (1)$$

where R is the total reaction on column i without considering its vertical displacements and R_δ is the total reaction on column i taking into account its settlements. In these equations R and R_δ are the total reactions obtained until the stage of construction being considered. Actually, the coefficient *FR* represents, in percentage terms, the increase or relief of the load on the support due to the settlements.

By taking the values of *FR* obtained it was possible to define two groups of columns with distinct behaviour. In the first group we have columns which suffered an increase in load when taking into account the settlement, and have positive *FR* values. In the second group we have those which suffered a decrease in load with negative *FR* values. Considering the maximum and minimum values of each group over the time of construction, it was possible to draw the curves show in Fig. 9. In this figure we also indicate, for each group, the columns which presented extreme values.

We find the highest load increases and reliefs in the first stages of construction. It can be seen that as the number of floors of the building increases, the amplitude between the values of load increases and relief among the columns tends to reduce. Symmetry of the curves is observed in relation to the horizontal axis that passes through the origin, indicating the redistribution of the forces that occurs, caused by the structure-soil interaction.

In the first half of the construction higher variations of loads are observed in deep foundations (columns P7, P8, P9 e P11) while in the second half higher values are observed in footing foundations (columns P23, P24, P25 e P30). This observation shows that, due to the stiffness of the structure, a transfer of loads still continues, even for foundations which end on the 2nd and 3rd floors.

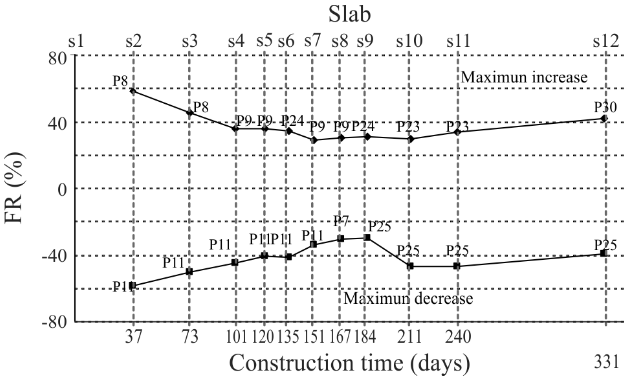

Figure 9 - Variation in maximum load increase and relief during the course of construction.

A worrying fact can be observed in this figure. For almost all monitoring stages the value of *FR* for pillars suffering an additional load is more than 30%. For the last stage (the pouring of the 12th slab) this difference is about 43%. Note that at this stage a uniformization of settlements is attained and this difference may persist for the life cycle of the building. This increase is a cause for concern from a structural point of view, and therefore deserves attention.

Uniformity of load distribution may be found when we analyse the coefficient of variation (CV) of the redistribution factor (*FR*) for each stage of construction, as presented in Fig. 10. This coefficient of variation is defined by the ratio between the standard deviation and the mean of the *FR*s. It can be seen that with the increase in the number of floors, the redistribution factor tends to decrease and stabilize. This fact, as observed previously, is a consequence of making the settlements uniform due to the influence of the stiffness of the structure.

5.2. Evaluation of spring foundation coefficient

To perform the analysis of structures considering the foundation settlements, one of the simplifications adopted in the computational modelling assumes the use of an ideal spring, with a vertical degree of freedom, connected with the support points of the structure on the soil. This resource is incorporated in the computational design of structures as an option dealing with a more realistic representation of the behaviour of the structures.

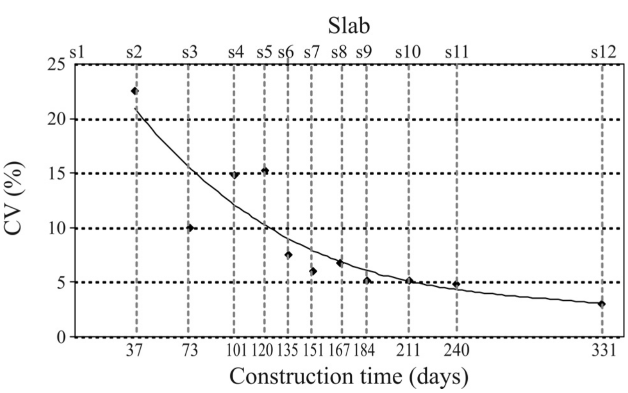

Figure 10 - Variation coefficient of the load redistribution during the course of construction.

In order to evaluate the magnitude of this parameter and to verify the feasibility of this assumption, we back-calculate here the spring coefficient based on experimental data. This spring coefficient of the soil-foundation set (K_{sf}) represents the relationship between the foundation load and the measured settlement and can be determined through Eq. (2),

$$R_{sf\,(i)} = \frac{R_{\delta(i)}}{\delta(i)} \qquad (2)$$

where $K_{sf(i)}$ is the spring coefficient of the support *i*, R_δ is the reaction of the support *i* of the structure, until the stage of construction considered, when it is analysed considering the measured settlements $\delta_{(i)}$ of the same support.

Figure 11 shows the contours of the coefficient referring to the execution of the 12th slab. It is evident that the coefficient K_{sf} is not constant along the ground surface, as also observed by Russo Neto *et al.* (2002) in their research carried out in a pre-cast concrete building. This can be explained by the fact that this coefficient is determined using the reactions of the supports when the measured settlements are considered. In this way, the values of K_{sf} depend not only on the type of soil and foundation but also on the features of the structure of the building. Therefore, the hypothesis using the same spring coefficient for all foundations often used in design is not a feasible representation of the actual problem.

In Fig. 11 it is possible to see the formation of four distinct zones clustered according to the magnitude of *Ksf.* The peripheral region, defined as Zone A, has the lowest values of K_{sf}. Low values of K_{sf} are also found in the zone near the lift shaft and stairs, defined as Zone B. The highest values of K_{sf} are found in Zone D, in the neighbourhood of the columns P2 and P19. There is also an intermediate region, Zone C, located in the peripheral projection of the typical floor.

The average values of K_{sf} during construction for the four zones described above are illustrated in Fig. 12. For zones C and D, we observe an increase of K_{sf} values at the beginning of construction, when the soil is receiving a significant amount of load. At the end of construction, these zones present an increase of, approximately, 56% and 33%, respectively, compared with the initial values. On the other hand, zones A and B experience a decrease of this parameter of about 13% and 22%, respectively. In fact, both forces and settlements tend to increase over the time of construction. As regards the definition of K_{sf}, which is the ratio of these two quantities, regions A and B experience an increase in settlement higher than the increase in load, while different behaviour is observed in regions C and D. Thus, the redistribution of load as a function of settlement is also observed in this analysis.

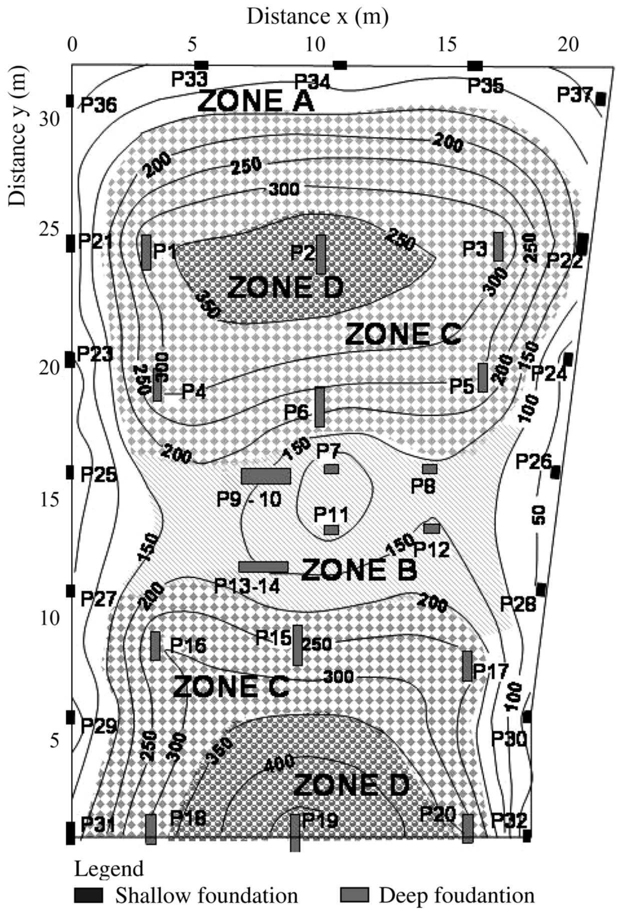

Figure 11 - Contours of K_{sf} for the last stage of construction (MN/m).

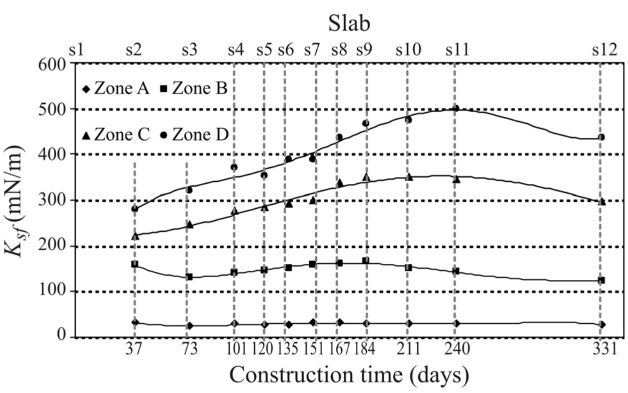

Figure 12 - Curves of average values of K_{sf} coefficient for zones SFA, SFB, SFC and SFD during construction.

It is clear that we have, again, a great disparity in the magnitude of this parameter among these four zones and during the construction of the building.

5.3. Influence of the stiffness of the structure on the static SSI mechanism

In this case study, the features of the structure make it difficult to use the methodology proposed by Meyerhof (1953), who considered, for the static SSI analysis, the frame of the structure as an equivalent beam. Thus, in order to analyse the influence of the stiffness of the structure on the redistribution of loads, another procedure was adopted. In this procedure, a parameter, defined here as an equivalent stiffness of the structure on each support (K_e), was obtained by applying unit settlements for each support and for each stage of construction. The necessary forces, that is, reaction values, to keep this displacement were interpreted as a stiffness coefficient of the structure related to a unit settlement of each support. It is important to stress that this procedure is similar to the idea of the direct displacement method for determination of the stiffness matrix of any kind of structure.

The variation of this parameter along the ground surface, for the 12[th] stage, can be observed in Fig. 13, where contours of K_e values are plotted. With regard to this figure, three distinct zones can be recognized according to the magnitude of the values of K_e. First, the zone called RA is characterized by lower values of K, of about 40 MN/m. This region corresponds to the periphery of the ground where the columns end in the second slab. Along the radial direction from the centre of the building, it is possible to observe a second region, called RB, with values of K_e between

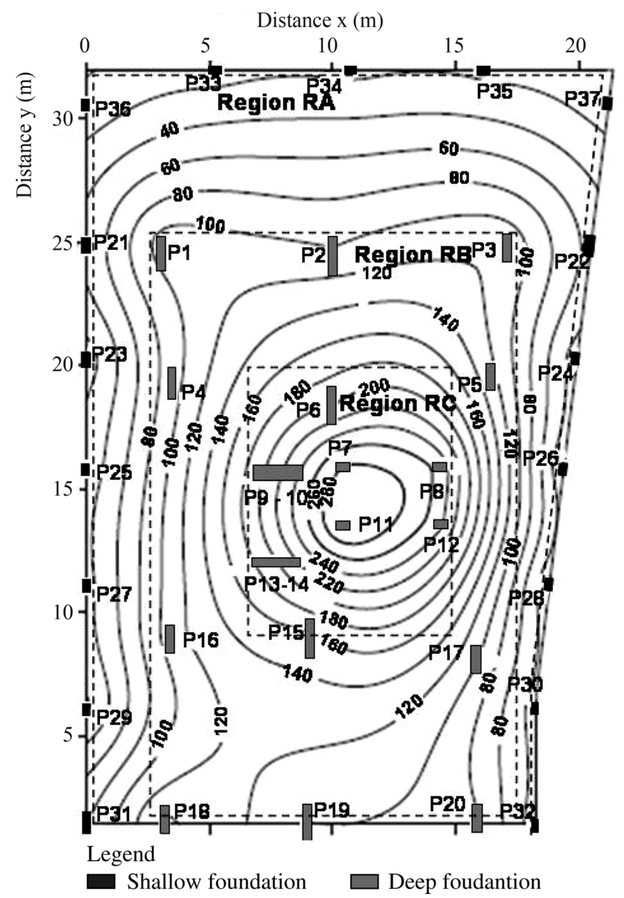

Figure 13 - Contours of equivalent coefficient curves (K_e) for the last stage of construction (MN/m).

80 MN/m and 120 MN/m. Finally, the third zone, located in the centre, called RC, has values of K_e over 160 MN/m.

In order to visualize the evolution of this parameter during the time of construction, the curves of mean values of K_e for regions RA, RB and RC are plotted in Fig. 14. It can be observed that regions RB and RC show a significant increase in the values of K_e during construction, but tend to stabilize in the final stages. On the other hand, the mean values in region RA stabilize just after the execution of the third slab. It should be noted that the columns in this region have shallow foundations and end at this stage of construction.

Another interesting result can be obtained if we compare Fig. 10 with Fig. 15 plotted below. The latter shows the variation curves of K_e during the construction stage, proportionally to the maximum values calculated for each region. It can be seen that all regions reached almost half the value of total stiffness after the third slab execution. Analysing Fig. 10, we can see that, after the execution of the fourth slab, the variation of the redistribution of load decreases. In other words, this confirms that significant effects of static SSI take place in the initial stages of construction. The same was observed by other researchers, like Gusmão & Calado Jr. (2002), Gonçalves (2004), Barros (2005), Danziger (2000) and Gusmão (2006).

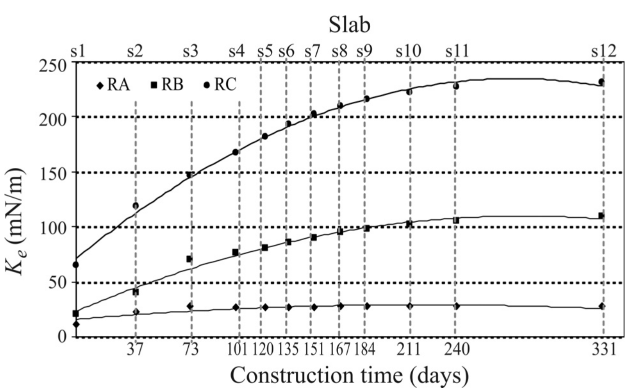

Figure 14 - Variation of the equivalent stiffness coefficient (K_e) for regions RA, RB and RC during construction.

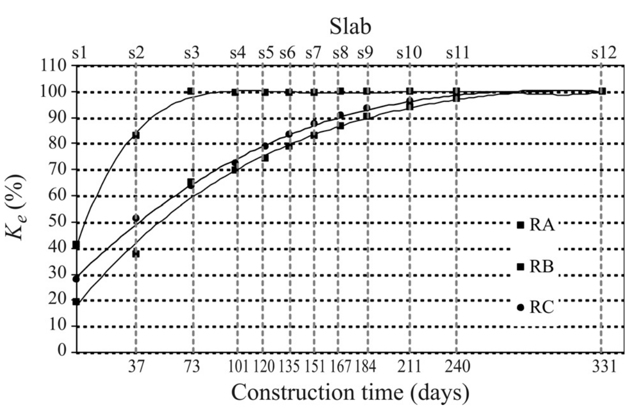

Figure 15 - Proportional evolution of the equivalent stiffness coefficient (K_e) of the structure for regions RA, RB and RC.

An analysis of the evolution of measured settlements was performed for each stage of construction and the results are plotted in Fig. 16. The initial stage of construction was characterized by a large displacement, generated by the removal of the casting forms of the first slab and execution of the second. It is possible to verify a uniform increase of settlements over time, which could be justified by the constant velocity imposed on the construction.

Figure 16 can also provide significant information on the static SSI mechanism. As observed, the average settlements in shallow foundations (region RA) have the same magnitude as in deep foundations in the first stages of construction. After the execution of the third slab, they continue to grow slightly and stabilize in the last stages. The increase of settlements in shallow foundations after the third pour slab suggests that, due to the stiffness of the structure, a transfer of loads from the central columns to the edge columns occurred. This effect is typical of the static SSI mechanism, as described in section 2.

Also in Fig. 16 the average loads for each stage of construction and for each section is provided. Note that there is a correlation between regions RA, RB and RC of Fig. 13 and zones A, B, C and D of Fig. 11. In fact, zone A corresponds to region RA, zone B corresponds to region RC and zones C and D correspond to region RB. In this way, we can observe the evolution of the stiffness coefficient in these regions by taking into account the evolution of the stiffness coefficient K_{sf} of Fig. 12.

In Fig. 17 an iso-settlement curve is presented for the stage related to the execution of the last slab. It is possible to observe the formation of a settlement basin, with higher depressions in the central region of the ground. This depression is due to the typical floors which generate the loads responsible for the increase of settlements in this region.

The influence of the stiffness of the structure on settlements can be verified using the variation coefficient of settlements, which is plotted in Fig. 18, and using the information provided by Fig. 13. Figure 16 shows, especially with regard to region RC, that the variation in settlement

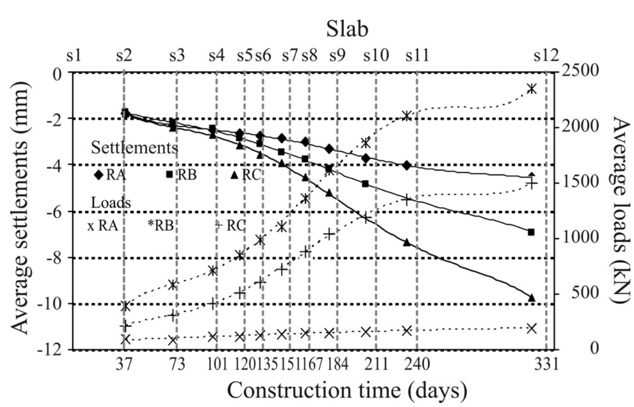

Figure 16 - Evaluation of mean settlement and loads during construction.

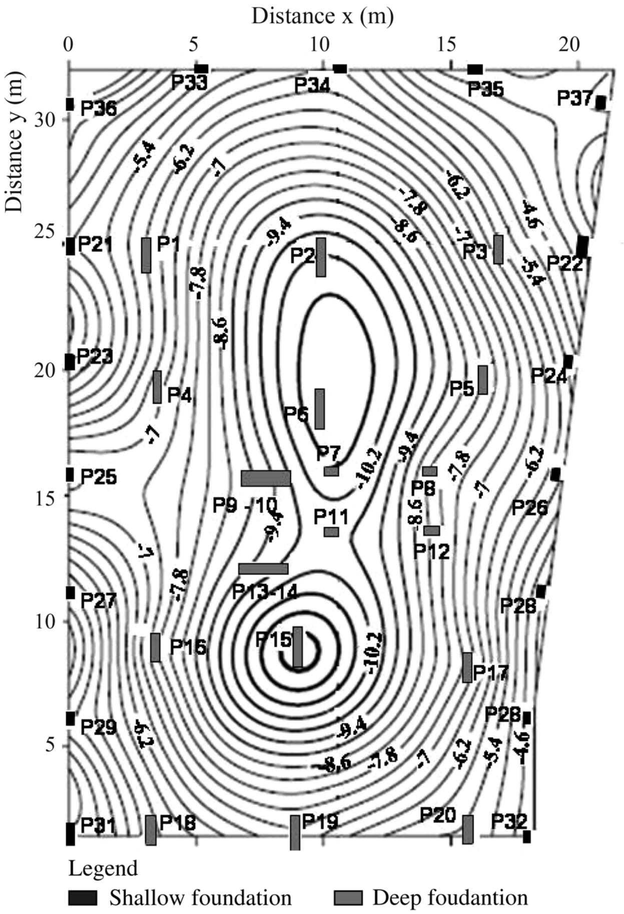

Figure 17 - Iso-settlement curve for stage 12.

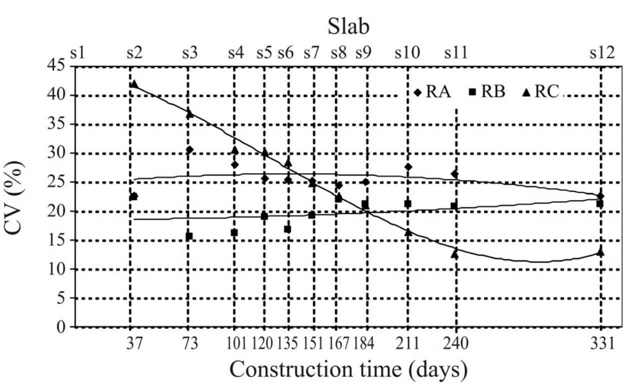

Figure 18 - Evolution of the settlement variation coefficients for regions RA, RB and RC over time of construction.

coefficient decreases over the time of construction, while the structure experiences an increase of the parameter K_e. This effect is more significant for the later stages of construction, where we have higher values of K_e. Thus, we suppose that the stiffness of the structure promotes the uniformization of settlements, as observed by Gusmão (1994), Danziger *et al.* (2000) and Gusmão (2006) in their respective research. Thus, the restriction of the structure to settlements depends on the number of floors and this dependence is more significant in the early stages of construction.

6. Conclusions

This work aimed to investigate the static soil-structure interaction mechanism. To achieve this, the behaviour of a structure which had its settlement monitored from the beginning of construction was analysed. The importance of this mechanism was demonstrated by analysing the behaviour of certain parameters, such as the redistribution of loads among columns, the spring soil coefficient and the stiffness of the structure. In general, it was found that:

• Numerical simulation of the building considering the execution of each slab and the two hypotheses, one with non-displaceable supports and other with the settlements applied to each model, was useful for evaluating the effects of settlements.

• The small settlements that occur in buildings, and which are frequently disregarded, cause disturbances in the structure, resulting in redistribution of loads among columns, with consequent greater uniformity of settlements.

• The hypothesis, often adopted in projects, which considers the support of foundations by means of a constant spring coefficient does not represent the real situation of the structure. In fact, the use of a spring coefficient in foundations must take into account not only the rigidity of the soil but also the rigidity of the structure because, according to the results obtained, these coefficients vary among the foundation elements.

• Due to the static SSI, a transfer of loads occurs from the columns which tend to settle more to those that tend to settle less. Load transfer among the columns causes a trend towards uniformization of settlements, resulting in smaller displacements than those estimated.

When observing the effects of the soil-structure interaction, it was concluded that it is of extreme importance to consider the settlements in the analysis of the structure. It is also important to include this procedure in drawing up projects in order to analyse their effects on the construction process.

Acknowledgments

The authors of this study thank UENF for the physical and academic structure that enabled them to conduct this study, and also thank CAPES for its support.

References

ABNT (1980) *Calculation of Loads* for *Building* Structures. Procedure. Standard Designation. NBR 6120, 5 pp.

ABNT (2003) Design of Concrete Structures. Procedure. Standard Designation. NBR 6118, 221 pp.

Almeida, V. (2003) Análise da Interação Solo Não-Homogêneo/Estrutura Via Acoplamento MEC MEF. Ph.D Thesis, São Carlos School of Engineering, University of São Paulo, São Carlos, 192 pp.

Aoki, N. & Cintra, J.C. (2004) Lecture Notes of the Discipline SGS-404 Foundations. Geotechnical Department, São Carlos School of Engineering, University of São Paulo, *apud* Mota *et al.* (2007).

Barros, R.A. (2005) Avaliação do Comportamento de Fundações em Estaca Hélice Através de Medidas de Recalques. Master Dissertation, Norte Fluminense State University *Darcy Ribeiro*, Rio de Janeiro, 118 pp.

Chamecki, S. (1954) Consideration of the stiffness in the calculation of settlements in foundations. Proc. I Brazilian Congress of Soil Mechanics and Foundations Engineering, Porto Alegre, v. 1, pp. 35-80; *apud* Gonçalves (2004).

Colares, G. (2006) Programa para Análise da Interação Solo-Estrutura no Projeto de Edifícios. Master Dissertation, São Carlos School of Engineering, University of São Paulo, São Carlos, 83 pp.

Crespo, V.A.S. (2004) Estudo da Sensibilidade de Edificações em Relação ao Solo. Campos dos Goytacazes. Master Dissertation, Norte Fluminense State University *Darcy Ribeiro*, Rio de Janeiro, 118 pp.

Danziger, F.A.B.; Danziger, B.R. & Crispel, F.A. (2000) A medida dos recalques desde o início da construção como um controle de qualidade das fundações. Proc. 4th Engineering Seminar of Special Foundations and Geotechnics - SEFE IV, pp. 191-202.

Gonçalves, J.C. (2004)) Avaliação da Influência dos Recalques das Fundações na Variação de Cargas dos Pilares de um Edifício. Master Dissertation, COPPE, Federal University of Rio de Janeiro, Rio de Janeiro, 126 pp.

Gonçalves, J.C.; Santa-Maria, P.E.L.; Danziger, F.A.B. & Carvalho, E.C. (2007) The influence of foundation settlements on the column loads of a building. Soils and Rocks, v. 30:3, p. 149-159.

Goshy, B. (1978) Soil-foundation-structure interaction. Journal of the Structural Division, ASCE, v. 104:ST5, p. 749-761; *apud* Gusmão (2006).

Gusmão, A.D. (1994) Aspectos relevantes da interação solo-estrutura em edificações. Revista Solos e Rochas. Solos e Rochas, v. 17:1, p. 47-55.

Gusmão, A.D. (2006) Desempenho de fundações de edifícios. Palestras XIII COBRAMSEG, Curitiba, pp. 215-240.

Gusmão, A.D. & Calado Jr., I.H. (2002) Estudo dos efeitos da interação solo estrutura em uma edificação com fundação em terreno melhorado. Proc. XII COBRAMSEG, São Paulo, ABMS, v. 3, pp. 1743-1752.

Iwamoto, R.K. (2000) Alguns Aspectos dos Efeitos da Interação Solo-Estrutura em Edifícios de Múltiplos Andares com Fundação Profunda. Master Dissertation, São Carlos School of Engineering, University of São Paulo, São Carlos, 140 pp.

Menegatti, M. (2004) A Protensão como um Conjunto de Cargas Concentradas Equivalentes. Masters Dissertation, Polytechnic School of São Paulo, University of São Paulo, São Paulo, 126 pp.

Meyerhof, G.G. (1953) Some recent foundation research and its application to design. Structural Engineer, v. 31, p. 151-167; *apud* Gusmão (1994).

Mota, M.M.C.; Pinheiro, L.M.; Aoki, N. & Mota, J.E. (2007) Método numérico para análise de edifícios com fundação profunda considerando a interação solo-estrutura. Proc. 49th Brazilian Congress in Concrete, CD-ROM, Bento Gonçalves, RS, Brazil.

Poulos, H.G. (1975) Soil-structure interaction. Proc. X ICSMFE, Stockholm, ISSMFE, v. IV, pp. 307-334; *apud* Iwamoto (2003).

Ribeiro, D. (2005) Análise da Interação Solo-Estrutura Via Acoplamento MEC MEF. Master Dissertation, São Carlos School of Engineering, University of São Paulo, São Carlos, 121 pp.

Savaris, G. (2008) Monitoração de Recalques de um Edifício e Avaliação da Interação. Masters Dissertation, Norte Fluminense State University *Darcy Ribeiro*, Rio de Janeiro, 177 pp.

Russo Neto, L.; Aoki, N. & Menegotto, M.L. (2002) Instrumento para medida de carga em pilares. Proc. XII COBRAMSEG, São Paulo, ABMS, v. 3, pp. 1785-1792.

Measurement of Drop Height and Impact Velocity in the Brazilian SPT System

E.H. Cavalcante, B.R. Danziger, F.A.B. Danziger

Abstract. The energy efficiency in SPT is generally evaluated based on the nominal drop height. Measurements of the drop height in systems different from those used in Brazil have shown that the drop height values can be significantly different from the nominal ones, inclusively in those systems where lifting-releasing operations are automatically performed. Measurements of the drop height have been carried out in a manual lifting-releasing pinweight hammer system regularly used in Brazil. The average value of the drop height was 0.79 m, with a standard deviation of 0.03 m and a coefficient of variation of 4%. Only 6 out of the 129 measured values provided drop height values smaller than 0.75 m, which is an indication of the tendency the operator has to lift the hammer above the standard height. The average potential energy error was only 5.1%. The obtained results may be attributed to the crew experience and cannot be considered typical values of Brazilian practice. However, they do represent a condition that can be achieved in practice, provided a proper operation is undertaken. Thus, it must be seen as a goal. The impact velocity of the hammer has also been evaluated from the instrumentation. The average ratio between kinetic energy and potential nominal energy (or e_1 value) was 0.74, and 0.70 if the measured potential energy is used instead of the nominal energy. An average value of 0.99 has been obtained for the energy below the anvil and kinetic energy ratio (or e_2 value).

Keywords: *in situ* testing, SPT, instrumentation, drop height, impact velocity, energy measurement.

1. Introduction

The Standard Penetration Test (SPT) is the most common in situ test performed all over the world (Décourt *et al.*, 1988). In foundation design in Brazil, it is in most cases the only available geotechnical investigation. Despite its simplicity and robustness, it is perhaps the in situ test most dependent on the attitude of the operator. A number of factors influencing the *N* value obtained from SPT has been discussed in a number of papers (*e.g.*, Fletcher, 1965; Ireland *et al.*, 1970; De Mello, 1971; Serota & Lowther, 1973; Kovacs *et al.*, 1977, 1978; Palacios, 1977; Schmertmann & Palacios, 1979; Kovacs, 1979, 1980, 1994; Kovacs & Salomone, 1982; Riggs *et al.*, 1983; Belincanta, 1985, 1998; Skempton, 1986; Belincanta & Cintra, 1998; Décourt *et al.*, 1988, 1989; Tokimatsu, 1988; Décourt, 1989; Clayton, 1990; Matsumoto *et al.*, 1992; Morgano & Liang, 1992; Teixeira, 1993; About-Matar & Goble, 1997; Aoki & Cintra, 2000; Fujita & Ohno, 2000; Cavalcante, 2002; Odebrechet, 2003; Daniel *et al.*, 2005; Youd *et al.* 2008).

Among these papers, the one by Schmertmann & Palacios (1979) has shown that the number of blows *N* varies inversely with the energy delivered to the rod stem, to *N* equal at least 50. After some discussions concerning the need of standardization and the choice of the proper energy to be used as a reference to the *N* value (*e.g.*, Kovacs & Salomone, 1982; Robertson *et al.*, 1983; Seed *et al.*, 1985; Skempton, 1986), ISSMFE (1989) has established 60% of the theoretical free fall energy (or nominal potential energy) as the international reference. Therefore the corresponding N_{60} is obtained as:

$$N_{60} = N\frac{E}{E_{60}} \quad (1)$$

where N = measured number of blows, E = energy corresponding to N and E_{60} = 60% of the theoretical free fall energy E^*, E^* = 474 J.

It must be emphasized that the potential energy E^* = 474 J mentioned in the International Reference Procedure for SPT (ISSMFE, 1989) is related to a 63.5 kgf weight hammer and a drop height of 0.76 m, while the nominal potential energy in the Brazilian Standard (ABNT, 2001) is 478.2 J, related to a 65 kg mass hammer and a drop height of 0.75 m. The difference between the potential nominal energies of the International Reference and that of the Brazilian Standard is only 1%.

Décourt (1989) and Kulhawy & Mayne (1990) have summarized the factors affecting the energy transmission from the hammer to the rods. According to Décourt (1989), the energy entering the rod stem (or enthru energy, E_i) can be obtained as

E.H. Cavalcante, Associate Professor, Departamento de Engenharia Civil, Centro de Ciências Exatas e Tecnologia, Universidade Federal de Sergipe, Campus São Cristóvão, 49100-000 São Cristóvão, SE, Brazil. e-mail: erinaldo@ufs.br.
B.R. Danziger, Associate Professor, Departamento de Estruturas e Fundações, Faculdade de Engenharia, Universidade do Estado do Rio de Janeiro, Maracanã, RJ, Brazil. e-mail: brdanzig@uerj.br.
F.A.B. Danziger, Associate Professor, COPPE and Escola Politécnica, Universidade Federal do Rio de Janeiro, 21945-000 Rio de Janeiro, RJ, Brazil. e-mail: danziger@coc.ufrj.br.
Submitted on July 19, 2010; Final Acceptance on January 27, 2011; Discussion open until April 30, 2012.

$$E_i = e_1 \times e_2 \times e_3 \times E^* \quad (2)$$

where e_1, e_2 and e_3 are efficiency (or correction) factors. The efficiency factor e_1 relates the kinetic energy just before the impact to the free fall energy and is mainly dependent on the way the hammer is lifted and released. A number of researches have been carried out on this subject (*e.g.*, Kovacs *et al.*, 1977, 1978; Kovacs, 1979, 1980; Kovacs & Salomone, 1982; Skempton, 1986; Tokimatsu, 1988; Décourt, 1989). Figure 1 summarizes the results obtained from different types of equipment.

The factor e_2 is associated to the loss of energy due to the presence of the anvil (Skempton, 1986). Décourt (1989) summarizes the main existing results (Fig. 2).

The efficiency factor e_3 is related to the rod length and e_3 values smaller than 1 have been proposed (*e.g.*, Schmertmann & Palacios, 1979; Skempton, 1986) to take into account the separation between hammer and anvil for rod lengths smaller than 10 m, due to the upcoming stress wave. However, recent research (Cavalcante, 2002; Odebrecht, 2003; Daniel *et al.*, 2005; Odebrecht *et al.*, 2005; Danziger *et al.*, 2006) has shown that a number of impacts may occur in a single blow, each impact being responsible for part of the energy delivered to the rod stem. Thus, e_3 should be taken as 1 (Fig. 3).

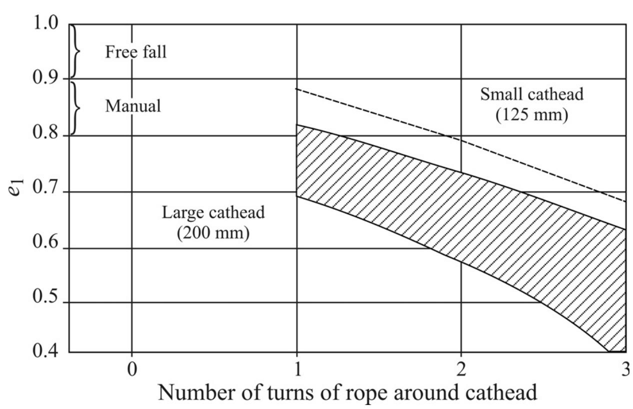

Figure 1 - Efficiency factor e_1 (adapted by Décourt, 1989 from Skempton, 1986).

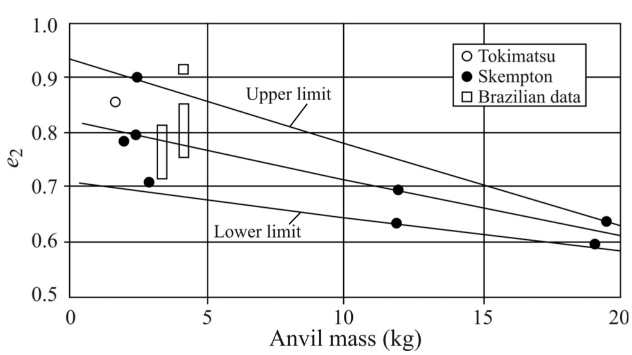

Figure 2 - Efficiency factor e_2 as a function of the anvil mass (Décourt, 1989).

Moreover, Odebrecht (2003) and Odebrecht *et al.* (2004, 2005) have shown (Fig. 4) that the potential energy resulting from the penetration ($\Delta\rho$) should be added to the nominal potential energy, which is significant in the case of soft (or loose) soils and small rod lengths.

Very few researches have measured the energy reaching the sampler, E_s, and Cavalcante *et al.* (2008) have presented results from recent researches (Fig. 5).

As shown before, the efficiency factors are related to the theoretical free fall energy, thus they are not the real ones. However, the efficiency factors are influenced by the errors associated with the non use of the real free fall energy during the test. The present paper presents a research aimed at the measurement of the potential energy of a pinweight hammer, hand lifted system commonly used in Brazil. Additionally, the impact velocity of the hammer has also been evaluated. The energy reaching the rod stem has been used to evaluate the efficiency factors based both on the theoretical free fall energy and on the measured energy as well.

2. The Free Fall Energy

The potential energy in fact used in SPT has been investigated by few researches. Riggs *et al.* (1983) gathered data from Goble & Ruchti (1981) and Kovacs *et al.* (1975) for the cathead and rope system, where two turns of rope on cathead were used. According to Riggs *et al.* (1983) the research from Goble & Ruchti (1981) involved the measurement of the impact velocity and the height of the hammer fall in more than 1500 blows. Fifteen experienced operators controlling various types of equipment participated in the

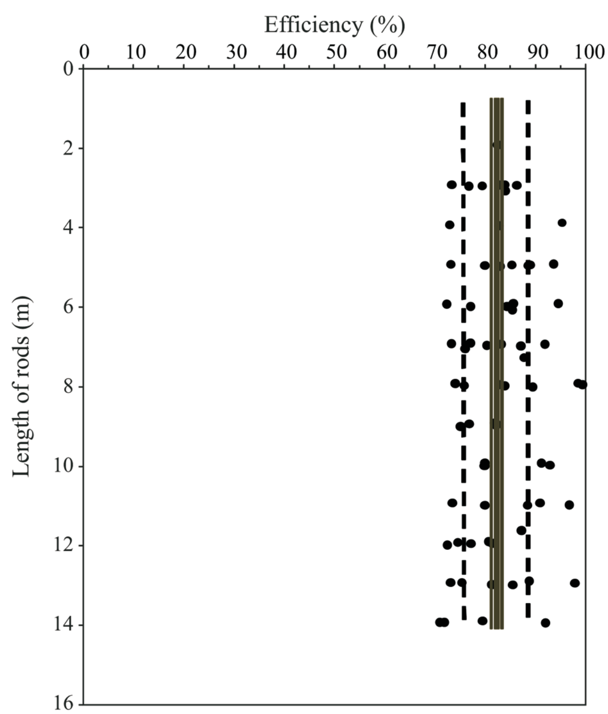

Figure 3 - Efficiency *vs.* rod length (adapted from Cavalcante, 2002; Cavalcante *et al.*, 2004).

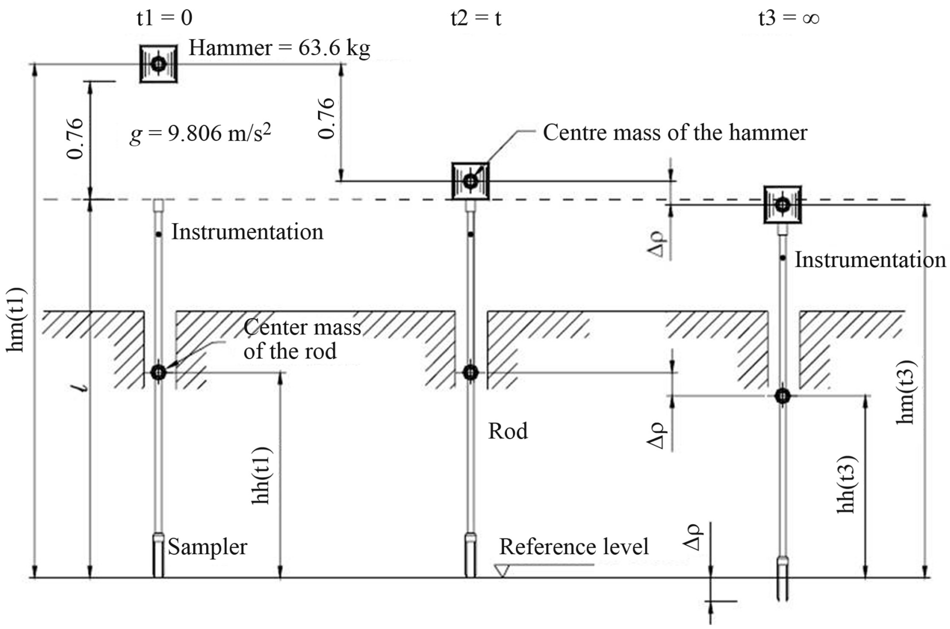

Figure 4 - Potential energy at different stages of the standard penetration test (Odebrecht, 2003; Odebrecht *et al.*, 2004, 2005).

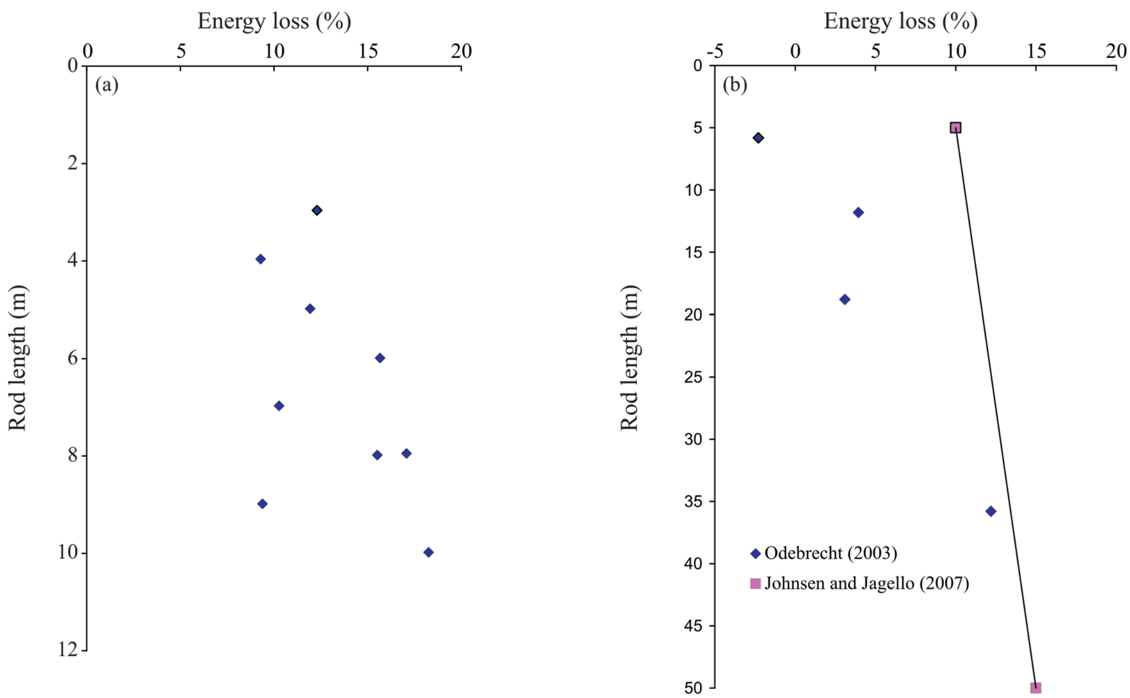

Figure 5 - Energy loss, $(E_i - E_s)/E_i$, *vs.* rod length. (a) Cavalcante *et al.* (2008), data from Cavalcante (2002); (b) Cavalcante *et al.* (2008), data from Odebrecht (2003) and general trend from Johnsen & Jagello (2007).

research. The results have shown that all the operators lifted the hammer higher than the standard 0.762 m, the average measured hammer fall being 0.817 m. The average efficiency taken from the measured impact velocity and the nominal (standard) hammer fall height was 86%. If the average efficiency had been related to the measured hammer fall height its value would have been naturally smaller. Figure 6 summarizes data obtained from Goble & Ruchti (1981) and Kovacs *et al.* (1975).

Even for the case of automatic hammers, some problems may arise on the mechanism of lifting and releasing the hammer, so that significant variations on the fall height may also occur. Kovacs (1979), for instance, presented some data from a Borros automatic free fall hammer that re-

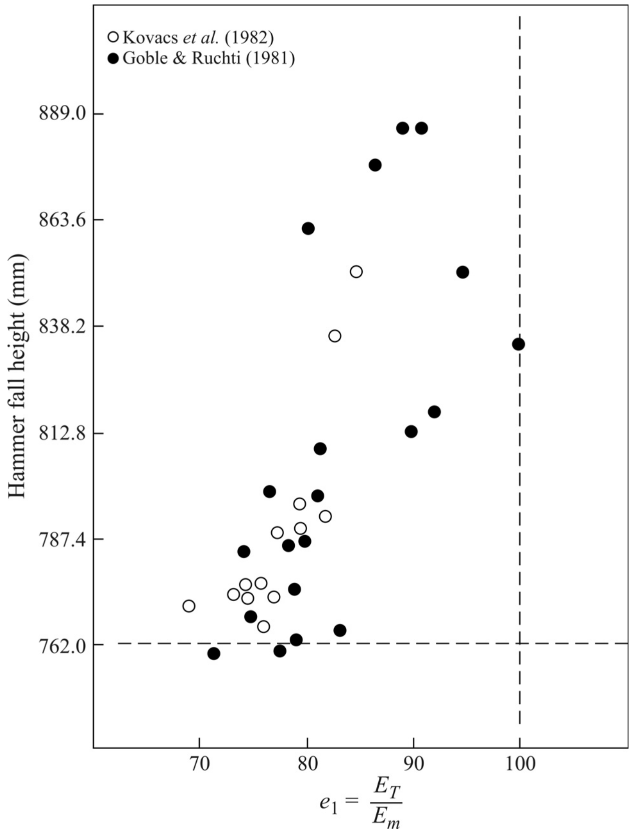

Figure 6 - Hammer fall height *vs.* efficiency, data from Goble & Ruchti (1981) and Kovacs *et al.* (1982) collected by Riggs *et al.* (1983).

vealed an increase in fall height when submitted to blow velocities greater than 15 blows per minute (Fig. 7).

Farrar & Chitwood (1999) have also shown that the hammer drop height is dependent on the blow count rate on an automatic hammer manufactured by the Central Mine Equipment Company (CME), as shown in Figure 8. In fact, the hammer drop height increases with the blow count rate. It must be pointed out that those authors have mentioned that the rate required to develop a 760 mm (30-inch) drop using the CME hammer is 50 to 55 blows per minute, and all drills are adjusted at the factory to provide the recommended rate. However, with time, these settings may change and should be checked. Farrar & Chitwood (1999) emphasized that if the operator fails to properly adjust the mechanical system that provides the rate, the SPT will be invalid unless the rate is recorded.

The first automatic SPT riggs have been recently introduced in Brazil (see *e.g.*, Hachich *et al.*, 2006), and a proper check of the hammer drop height is therefore very important.

3. Measurements of Hammer Impact Velocity

The systems used for measuring impact velocity in SPT hammers are based on: (i) scanners focalizing a series

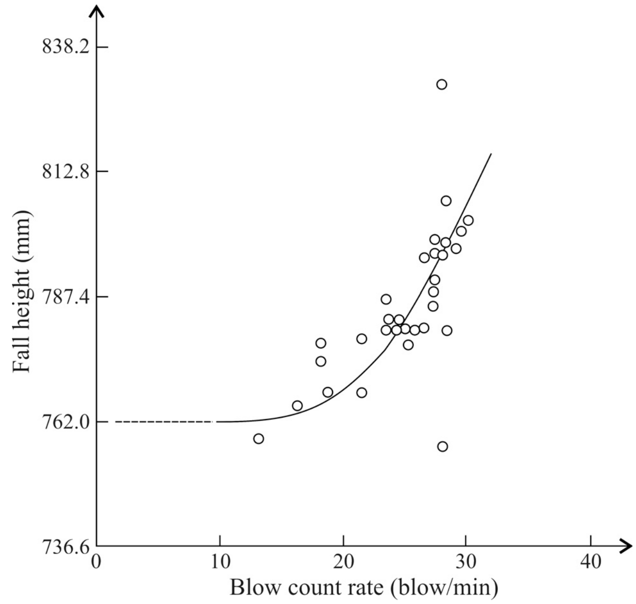

Figure 7 - Increase in fall height with blow velocity for automatic Borros free fall hammer (Kovacs, 1979).

of reflective light strips strategically positioned at the hammer (Kovacs *et al.*, 1977, 1978; Kovacs, 1979; Kovacs *et al.*, 1981; Kovacs & Salomone, 1982); (ii) generation of an electrical pulse in parallel wires spaced by a known distance that records the hammer passage and the elapsed time during the known course (Matsumoto *et al.*, 1992); (iii) more recently, the use of radar technology with a record system based on Doppler effect (Morgano & Liang, 1992; Abou-Matar & Goble, 1997).

Figure 9 shows details of the hammer impact velocity recording system with the use of scanners and reflective light strips of contrasting colors (black and white) put on donut hammer model (Kovacs *et al.*, 1978, 1981).

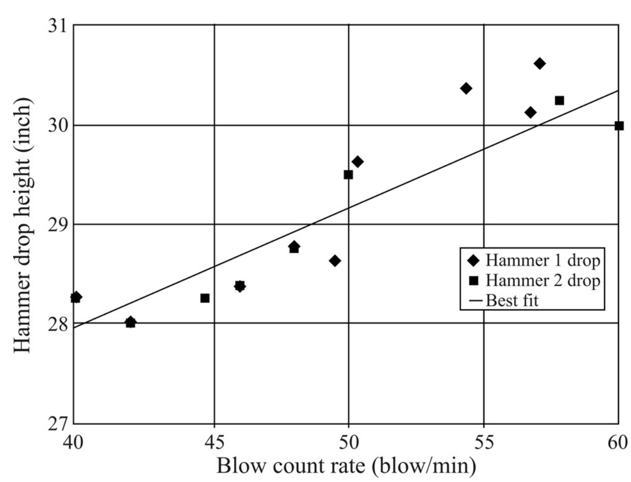

Figure 8 - Increase in fall height with blow velocity for automatic CME hammer (Farrar & Chitwood, 1999).

4. Tests Performed

SPTs have been instrumented at the district of Lapa, Rio de Janeiro, aiming at the measurement of the SPT efficiency considering both the nominal drop height and the measured values. Impact velocities have been measured in addition to the drop height. The energy just below the anvil (weight of 13 N) has been measured with a SPT Analyzer system.

A very experienced sounding crew composed of a 50 year-experience chief-operator and 2 auxiliary-operators were in charge of the SPT system.

A total of 129 hammer blows have been analyzed in 3 depths, ranging from nominal depths of 23 m to 25 m. Energy measurements below the anvil have been carried out in 96 blows. The soil nature at the tested depths consisted of a residual sand from weathered gneiss. Table 1 summarizes the measurements performed.

4.1. Drop height and impact velocity measurement system

The drop height has been measured by an equipment consisting of:

(i) a wood ruler, fixed in the rods in a way that the beginning of the scale coincided with the anvil top (Fig. 10);

(ii) an Invar ruler, manually held during the tests;

(iii) a metallic pointer, fixed at the base of the hammer, to provide a better reference for the measurements (Fig. 11);

(iv) a camera capable of filming at a speed of 30 pictures per second, placed at a level and at a distance able to properly record the blows (Fig. 12);

(v) additionally, one of the accelerometers used in connection with the energy measurements below the anvil was fixed in the hammer (Fig. 11).

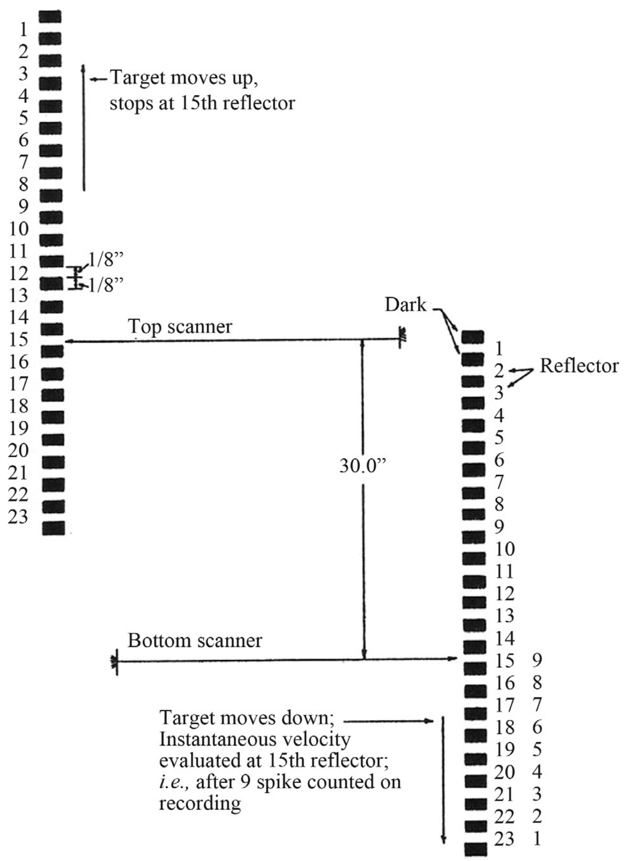

Figure 9 - Details of the reflective light strips used for the scanners to record the hammer impact velocity (Kovacs *et al.*, 1978).

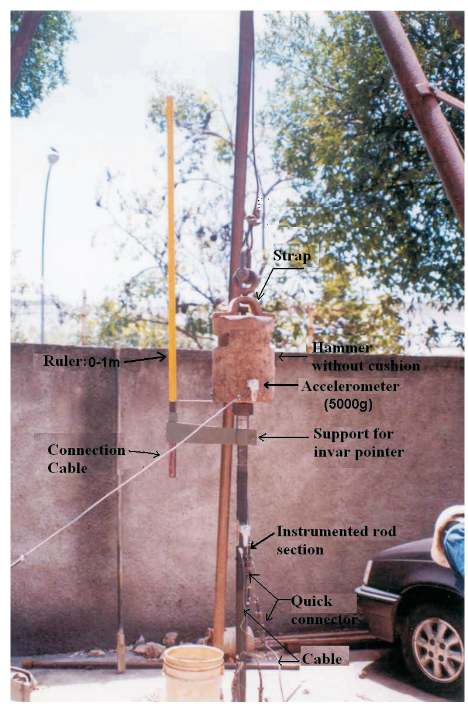

Figure 10 - Instrumentation used to measure drop height and impact velocity.

Table 1 - Measurements performed.

Nominal depth (m)	N	Rod length (m)	Number of filmed blows	Energy measured below the anvil
23	27	25.39	22	No
24	46	25.67	57	Yes
25	-*	26.80	50	Yes

*50 blows have been able to penetrate only 26 cm.

The blows have been filmed during both the operations of lifting and releasing the hammer (Figs. 13 and 14). The images have been analyzed by means of a cassette video and a video monitor. The speed of the camera has allowed an accurate definition of the drop height, *i.e.*, with the use of the commands “slow motion” and “pause” it has been possible to properly define the maximum height the hammer was lifted, following successive pictures with intervals of 0.033 s.

However, the camera speed did not allow to get the proper definition of the impact velocity. In fact, at the beginning of the releasing process, it was possible to get sharp images of successive pictures. However, as the rate increased, it was no longer possible to get the proper definition of 2 successive pictures, so from a certain time the drop rate could not be properly measured. Another method was then used to estimate the impact velocity. The drop height was divided in 3 sections, and both elapsed time and length in each section have been recorded. It has been assumed a linear velocity in each section, which corresponds to a constant acceleration. The initial velocity of each interval was taken as the final velocity of the previous interval, and the impact velocity was taken as the final velocity of the third section. An example of the obtained values is presented in Table 2 (see also Fig. 15).

In order to check the errors due to the assumed hypothesis, hammer equilibrium has been considered (Fig. 16), and Eq. (3) can be written

$$mg - F_{at} = m\frac{dv}{dt} = m\frac{d^2s}{dt^2} \tag{3}$$

where m = hammer mass, g = gravity acceleration, v = hammer velocity, s = covered distance (from hammer release), t = time (from hammer release) and F_{at} represents both the friction between the hammer guide and the anvil/rod (F_1) and also the force acting at the hammer top due to friction at the pulley (F_2).

If any friction effect is disregarded, a free fall condition is achieved, and $s = f(t)$ is a second degree equation. If F_{at} is not constant then $s = f(t)$ will be a polynomial with a degree higher than 2, and a 4th degree polynomial has been assumed as an approximation, according to Eq. (4).

$$s(t) = s_0 + s_1 t + s_2 t^2 + s_3 t^3 + s_4 t^4 \tag{4}$$

As doing so, one should arrive at a more approximate response of the event. Using the boundary conditions $s = 0$

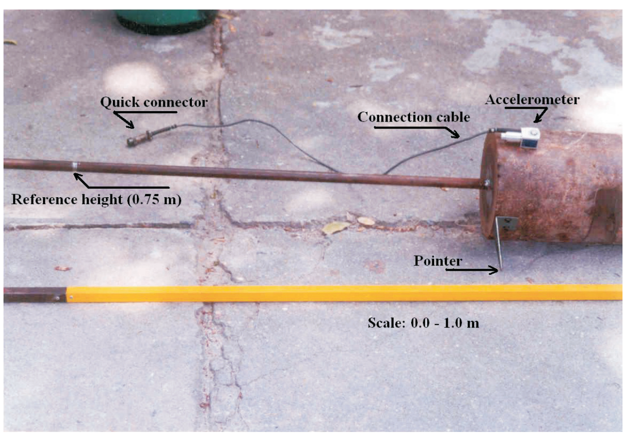

Figure 11 - Detail of the hammer, guide and part of instrumentation used to measure drop height and impact velocity.

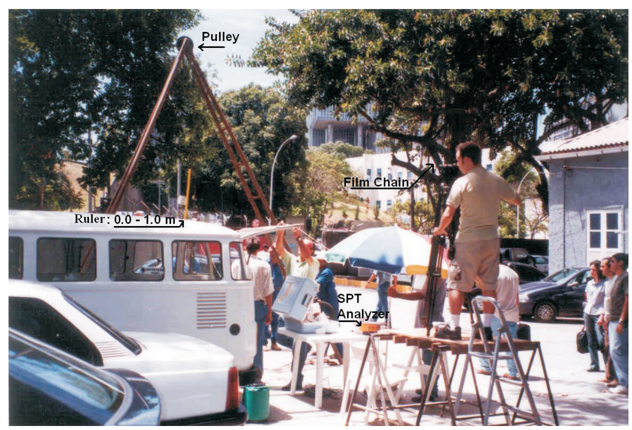

Figure 12 - System used to evaluate drop height, impact velocity and energy below the anvil.

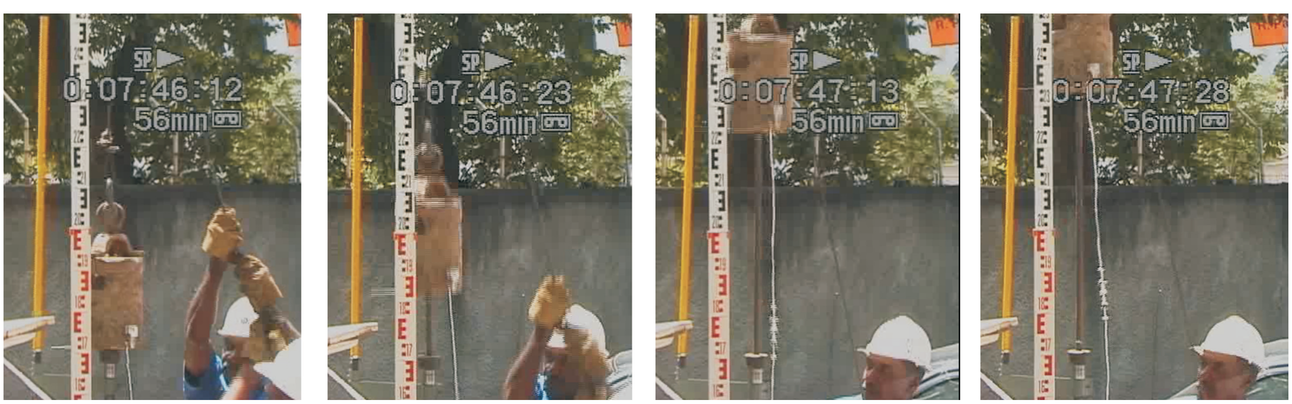

Figure 13 - Video frames during hammer lift.

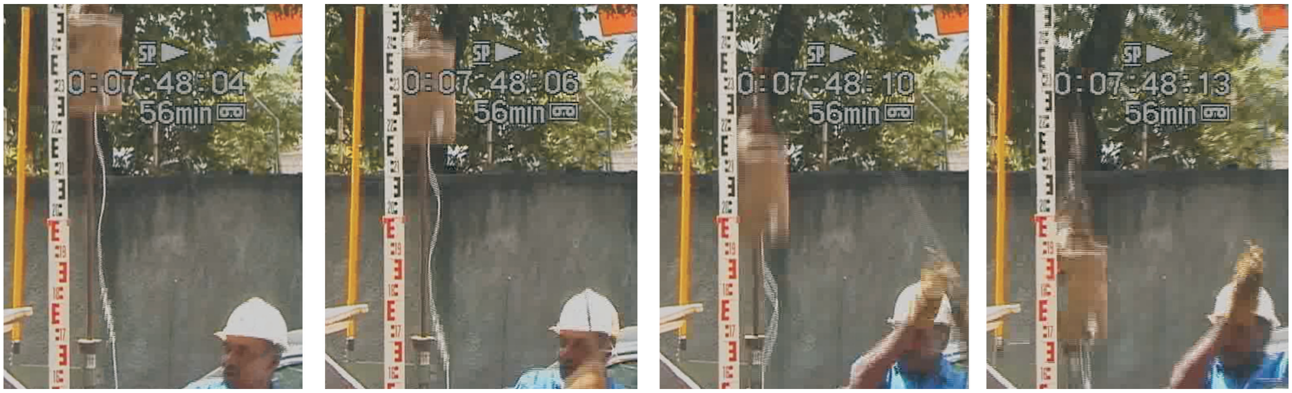

Figure 14 - Video frames during hammer fall.

Table 2 - Example of calculation of impact velocity.

Section	Length, Δh (m)	Elapsed time, Δt (s)	Initial velocity (m/s)	Final velocity (m/s)
1	0.15	0.23	0	1.30
2	0.21	0.13	1.30	1.93
3	0.44	0.17	1.93	3.25*

*Impact velocity.

for $t = 0$ and $v = 0$ for $t = 0$ the values $s_o = 0$ and $s_1 = 0$ can be respectively obtained. Thus, Eq. (4) can be simplified to

$$s(t) = s_2 t^2 + s_3 t^3 + s_4 t^4 \quad (5)$$

The use of Eq. (5) for each one of the 3 sections provides a system of 3 equations and 3 unknowns. The values included in Table 2 provide the equation

$$s(t) = 3.175t^2 - 2.141t^3 + 2.874t^4 \quad (6)$$

The velocity can then be obtained as

$$v(t) = 6.350t - 6.422t^2 + 11.496t^3 \quad (7)$$

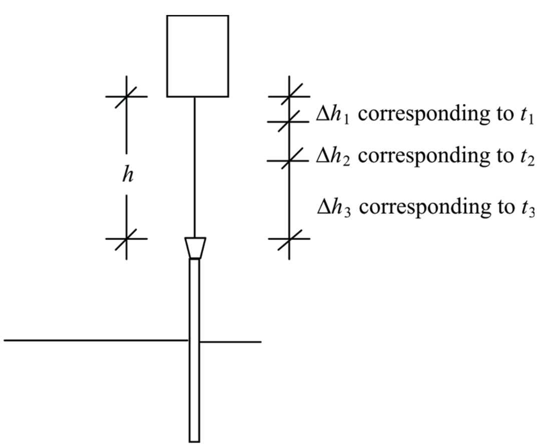

Figure 15 - Measured values used to evaluate the impact velocity.

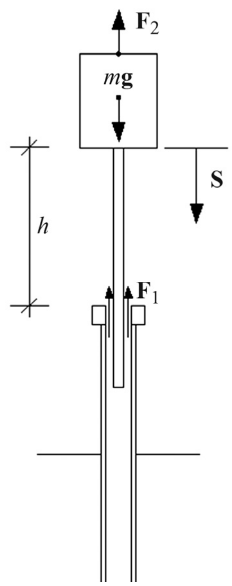

Figure 16 - Friction during hammer fall.

Eq. (7) provides the values included in Table 3, which also includes the values from the linear hypothesis (in each interval) assumption. The differences between both hypotheses are also included in the table.

As expected, the difference between both hypotheses decreases as time increases, *i.e.*, the velocity is closer to a linear behaviour approaching impact.

Table 3 - Hammer impact velocities.

t (s)	v (m/s)		Difference (%)
	Assuming linear variation in each interval	Assuming 4th degree equation for $s = f(t)$	
0.23	1.30	1.26	+3.2
0.36	1.93	1.99	-3.0
0.53	3.25*	3.27*	-0.6

*Impact velocity.

The SPT Analyzer system used to measure the energy just below the anvil has been tentatively used to measure the impact velocity, by fixing one accelerometer in the hammer, as mentioned in the previous section (see Fig. 11). However, owing to the longer interval of the fall height, nearly 400 ms, compared to the maximum time allowed by the SPT Analyzer system, 102.4 ms, it has not been possible to record the impact hammer velocity.

4.2. Test results

The histograms of drop height measured values (h) are shown in Figs. 17, 18 and 19, respectively for the 23 m, 24 m and 25 m nominal depths. The average values are included in Table 4. The corresponding values of potential energy ($E_{pot,\ meas}$) are also included in the table.

The average drop height for the 23 m nominal depth is 0.78 m, associated with a small standard deviation of 0.01 m and a coefficient of variation of 1.7%. In no case has the hammer been released at a drop height lower than 0.75 m. It must be taken into account that the first series of measurements deserved a very special attention of the crew as far as the use of the correct drop height is concerned. Due to the small difference of the drop height with respect to the nominal one, the average potential energy error was only 4.5%.

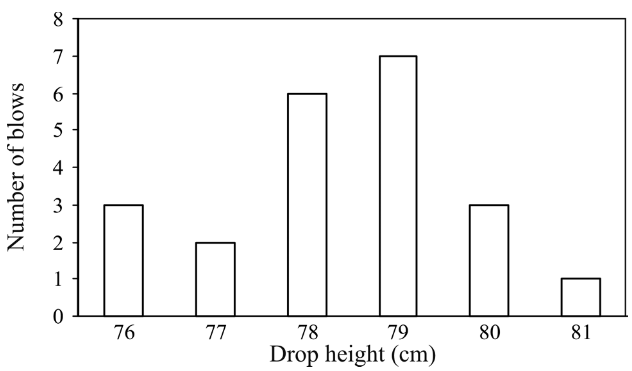

Figure 17 - Drop height values measured at 23 m nominal depth.

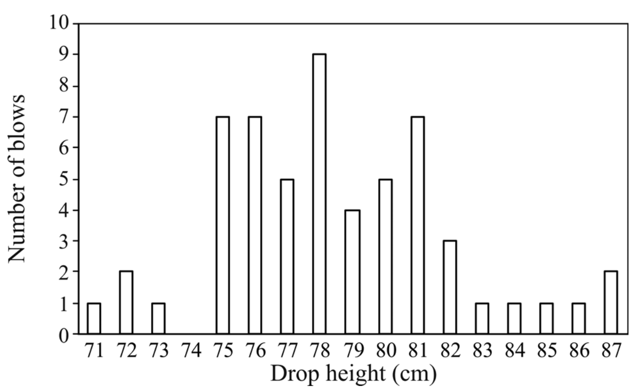

Figure 18 - Drop height values measured at 24 m nominal depth.

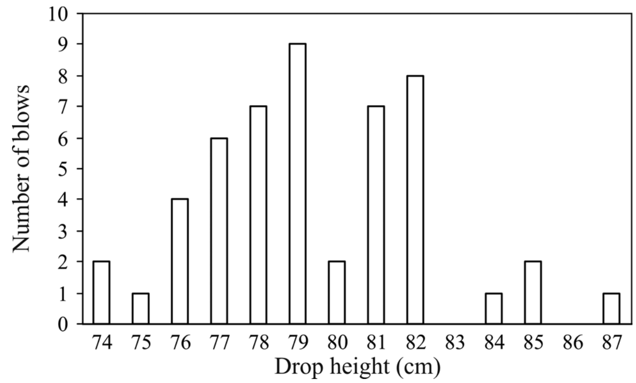

Figure 19 - Drop height values measured at 25 m nominal depth.

Similar results have been obtained for the other nominal depths (24 m and 25 m). However, the crew was asked to behave more naturally during the second and third series of measurements. As a consequence, the standard deviation and the coefficient of variation were higher at those depths (see Table 4).

If all data is now analyzed, the average value of the drop height is 0.79 m, with a standard deviation of 0.03 m and a coefficient of variation of 4%. Only 6 out of the 129 measured values provided drop height values smaller than 0.75 m, which is indeed an indication of the tendency the operator has to lift the hammer above the standard height, as shown previously for other SPT systems, as shown *e.g.* by Riggs *et al.* (1983), see Fig. 6.

The average potential energy error was only 5.1%. The very good results obtained may be attributed to the crew experience and cannot be considered typical values of Brazilian practice. However, they do represent a condition that can be achieved in practice, provided a proper operation is undertaken. Thus, it must be seen as a goal.

The average values of impact velocity (v_{imp}) and the corresponding values of kinetic energy (E_{kin}) are included in Table 5.

As a consequence of the smaller scatter of the drop height at the nominal depth of 23 m, there was a smaller scatter of the impact velocity data with respect to the other depths, as can be seen in Table 5.

The average impact velocity was 3.29 m/s, indicating a loss compared to the nominal value ($v_{imp} = \sqrt{2gh}$, h = 0.75 m) of 14.2%. If one now considers the average measured drop height value of 0.79 m, the loss in velocity is 16.4%. As the kinetic energy takes the square of the velocity, the average ratio between kinetic energy and potential nominal energy, $E_{pot,\ nom}$ (or e_1 value) is 0.74; if the measured potential energy is used, the obtained value is even smaller, about 0.70 (see Table 5). Those values are smaller than the ones included in Fig. 1, suggested by Décourt (1989).

Besides the evaluation of drop height and impact velocity, the energy below the anvil has also been measured at the nominal depths of 24 m and 25 m with a SPT Analyzer

Table 4 - Summary of drop height measurements.

Nominal depth (m)	Number of blows	h (m)	Standard dev. (m)	Coef. var.	$E_{pot,\ meas}$ (J)	$E_{pot,\ meas}$ error*(%)
23	22	0.78	0.01	1.7%	499.69	4.5
24	57	0.78	0.04	4.5%	500.39	4.6
25	50	0.79	0.03	3.5%	506.29	5.9
Whole data	129	0.79	0.03	3.8%	502.56	5.1

*with respect to the nominal value of 478.24 J.

system, and accelerometers and force transducers (strain-gauge based) have been used. Details of the energy measurement have been presented by *e.g.*, Cavalcante (2002), Cavalcante *et al.* (2003; 2004). The average energy values (*EFV*) are included in Table 6. Those values are lower than the ones obtained in other places in the same research, although in smaller depths (Cavalcante, 2002; Cavalcante *et al.*, 2004). In fact, those values do represent an energy ratio $EFV/E_{pot,nom}$ of 73%, smaller than the average of those other depths (see Fig. 3), with an average ratio of 0.82.

If the measured potential energy is used rather than the nominal one, *i.e.*, if one considers the energy ratio $EFV/E_{pot,meas}$, an even smaller value, 0.70, is obtained (see Table 6).

The most plausible explanation for the smaller energy ratio in the data herein reported is that smaller drop height values have been used only in the tests herein reported, due to the crew experience. Since drop height values have not been measured in the other mentioned tests, more research is needed relating the average ratio with the potential energy indeed used in the tests.

When the EFV/E_{kin} average ratio is analyzed, it can be observed that it is very close to 1, indicating a value of e_2 around 1. This value is higher than the range suggested by Décourt (1989), included in Fig. 2. In various blows the energy measured below the anvil was greater than the kinetic energy, a fact that seems inconsistent, even considering any increase of the potential energy suggested by Odebreht (2003). This has been attributed to the scatter related to the impact velocity measurements. However, the average values have shown clearly the trend of EFV/E_{kin} to be around 1, as mentioned.

5. Conclusions

Drop height and impact velocity have been measured in 129 blows in 3 nominal depths in SPTs performed in Rio de Janeiro. The first series of measurements (23 m nominal depth) deserved a very special attention of the crew as far as the use of the correct drop height is concerned, and the average drop height was 0.78 m, associated with a small standard deviation of 0.01 m and a coefficient of variation of 1.7%. In no case has the hammer been released at a drop height lower than the Brazilian standard 0.75 m. The average potential energy error was only 4.5%. The crew was asked to behave more naturally during the second and third series of measurements, and although the average drop height was only 0.01 m greater (0.79 m), the standard deviation and the coefficient of variation were higher. If the whole data is now analyzed, the average value of the drop height was 0.79 m, with a standard deviation of 0.03 m and a coefficient of variation of 4%. Only 6 out of the 129 measured values provided drop height values smaller than 0.75 m, which is indeed an indication of the tendency the operator has to lift the hammer above the standard height,

Table 5 - Summary of impact velocity measurements.

Nominal depth (m)	Number of blows	v_{impact} (m/s)	Standard dev. (m/s)	Coef. var.	E_{kin} (J)	$E_{kin}/E_{pot,\ nom}$ (%)	$E_{kin}/E_{pot,\ meas}$ (%)
23	21	3.29	0.24	7.4%	354.61	0.74	0.71
24	57	3.23	0.33	10.1%	342.44	0.72	0.68
25	50	3.35	0.29	8.7%	366.36	0.77	0.72
Whole data	128	3.29	0.30	9.3%	353.78	0.74	0.70

Table 6 - Summary of energy below the anvil measurements.

Nominal depth (m)	Number of blows	*EFV* (J)	Standard dev. (J)	Coef. var.	EFV/E_{kin}*	$EFV/E_{pot,\ nom}$	$EFV/E_{pot,\ meas}$
24	53	348.96	26.54	7.6%	1.02	0.73	0.70
25	45	348.85	20.48	5.9%	0.95	0.73	0.70
Whole data	98	348.91	23.95	6.9%	0.99	0.73	0.70

as shown for other SPT systems. The average potential energy error was only 5.1%. The very good results obtained may be attributed to the crew experience and cannot be considered typical values of Brazilian practice. However, they do represent a condition that can be achieved in practice, provided a proper operation is undertaken. Thus, it must be seen as a goal.

The average impact velocity was 3.29 m/s, indicating a loss compared to the nominal value of 14.2%. If the average measured drop height value of 0.79 m is considered, the loss in velocity is 16.4%. The average ratio between kinetic energy and potential nominal energy (or e_1 value) is 0.74; if the measured potential energy is used, the obtained value is even smaller, about 0.70.

The energy below the anvil has also been measured at the nominal depths of 24 m and 25 m. An average energy ratio of 73% has been obtained, if the potential nominal energy is considered (as the usual procedure). If the measured energy is considered, instead of the nominal one, an average energy ratio of 70% is obtained. Those values are smaller than the ones obtained in other places in the same research (Cavalcante, 2002; Cavalcante *et al.*, 2004). The most plausible explanation for the smaller energy ratio in the data herein reported is that smaller drop height values have been used only in the tests herein reported, due to the crew experience. Since drop height values have not been measured in the other mentioned tests, more research is needed in order to properly relate the average energy ratio below the anvil to the potential energy indeed used in the tests.

An average value very close to 1 (0.99) has been obtained for the EFV/E_{kin} ratio (or e_2 value).

Acknowledgments

The SPT Analyzer was purchased with financial support from Fundação Universitária José Bonifácio (FUJB) under Prof. Dirceu Velloso administration. The senior author received a PhD scholarship from the Brazilian Research Council, CNPq. Tengel Técnica de Engenharia Ltda., performed the SPTs and provided assistance for the measurements.

References

ABNT (2001) Solo - Sondagens de Simples Reconhecimento com SPT - Método de Ensaio, NBR 6484, 17 pp.

Abou-Matar, H. & Goble, G.G. (1997) SPT Dynamic Analysis and Measurements. Journal of Geotechnical and Geoenvironmental Engineering, ASCE, v. 123:10, p. 921-928.

Aoki, N. & Cintra, J.C.A. (2000) The application of energy conservation Hamilton's Principle to the determination of energy efficiency in SPT tests. Proc. 6th Int. Conf. on the Application of the Stress-Wave Theory to Piles, São Paulo, v. 1, pp. 457-460.

Belincanta, A. (1985) Energia Dinâmica no SPT - Resultados de uma Investigação Teórico-Experimental. MSc Thesis, Escola Politécnica, Universidade de São Paulo, São Paulo, 217 pp.

Belincanta, A. (1998) Avaliação de Fatores Intervenientes no Índice de Resistência à Penetração do SPT. DSc Thesis, Escola Politécnica, Universidade de São Paulo, São Paulo, 141 pp.

Belincanta, A. & Cintra, J.C.A. (1998) Avaliação de fatores intervenientes no índice de resistência à penetração do SPT. Soils and Rocks, v. 21:3, p. 36-40.

Cavalcante, E.H. (2002) Investigação Teórico-Experimental sobre o SPT. DSc Thesis, Universidade Federal do Rio de Janeiro, Rio de Janeiro, 430 pp.

Cavalcante, E.H.; Danziger, F.A.B. & Bezerra, R.L. (2003) Recent experience on SPT instrumentation in Brazil. Proc. 12th Panamerican Conference on Soil Mechanics and Geotechnical Engineering, Cambridge, v. 1, pp. 423-428.

Cavalcante, E.H.; Danziger, F.A.B. & Danziger, B.R. (2004) Estimating the SPT penetration resistance from rod penetration based on instrumentation. Proc. 2nd Conference on Site Characterization - Geotechnical and Geophysical Site Characterization, Milpress Netherlands, v. 1, pp. 293-298.

Cavalcante, E.H.; Danziger, B.R. & Danziger, F.A.B. (2008) On the energy reaching the sampler during SPT. Proc. 8th International Conference on the Application of Stress-Wave Theory to Piles, Lisbon, v. 1, pp. 737-742.

Clayton, C.R.I. (1990) SPT energy transmission: Theory, measurement and significance. Ground Engineering, v. 23:10, p. 35-43.

Daniel, C.R.; Howie, J.A.; Jackson, R.S. & Walker, B. (2005) Review of standard penetration test short rod corrections. Journal of Geotechnical and Geoenvironmental Engineering, ASCE, v. 131:4, p. 489-497.

Danziger, F.A.B.; Danziger, B.R. & Cavalcante, E.H. (2006) Discussion of Review of Standard penetration test short rod corrections, by Chris R. Daniel, John A. Howie, R. Scott Jackson, and Brian Walker. Journal of Geotechnical and Geoenvironmental Engineering, ASCE, v. 132:12, p. 1634-1637.

Décourt, L. (1989) The standard penetration test - State-of-the-art report. Proc. 12th Int. Conference on Soil Mechanics and Foundation Engineering, Rio de Janeiro, v. 4, pp. 2405-2416.

Décourt, L.; Muromachi, T.; Nixon, I.K.; Schmertmann, J.H.; Thorburn, S. & Zolkov, E. (1988) Standard Penetration Test (SPT): International reference test procedure. Proc. of the ISSMFE Technical Committee on Penetration Testing - SPT Working Party, ISOPT I, Orlando, v. 1, pp. 3-26.

Décourt, L.; Belincanta, A. & Quaresma Filho, A.R. (1989) Brazilian experience on SPT, supplementary contributions by the Brazilian Society of Soil Mechanics. Proc.

12th Int. Conf. on Soil Mechanics and Foundation Engineering, Rio de Janeiro, pp. 49-54.

De Mello, V.F.B. (1971) Standard penetration test. Proc. of the 4th Panamerican Conference on Soil Mechanics and Foundation Engineering, Porto Rico, v. l, pp. 1-86.

Farrar, J.A. & Chitwood, D. (1999) CME Automatic Hammer. Operations Bulletin DSO-99-03, Earth Sciences and Research Laboratory, U.S. Department of the Interior, Bureau of Reclamation.

Fletcher, G.F.A. (1965) Standard penetration test: Its uses and abuses. Journal of the Soil Mechanics and Foundations Division, ASCE, v. 91:SM4, p. 67-75.

Fujita, K. & Ohno, M. (2000) Stress wave application to standard penetration test in Japan. Proc. 6th Int. Conference on the Application of Stress-Wave Theory to Piles, São Paulo, v. 1, pp. 469-475.

Goble, G.G. & Ruchti, P. (1981) Measurements of Impact Velocity on Penetration Testing Systems. Report, Department of Civil, Environmental and Architectural Engineering, University of Colorado, Boulder.

Hachich, W.; Villefort, L.F.C.B. & Schmidt, C.F. (2006) Comparação de N_{SPT} entre os processos manual e mecanizado. Anais do XIII COBRAMSEG, Curitiba, v. 2, pp. 613-618.

Ireland, H.O.; Moretto, O. & Vargas, M. (1970) The dynamic penetration test: A standard that is not standardized. Géotechnique, v. 20:2, p. 185-192.

ISSMFE (1989) International reference test procedure for the standard penetration test (SPT). Report of the ISSMFE-TC 16 - Technical Committee on Penetration Testing of Soils, with Reference Test Procedures - CPT- SPT - DP - WST, pp. 17-19.

Johnsen, L.F. & Jagello, J.J. (2007) Discussion of Energy efficiency for standard penetration tests, by Edgar Odebrecht, Fernando Schnaid, Marcelo Maia Rocha and George de Paula Bernardes. Journal of Geotechnical and Geoenvironmental Engineering, ASCE, v. 133:4, p. 486-487.

Kovacs, W.D. (1979) Velocity measurement of free-fall SPT hammer. Journal of the Soil Mechanics and Foundations Division, ASCE, v.105:GT1, p. 1-10.

Kovacs, W.D. (1980) What constitutes a turn? Geotechnical Testing Journal, ASTM, v. 3:3, p. 127-130.

Kovacs, W.D. (1994) Effects of SPT equipment and procedures on the design of shallow foundations on sand. Proc. Settlement'94, ASCE, New York: v. 1, pp. 121-131.

Kovacs, W.D.; Evans, J.C. & Griffith, A.H. (1977) Towards a more standardized SPT. Proc. 9th International Conference on Soil Mechanics and Foundation Engineering, Tokyo, v. 2, pp. 269-276.

Kovacs, W.D.; Evans, J.C. & Griffith, A.W. (1975) A Comparative Investigation of the Mobile Drilling Company's Safe-T-Driver with the Standard Cathead with Manila Rope for the Performance of the Standard Penetration Test. Report of the Geotechnical Engineering, Purdue University, W. Lafayette, 127 pp.

Kovacs, W.D.; Griffith, A.W. & Evans, J.C. (1978) An alternative to the cathead and rope for the standard penetration test. Geotechnical Testing Journal, ASTM, v. 1:2, p. 72-81.

Kovacs, W.D. & Salomone, L.A. (1982) SPT hammer energy measurement. Journal of the Soil Mechanics and Foundations Division, ASCE, v. 108:GT4, p. 599-620.

Kovacs, W.D.; Salomone, L.A. & Yokel, F.Y. (1981) Energy Measurement in the Standard Penetration Test. NBS Building Science Series 135, National Bureau of Standards, Washington, DC.

Kulhawy, F.H. & Mayne, P.W. (1990) Manual on Estimating Soil Properties for Foundation Design. Prepared by Cornell University for Electric Power Research Institute.

Matsumoto, T.; Sikigushi, H. & Yoshida, H. (1992) Significance of two point strain measurement in SPT. Soils and Foundations, v. 32:2, p. 67-82.

Morgano, C.M. & Liang, R. (1992) Energy transfer in SPT - Rod length effect. Proc. 4th International Conference on the Application of Stress-Wave Theory to Piles, Netherlands, v. 1, pp. 121-127.

Odebrecht, E. (2003) Medidas de Energia no Ensaio do SPT. DSc Thesis, Universidade Federal do Rio Grande do Sul, 230 pp.

Odebrecht, E.; Schnaid, F.; Rocha, M.M. & Bernardes, G.P. (2004) Transferência de energia no ensaio SPT: Efeito do comprimento de hastes e da magnitude dos deslocamentos. Solos e Rochas, v. 27:1, p. 69-82.

Odebrecht, E.; Schnaid, F.; Rocha, M.M.& Bernardes, G.P. (2005) Energy efficiency for standard penetration tests. Journal of Geotechnical and Geoenvironmental Engineering, ASCE, v. 131:10, p. 1252-1263.

Palacios, A. (1977) Theory and Measurements of Energy Transfer During Standard Penetration Test Sampling. Ph.D Thesis, University of Florida, Gainesville, 391 pp.

Riggs, C.O.; Schmidt, O.N. & Rassieur, C.L. (1983) Reproducible SPT hammer impact force with an automatic free fall SPT hammer system. Geotechnical Testing Journal, ASTM, v. 6:3, p. 201-209.

Robertson, P.K.; Campanella, R.G. & Wightman, A. (1983) SPT-CPT correlations. Journal of Geotechnical Engineering, ASCE, v. 109:11, p. 1449-1459.

Schmertman, J.H. & Palacios, A. (1979) Energy dynamics of SPT. Journal of the Soil Mechanics and Foundations Division, ASCE, v. 105:GT8, p. 909-926.

Seed, H.B.; Tokimatsu, K.; Harder, L.F. & Chung, R.M. (1985) Influence of SPT procedures in soil liquefaction resistance evaluations. Journal of Geotechnical Engineering, ASCE, v. 111:12, p. 1425-1445.

Serota, S. & Lowther, G. (1973) SPT practice meets critical review. Ground Engineering, v. 6:1, p. 20-22.

Skempton, A.W. (1986) Standard penetration test procedures and the effects in sands of overburden pressure, relative density, particle size, aging and overconsolidation. Géotechnique, v. 36:3, p. 425-447.

Teixeira, A.H. (1993) Um Aperfeiçoamento das Sondagens de Simples Reconhecimento à Percussão. Solos do Interior de São Paulo, ABMS-NRSP, São Carlos, pp. 75-93.

Tokimatsu, K. (1988) Penetration Tests for Dynamic Problems. Proc. of the First International Symposium on Penetration Testing, ISOPT-1, Orlando, pp. 117-136.

Youd, T.L.; Bartholomew, H.W. & Steidl, J.H. (2008) SPT hammer energy ratio versus drop height. Journal of Geotechnical and Geoenvironmental Engineering, ASCE, v. 134:3, p. 397-400.

On the Erosive Potential of Some Weathered Soils from Southern Brazil

R.A.R. Higashi, M. Maccarini, R. Davison Dias

Abstract. This paper presents a parametric study on erodibility of soils which occurs in Southern Brazil. Different methodologies were carried out and soils more vulnerable to these phenomena were identified. The research lays mainly on erodibility criteria based on infiltrability tests, weight loss by immersion, direct shear tests and modified Inderbitzen tests. Results obtained allowed a comparison and interpretation of the erosive potential of some soil units from the states of Paraná, Santa Catarina and Rio Grande do Sul. By the applied methodologies and their respective criteria, it was observed that Cambisols units present a high erosive potential compared to other soils studied, like Latosols and Red-Yellow Podzolic soils. It was also observed that fine sandy soils were more vulnerable to erosion despite the fact of belonging to the same group. This was due to the different degree of weathering of the stratum from where samples were obtained. Finally, the results also showed that it seems to be possible to successfully correlate the erosive potential of soils with simple indices, which may reflect the characteristics related to certain peculiarities of the soil, such as specific gravity.

Keywords: erosion, tropical soils, laboratory tests.

1. Introduction

Erosive processes caused by water are of great interest, especially in areas of high pluviometric indices and intense use and occupation, as occurs in the south region of Brazil. The siltation mechanism, reflex of erosion phenomenon, tends to accelerate with the expansion of urban areas, mainly due to the suppression of vegetation, exposing high vulnerable soils to erosion. This process results on the decrease of the superficial thickness of soil horizons and on the rising of river water levels during catastrophic climatic events.

Although several studies have been carried out to analyze erosive potential of soils from other parts of Brazil, the relationship between geotechnical parameters obtained by laboratory tests and the tropical soil units have not usually been done.

Due to this reason, a diagnostic study was carried out between the erosive potential of soils determined by different mechanisms of evaluation of geotechnical parameters involved in the process (Criterion of erodibility - Nogami & Villibor, 1979; Modified Inderbitzen - Freire, 2001 and Direct Shear Tests - Bastos *et al.*, 2002) and their pedologic classification.

2. Soil Samples Location

All studied soil samples come from south Brazil, which is formed by states of Paraná, Santa Catarina and Rio Grande do Sul. Fig. 1 shows the map details.

Despite all three states of south Brazil are well away from the equator line, they present soils with tropical characteristics, with thick residual soil layer showing intensive weathering action. In this region, apart from sedimentary soils, which are not the subject of this study, the more important units are formed by Latosols (Oxisols), Cambisols and Red-Yellow Podzolic soils originated from several geologic formations.

The main characteristics of Latosols from this region are that, despite their high permeability (average of 10^{-4} cm/s, mainly due to their structures formed by micro-aggregates - Davison Dias, 1987) they present a high percentage of clay size particles. They also show a deep and relatively homogeneous B horizon with water table well below from soil surface.

Cambisols and Red-Yellow Podzolic soils, which tend to be developed in steep topographic areas, show some similar geotechnical characteristics. Among them, they present a deep C horizon containing low weathered minerals and high strength increasing with depth. They also show deep water table and a significant variability of others geotechnical properties as the matrix rock changes.

Lithologically, the studied areas are composed of basaltic rocks (Serra Geral Formation), granites (Granite-Gneiss Complex) and sedimentary rocks (Guabirotuba Formation).

3. Tests Procedures

Laboratory erodibility tests have been carried out more frequently from the sixties on. They allow to analyse

R.A.R. Higashi, PhD, Associate Professor, Departamento de Engenharia Civil, Universidade Federal de Santa Catarina, 88037-001 Florianópolis, SC, Brazil. e-mail: rrhigashi@gmail.com.
M. Maccarini, PhD, Professor, Departamento de Engenharia Civil, Universidade Federal de Santa Catarina, 88035-420 Florianópolis, SC, Brazil. e-mail: ecv1mac@ecv.ufsc.br.
R. Davison Dias, PhD, UNA Tecnológica, Universidade do Sul de Santa Catarina 88053-516 Florianópolis, SC, Brazil. e-mail: redavison@gmail.com.
Submitted on September 28, 2010; Final Acceptance on February 2, 2011; Discussion open until April 30, 2012.

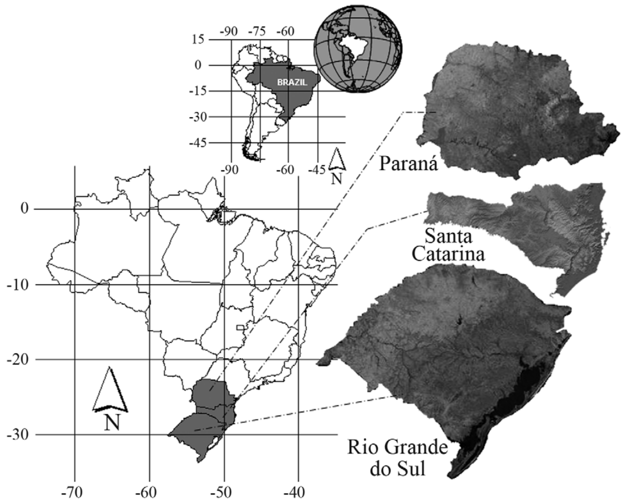

Figure 1 - Studied area Location.

the influence of the several states the soils experiment, such as humidity during erosion is taking place, the rain drops impact energy or water percolation (Chamecki & Silva, 2004).

Several papers on erodibility have been published, among them, Moore and Masch (1962), the Inderbitzen tests (Inderbitzen, 1961), pinhole test and crumb test (Sherard *et al.*, 1976a and 1976b), desegregation (Brazil, 1979; Fonseca & Ferreira, 1981), the MCT erodibility criterion (Nogami & Villibor, 1979) and the Modified Inderbitzen criterion (Freire, 2001).

Due to the high variety of existing geotechnical tests, only three different procedures have been chosen by this research to evaluate the mechanisms influencing soils erosive potential, as follows:

- MCT erodibility criterion (Nogami & Villibor, 1979);
- Erodibility criterion based on Modified Inderbitzen tests (Freire, 2001) and;
- Erodibility criterion based on direct shear tests (Bastos *et al.*, 2002).

The paper searched for relationship between results obtained by the three methodologies and also between physical indices, such specific gravity, taking account samples of Cambisols, Latosols and Red-Yellow Podzolic soils from South Brazil.

3.1. MCT erodibility criterion (Nogami & Villibor, 1979)

Erodibility criterion using the MCT methodology, as been proposed by Nogami & Villibor (1979) is essentially empirical and is based on correlations with the behaviour of a great number of tropical soils observed in roads cuts.

Nogami & Villibor (1995) stress the complexity of erodibility due to the great number of factors involved and because they are generally interdependent. According to these authors, erodibility depends mainly on the following characteristics: grain size distribution, structure and macro-fabric, permeability, infiltration rate and cohesion.

According to the authors, the prediction of the behaviour of tropical soils against hydric erosion can be obtained by infiltrability tests which determines the water absorption index (s) and the specific erodibility (modified loss of mass by immersion) which indicates the percentage of dry weight loss in relation to the total weight of the sample (pi).

From results of these two tests, the relationship called erodibility index ($E = 52s/pi$) is obtained, which establishes the limit of the erodibility criterion, based on field observations. This way, soils presenting $pi/s > 52$ are considered of high erodibility and soils showing $pi/s < 52$ are classified as medium to low erodibility.

Despite the erodibility criterion proposed by Nogami & Villibor (1979) has been used for decades and by different studies, Pejon (1992) presented a criterion using as boundary the value $pi/s = 40$ for some deep tropical soils from southern Brazil. This condition is emphasized by this paper for some tropical soils whose origin and formation are similar to those studied by Pejon (1992), as for example, Latosols.

3.2. Erodibility criterion by direct shear tests (Bastos *et al.*, 2002)

The methodology proposed by Bastos *et al.* (2002) is based on considerations made by Nascimento and Castro (1976). These authors consider that the most important parameters affecting the erosive processes of tropical soils are: grain size distribution (for sandy soils), expansion and *petrification* (the last one representing the ability of a clayey soil to maintain its cohesion immediately after submersion). Therefore, Bastos *et al.* (2002), evaluate the potential erodibility of tropical soils by the analysis of the decrease in cohesion due to submersion of the soil samples during the stage of consolidation in the direct shear tests. According to the authors, a change in cohesion (Δc), given by Eq. (1), of at least 85%, classify soils as potentially erodible.

$$\Delta c = \frac{(c_{nat} - c_{inu})}{c_{inu}} \tag{1}$$

where c_{nat} and c_{inu} are, respectively, the cohesion determined by samples under natural water content and after submersion.

3.3. Erodibility criterion based on modified inderbitzen tests (Freire, 2001)

The erodibility criteria of soils presented so far, evaluate with efficiency the erosive effects by loss of solid particles and modification of soil structure due to submersion. Nevertheless, these tests are not able to simulate the soil particles desegregation due to the impact of rain drops and superficial running water after intensive rains.

The importance of rain drops impact in the erosive processes can be observed directly by laboratory tests developed by Laws (1940), Ellison (1947a-e), Musgrave (1947), Guerra & Cunha (1995) and Chamecki & Silva (2004).

In this way, Freire (2001) presents the modified Inderbitzen test which adds to the superficial running water effect (Inderbitzen, 1961), the rain drops impact effect. In the authors opinion, the latest one is considered to be the most representative of all the three methodologies presented.

The test apparatus is mainly composed of an inclined plane structure which serves as a bed to set up undisturbed samples on it. In addition, there are two parallel lines of "showering" made of perforated tubes which lies, on average, 0,20 m above the undisturbed samples.

The samples, with dimensions 10.16 cm x 10.16 cm x 2 cm, are submitted to showering at constant water flow for a period of 2 h, under different humidity conditions.

Water and sediments are collected under the inclined plane structure in a first recipient. Afterward, they are oriented to a second recipient where sedimentation process occurs. After the sediments are separated from water, it is sieved to determine the grain size distribution of the eroded soil.

Figure 2 presents the apparatus setup for infiltrability tests, weight loss by immersion and modified Inderbitzen tests.

Through field observations and laboratory tests, Higashi (2006) obtained a value of 6% loss of weight by water dropping for residual samples that occur in some coastline regions of south Brazil. According to the author, this value should be considered the limiting value defining the erosive potential of soils. Despite this, studies involving this type of tests are recent and there is no agreement among researchers about the criteria which define erosive potential of soils. Some variations are expected for soils from different places.

4. Soil Erodibility Evaluation

A laboratory test program was conducted to study the erodibility of typical tropical soils, such as Latosols, Cambisols and Red-Yellow Podzolic from southern Brazil by several tests, as mentioned previously. The main geotechnical soil properties are presented in Table 1.

In this study, 898 samples were tested, from which, 380 specimens according to MCT methodology, 38 by Inderbitzen Modified tests and 160 by Mohr-Coulomb failure envelope (with at least three specimens for each envelope), carried out by direct shear test.

The same criterion was applied for collecting all samples, that is, three sun shining days after the last rain stopped.

4.1. Erodibility evaluation by MCT criterion

It was observed from results obtained by MCT testing procedures that there is a tendency towards a relationship, between pedologic evolution and the erosive potential of soils.

Figure 3 shows the relationship between *pi* and *s* for Cambisols and Red-Yellow Podzolic soils, based on pa-

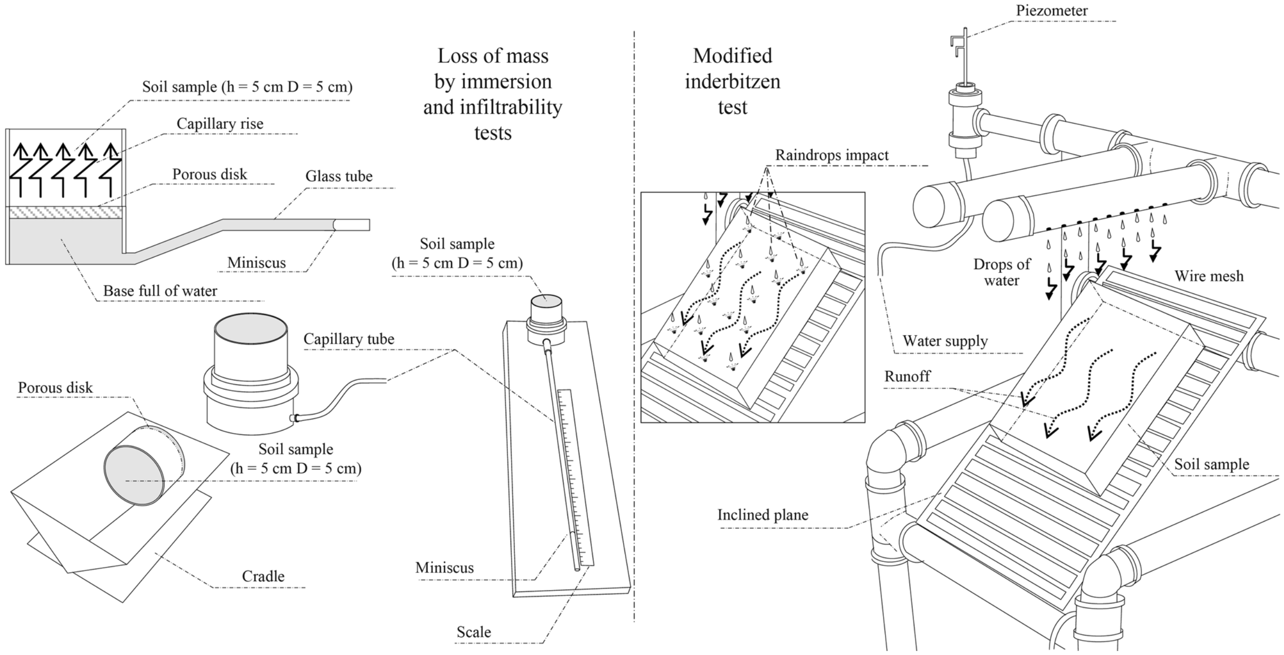

Figure 2 - Apparatus setup for infiltrability tests, weight loss by immersion and modified Inderbitzen tests (Modified from Nogami & Villibor, 1979 and Freire, 2001).

Table 1 - Main geotechnical properties for soils such Latosols, Cambisols and Red-Yellow Podzolic soils from southern of Brazil.

Property		Cambisols	Red-Yellow Podzolic	Latosols	
				Dusk	Dark Red
Medium grain size distribution (%)[1]	Sand	48.51	36.43	6.52	48.83
	Silt	42.39	23.21	29.73	19.62
	Clay	9.10	40.36	63.75	31.55
Origin rock		Granite	Granite	Basalt	Sandstone
Horizon sampling		C	B/C and C	B	B
Average specific gravity		2.67	2.77	2.83	2.74
Water content (%)		14.23-15.31	19.24-25.18	29.42-49.61	7.50-24.25
Optimum moisture content[2] (%)		10.5-32.7	13.7-35.4	32.3-36.9	10.9-16.5
Maximum dry density (kN/m3)		12.2-18.6	13.1-19.8	12.4-13.7	14-19.5
Natural cohesion (kPa)		8.1-104.1	22.3-74.1	17.4-57.0	8.0-54.0
Submerged cohesion (kPa)		36.5-0	17.5-6.4	6.3-37.9	2.5-17.5
Natural friction angle (degrees)		31.9-46.1	28.7-37.3	11.8-35.0	23.8-32.1
Submerged friction angle (degrees)		23.2-41.3	20.1-35.6	21.1-31.2	21.1-28.4
Average CBR[2] (%)		18	16	11	13

Notes: (1) With deflocculating agent; (2) Normal proctor energy.

rameters obtained by Nogami & Villibor (1979) and Pejon (1992).

Soils with higher degree of weathering (Red-Yellow Podzolic and mainly Latosols soils) showed lower values of *pi*/*s*. This behaviour indicates a lower tendency to erodibility, especially based on criterion of $pi = 52\ s$.

Despite this and the fact that the great majority of results obtained by Cambisols indicated a high erosive potential, most of the data obtained fell in between the interval $40 < pi/s < 52$. For these soil samples, the authors observed a direct relationship between grain size distribution and erosive potential. More erodible soils presented a higher content of sand particles size.

Despite the high depths of C horizon in Cambisols soils of Southern Brazil, even the top part of these strata presents a low degree of weathering. In many cases, a significant number of samples collected from different places presented a significant percentage of quartz, a mineral known to be more resistant to weathering. This aspect ensures to these soils a higher percentage of sand in their composition, with an unstable structure, which by its turn may trigger the process of erosion.

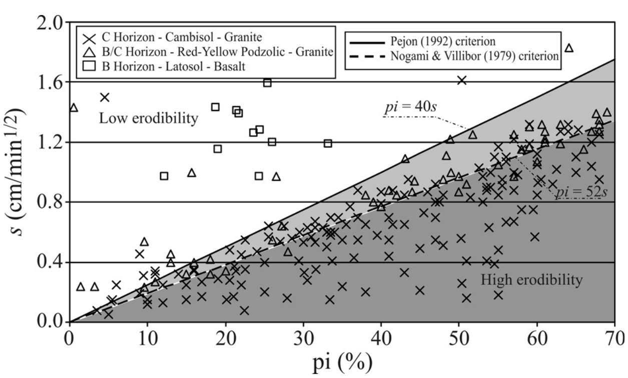

Figure 3 - Water absorption index (s) *vs.* loss of mass by immersion (pi).

Based on the data studied, it seems clear that the weight loss by immersion is the main parameter separating the erodibility of soils samples. More important than the water absorption index.

Nevertheless, Pejon and Silveira (2007) emphasize that there is a relationship between specific gravity of particles (ρ_s) in the range between 25.1 to 27 kN/m^3 and high erodibility index.

Based on data presented by Fig. 4 and comparing results with those obtained by the MCT criterion, it was observed that soils with ρ_s in between 25.31 to 26.69 kN/m^3 show higher erodibility. This range was determined by a statistical analysis.

4.2. Erodibility evaluation by direct shear tests

Fig. 5 shows the relationship between natural and submerged cohesion, according to criterion presented by Bastos *et al.* (2002) and Bastos *et al.* (1998).

The behaviour of cohesion, under these two conditions, is reflected on the desegregation of superficial particles, especially in less weathered soils, the Cambisols. As already mentioned previously, though Cambisols and Red-Yellow Podzolic soils do present a structure more similar to that of the origin rock, these soils also present their superficial strata with considerable quantities of quartz,

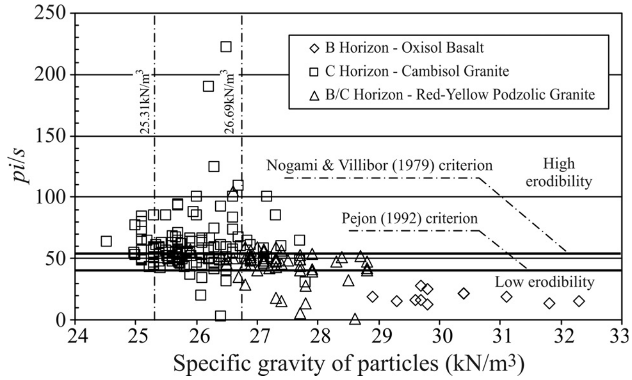

Figure 4 - Relationship between specific gravity, loss of mass by immersion and water absorption index.

which due to this aspect turn them more vulnerable to erosion. Even Cambisols, considered the most structured ones, which present high natural cohesion, showed significant decrease after being submerged. For these cases, in many times the criterion proposed by Bastos *et al.* (2002), was reached.

By the other hand, results obtained with samples collected from B horizon, formed by basaltic and sandstones Latosols, showed low erodibility. Despite structural instability, typical to these types of soils, originated from a structure formed by strongly bonded clayey micro-aggregates and weakly bonded micro-aggregates formed by clay-bridges, the variation of cohesion intercept was considered low, especially when interpreted by criterion proposed by Bastos *et al.* (2002).

Nevertheless, it was noticed that samples collected from very weathered soil strata, like sandstones, showed lower values of natural cohesion and higher cohesion drops after submersion, compared to results obtained from very weathered Latosols derived from basaltic rocks. This characteristic is associated to the bigger amount of fine sand particles present in the Latosol B horizon derived from the sandstone. The fine sand fraction in this case, was above 40% in all samples, while in samples derived from basaltic rocks this value was less than 25%.

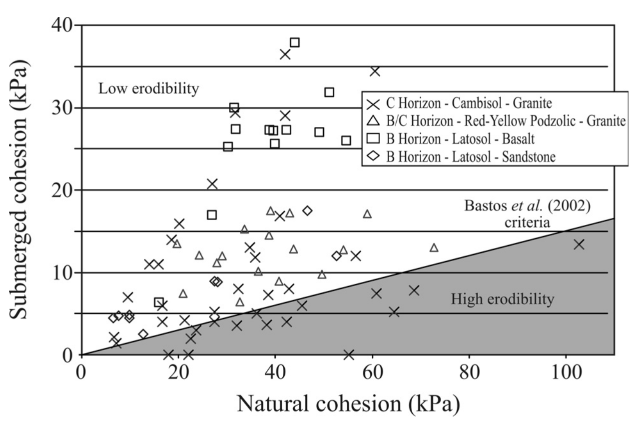

Figure 5 - Relationship between values of submerged and natural cohesion.

Related to variation in friction angles, one assume that minor changes were due to new spatial arrangements of particles after submersion and are not indicative of erosive characteristics.

4.3. Erodibility evaluation by modified inderbitzen tests

Modified Inderbitzen tests were carried out on samples at natural water content and air dried for 72 h, as recommended by Freire (2001). Figure 6 shows the results.

The soil behaviour determined by this test, considered by Higashi (2006) the most representative method to evaluate the erosive potential, confirms the results obtained by other methodologies used in this research.

Besides the fact that the majority of the samples show considerable weight loss, under a constant simulation of dripping rain water, it was observed that for granitic Cambisols samples the loss of solid particles was more significant.

Though Latosols derived from basalt show structural instability (Davison Dias, 1987), simulation under constant dripping process on these samples has indicated a weight loss considered low, compared to other soils studied. This aspect emphasizes the necessity of some adjustment in the criterion proposed by Higashi (2006). This author establishes as 6% the weight loss of solids as the limit between low and high erodibility (Fig. 6).

Referring to grain size distribution of eroded soil, though some samples did not present enough material for the test, in order to comply with the standards, it was observed a tendency for the curves, under different conditions, to be somewhat parallel. This indicates that the weight loss, during the tests, has occurred approximately with the same intensity for the whole range of diameter particles, and for different soil types.

Figure 7 shows a comparison between grain size distribution for Red-Yellow Podzolic soils before Modified Inderbitzen tests under conditions of natural water content and for its respective eroded material. Figure 8 presents this comparison for the same soil after being dried out for 72 h.

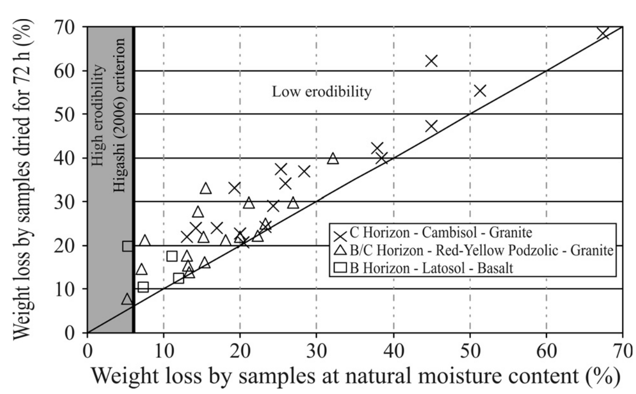

Figure 6 - Weight loss of soils under different conditions of humidity.

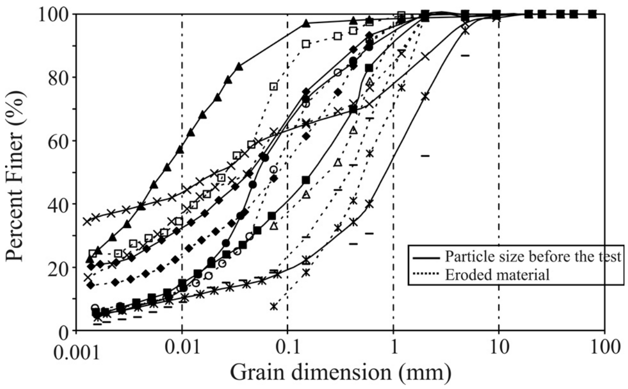

Figure 7 - Comparison of grain size distribution for soil and respective eroded material for Red-Yellow Podzolic soils under Modified Inderbitzen tests - samples tested at natural water content.

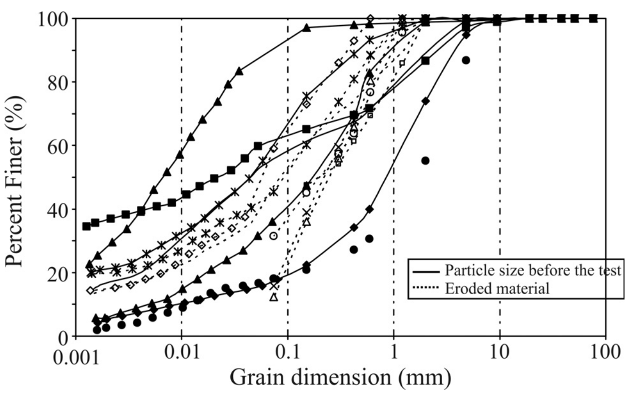

Figure 8 - Comparison of grain size distribution for soil and respective eroded material for Red-Yellow Podzolic soils under Modified Inderbitzen tests - samples tested after being dried for 72 h.

5. Conclusions

There is a great variety of tropical residual soils in Brazil, which underwent intensive processes of weathering. The most common ones in southern part are Latosols, Cambisols and Red-Yellow Podzolic soils. Under present climate conditions, these soils suffer a continuous weathering, which results in structures in constant changes. Therefore, due to the differences of weathering, from where samples have been collected and the different types of parent rocks, to establish a parameter defining the erodibility of soils is a very complex task.

Nevertheless, the analysis of the erosive potential, based on the methodologies applied and their respective criteria, carried out in this research, showed high values of erosive potential for Cambisols, especially when compared to other soils studied. This aspect is still more significant due to the high slopes in which these units are formed.

Furthermore, it was also observed that soils composed of grain size fraction of fine sand, are more vulnerable to erosion, as for instance, the dusk and dark red Latosols. It is important to emphasize that in the field, these soils present their structures in the form of micro-aggregates, in the range of fine sand particles, strongly bonded. Despite this characteristic, the micro-aggregates also present weak bonding, especially in the B horizon of Latosols derived from sandstones.

Finally, it was also observed that methods applied to differentiate soils of high and low erodibility presented coherent results by their classifications. All methods classified Cambisols as highly erodible, Latosols as less erodible and an erodibility medium to high to the Red-Yellow Podzolic soils. Besides, this work has shown also that simple indices, as specific gravity, can be successfully used to evaluate tropical soil erodibility and thus aid the prevention of erosion and the losses of its entails.

References

Bastos, C.A.B.; Gehling, W.Y.Y. & Bica, A.V.D. (1998) Some considerations about the shear strength an erodibility of unsaturated residual soils. In: Proc. International Conference on Unsaturated Soils, ISSMGE/CISMGE-CCES, Beijing, v. 1, pp. 19-24.

Bastos, C.A.B.; Gehling, W.Y.Y. & Milititski, J. (2002) Avaliação geotécnica da erodibilidade de solos residuais - Uma proposta metodológica. Anais XII Congresso Brasileiro de Mecânica dos Solos e Engenharia Geotécnica, São Paulo, v. 2, pp. 1193-1203.

Brasil, Ministério dos Transportes (1979) Recomendações para Proteção de Taludes Contra a Erosão. Instituto de Pesquisas Rodoviárias, Rio de Janeiro, 59 pp.

Chamecki, P.R. & Silva, E.T. (2004) Erosão hídrica em argilas da Formação Guabirotuba: comportamento e parâmetros em ensaios e simulações em laboratório. Proc. GEOSUL - Simpósio de Prática de Engenharia Geotécnica da Região Sul, Curitiba, pp. 131-138.

Davison Dias, R. (1987) Aplicação de Pedologia e Geotecnia no Projeto de Fundações de Linhas de Transmissão. Tese de Doutorado em Engenharia, Universidade Federal do Rio de Janeiro, Rio de Janeiro, 309 pp.

Ellison, W.D. (1947a) Soil erosion studies - Part I. Agricultural Engineering, v. 28:4, p. 145-146.

Ellison, W.D. (1947b) Soil erosion studies - Part II: Soil detachment hazard by raindrop splash. Agricultural Engineering v.28:5, p. 197-201,.

Ellison, W.D. (1947c) Soil erosion studies - Part III: Effects of soil erosion on infiltration and surface runoff. Agricultural Engineering, v. 28:6, p. 245-248.

Ellison, W.D. (1947d) Soil erosion studies - Part IV: Soil erosion, soil loss, and some effects of soil erosion. Agricultural Engineering, v. 28:7, p. 297-300.

Ellison, W.D. (1947e) Soil erosion studies - Part V: Soil transportation in the splash process. Agricultural Engineering, v. 28:8, p. 349-351, 353.

Fonseca, A.M.M.C.C. & Ferreira, C.S.M. (1981) Metodologia para determinação de um índice de erodibilidade dos solos. Proc. I Simpósio Brasileiro de Solos Tropicais em Engenharia, COPPE, CNPq e ABMS, Rio de Janeiro, pp. 646-667.

Freire, E.P. (2001) Ensaio Inderbitzen modificado: Um novo modelo para avaliação do grau de erodibilidade do solo. Proc. VII Simpósio Nacional de Controle de Erosão, Goiânia, CD-ROM, pp. 1-8.

Guerra, A.T. & Cunha, S.B. (1995) Geomorfologia, Uma Atualização de Bases e Conceitos. Ed. Bertrand, Rio de Janeiro, 443 pp.

Higashi, R.A.R. (2006) Metodologia de Uso e Ocupação dos Solos de Cidades Costeiras Brasileiras Através de SIG com Base no Comportamento Geotécnico e Ambiental. Tese de Doutorado em Engenharia Civil, Universidade Federal de Santa Catarina, 486 pp.

Inderbitzen, A.L. (1961) An erosion test for soils. Materials Research Standards, v. 1:7, p. 553-554.

Laws, J.O. (1940) Recent studies in raindrops and erosion. Agricultural Engineering, v. 21, p. 431-433.

Moore, W.L. & Masch, F.D. (1962) Experiments on the scour resistance of cohesive sediments. Journal Geophysical Research, v. 67:4, p. 1437-1446.

Musgrave, G.W. (1947) The quantitative evaluation of factors in water erosion, a first approximation. Journal of Soil and Water Conservation, v. 2, p. 133-138.

Nascimento, U. & Castro, E. (1976) Erosão: critérios de seleção de solos. Geotecnia, n. 20, p. 17-33.

Nogami, J.S. & Villibor, D.F. (1979) Soil characterization of mapping units for highway purposes in a tropical area. Bulletin of IAEG, n. 19, pp. 196-199, DOI 10.1007/BF02600475.

Nogami, J.S. & Villibor, D.F. (1995) Pavimentação de Baixo Custo com Solos Lateríticos. Ed. Villibor, São Paulo, 240 pp.

Pejon, O.J. (1992) Mapeamento Geotécnico de Piracicaba 1:100.000: Estudo de Aspectos Metodológicos, de Caracterização e de Apresentação dos Atributos. Tese de Doutorado, Escola de Engenharia de S. Carlos, Universidade de São Paulo.

Pejon, O.J. & Silveira, L.L.L. (2007) Index properties to predict erodibility of tropical soils. Bulletin of Engineering Geology and the Environment, v. 66:2, DOI 10.1007/s10064-006-0067-9.

Sherard, J.L.; Dunningan, L.P. & Decker, R.S. (1976a) Identification and nature of dispersive soils. Journal of the Geotechnical Engineering Division, ASCE, v. 102:GT4, p. 287-301.

Sherard, J.L.; Dunningan, L.P.; Decker, R.S. & Steele, E.F. (1976b) Pinhole test for identifying dispersive soils. Journal of the Geotechnical Engineering Division, ASCE, v. 102:GT1, p. 69-85.

Mobility of Manganese in a Compacted Residual Gneissic Soil Under Laboratory Conditions

R. Nascentes, I.C.D. Azevedo, A.T. Matos, M.P.F. Fontes, R.F. Azevedo, L.M. Guimarães

Abstract. Given the shortage of information available in the literature on transport parameters of heavy metals in Brazilian tropical soils, the mobility of manganese (Mn^{2+}) in a residual gneissic compacted soil is studied in this work. Manganese can be found in toxic concentrations in landfill leachate, besides being one of the main contaminants from acid mine drainage. Column tests were performed in two groups of compacted soil samples to determine the manganese retardation factor. The sample groups presented slightly different soil compaction degrees and water contents. Soil samples were initially saturated by upward percolation of distilled water without applied counter pressure. A multi-species contaminant solution was then percolated through the soil columns. A different behavior of the hydraulic conductivity along time was observed between the two groups, during water as well as solution percolation. Manganese mobility was observed to be independent of soil hydraulic conductivity, *k*, for the range of *k*-values attained in this investigation, emphasizing the importance in evaluating the mobility of this metal in compacted soil barriers. Even when these barriers present low hydraulic conductivity values, this cation high mobility may cause it to reach soil layers below the compacted layer resulting in groundwater contamination.
Keywords: adsorption, hydraulic conductivity, manganese, mobility, tropical soils, column tests.

1. Introduction

Municipal solid waste (MSW) dump sites and areas surrounding mining activities are normally subjected to heavy metal contamination. The leachate produced by MSW generally contains high concentrations of metals, including manganese, while acid mine drainage exhibits low pH and high concentrations of iron, aluminum and manganese.

Heavy metals are chemical elements frequently associated with contamination since they may accumulate and cause disturbances in living organisms in a given environment. Studies concerning their behavior in soil have received considerable attention, and have helped to increase our understanding of the phenomena related to mobility and retention of these elements in the environment and their inclusion in the food chain.

Concern over manganese is relatively recent. However, like other essential elements such as zinc and copper, it can be responsible for soil and groundwater contamination when it is present above certain concentrations. Groundwater pollution below contaminated areas is related to contaminant mobility. When it is high, a greater risk exists.

Manganese, a plant and animal micronutrient, is a transition element of the iron family. It is among the most abundant elements (Group VII B), representing 0.09% of the weight of the Earth's crust (Wills, 1992). It is employed in metallurgy as well as in the production of fertilizers, electrolytic batteries, ceramics, varnish and paints, among other uses. According to Barceloux (1999), manganese is present in almost all types of soils in divalent and tetravalent forms and in concentrations varying between 40 and 900 mg kg^{-1}. In mining areas its concentration can reach levels of about 7000 mg kg^{-1}. The formation of Mn^{2+} complexes in the process of adsorption and the consequent mobility depend on the properties of that metal, the type and amount of ligands, the composition of soil solution and soil pH (Alleoni *et al.*, 2005).

Therefore, the main objective of this work was to evaluate Mn^{2+} mobility and determine its retardation factor when percolating a multi-species contaminant solution through compacted gneissic residual soil columns.

R. Nascentes, DSc, Associate Professor, Departamento de Engenharia Civil, Universidade Federal de Viçosa, Campus Rio Paranaíba, 36571-000 Rio Paranaíba, MG, Brazil. e-mail: rejanenascentes@yahoo.com.br.
I.C.D. Azevedo, DSc, Associate Professor, Departamento de Engenharia Civil, Universidade Federal de Viçosa, Campus Universitário s/n, 36571-000 Viçosa, MG, Brazil. e-mail: iazevedo@ufv.br.
A.T. Matos, DSc, Associate Professor, Departamento de Engenharia Agrícola, Universidade Federal de Viçosa, Campus Universitário s/n, 36571-000 Viçosa, MG, Brazil. e-mail: atmatos@ufv.br.
M.P.F. Fontes, PhD, Full Professor, Departamento de Solos, Universidade Federal de Viçosa, Campus Universitário s/n, 36571-000 Viçosa, MG, Brazil. e-mail: mpfontes@ufv.br.
R.F. Azevedo, PhD, Full Professor, Departamento de Engenharia Civil, Universidade Federal de Viçosa, Campus Universitário s/n, 36571-000 Viçosa, MG, Brazil. e-mail: razevedo@ufv.br.
L.M. Guimarães, MSc, Departamento de Engenharia Civil, Universidade Federal de Viçosa, Campus Universitário s/n, 36571-000 Viçosa, MG, Brazil. e-mail: lucasmguimaraes@bol.com.br.
Submitted on October 7, 2010; Final Acceptance on September 27, 2011; Discussion open until April 30, 2012.

2. Material and Methods

2.1. Soil

The soil used in this study, extracted from a slope of Visconde do Rio Branco, MG, sanitary landfill, was collected from the B horizon of a yellow red latosol classified, according to Unified System of Soil Classification (USCS), as inorganic silt of high compressibility (MH) and according to the Highway Research Board (HRB) system as A-7 soil with group index 12 (Azevedo *et al.*, 2006). The soil was characterized through geotechnical tests, clay fraction mineralogical analysis and chemical and physicochemical analyses. Soil characterization and compaction tests were performed according to the Brazilian Standards ABNT NBR-7181/84 for particle size; ABNT NBR-6459/84 and NBR-7180/84 for consistency limits; ABNT NBR-6508/84 for specific weight of solids; and ABNT NBR-6457/86 for compaction. The chemical and physicochemical analyses were determined according to EMBRAPA (1987).

Geotechnical properties are presented in Tables 1 and 2 while the results of chemical and physicochemical analyses are listed in Table 3.

X-ray analysis was conducted with a Rigaku D-Max diffractometer equipped with a cobalt tube (Co-Kα radiation) and a graphite curved crystal monochromator operated at 40 kV and 30 mA. The X-ray analysis of the soil clay fraction was performed in three different types of samples: (i) random-powder, prepared on a glass slide with a cavity in which the natural clay was packed in powder form; (ii) oriented-aggregate, prepared with natural clay by the paste method according to Theisen and Harward (1962) for better mineral preferential orientation; and (iii) oriented-aggregate, prepared after treating the clay to remove the iron oxides, to enhance the preferential orientation of the silicate layer species present (Fig. 1). Analysis of these three sam-

Table 1 - Soil grain size distribution and Atterberg limits.

Grain size distribution				Atterberg limits			
Clay (%)	Silt (%)	Sand (%)	Gravel (%)	w_L[1]	w_P[2]	*PI*[3]	Activity
42.0	10.0	47.1	0.9	52	30	22	0.52

[1]w_L - liquid limit; [2]w_P - plastic limit; [3]*PI* - plasticity index.

Table 2 - Soil physical indexes.

γ_s[0] (kN m^{-3})	γ_{dmax}[1] (kN m^{-3})	γ_{dmax}[2] (kN m^{-3})	γ_{dmax}[3] (kN m^{-3})	w_{opt}[1] (%)	w_{opt}[2] (%)	w_{opt}[3] (%)
27	16.45	15.97	15.82	22.3	23.9	24.1

[0]γ_s - solids unit weight; [1]γ_{dmax} and [1]w_{opt} - soil maximum dry unit weight and optimum moisture content for Standard Proctor; [2]γ_{dmax} and [2]w_{opt} - idem for 291 kJ/m^3; [3]γ_{dmax} and [3]w_{opt} - idem for 233 kJ/m^3.

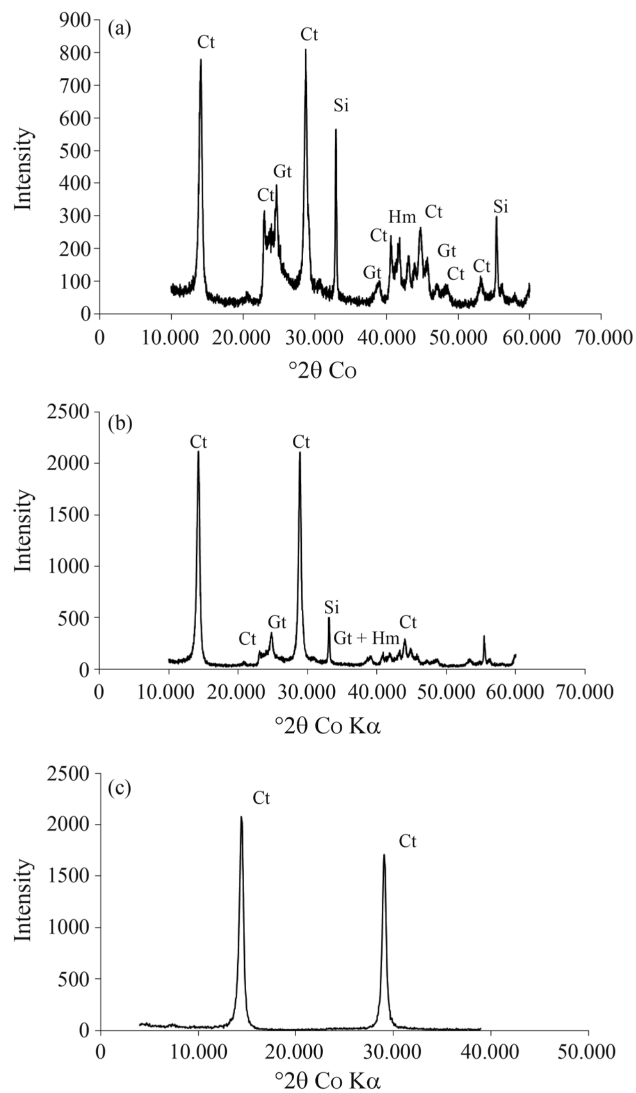

Figure 1 - Soil clay fraction X-ray: (a) random-powder, (b) oriented-aggregate, prepared with natural clay by the paste method, and (c) oriented-aggregate, prepared with the clay after removal of iron oxides. Ct - kaolinite, Gt - goethite, Si - silicon, Hm - hematite.

Table 3 - Chemical and physicochemical analyses.

Mn^{2+} (cmol$_c$ kg^{-1})	Ca^{2+} (cmol$_c$ kg^{-1})	Mg^{2+} (cmol$_c$ kg^{-1})	K^+ (cmol$_c$ kg^{-1})	Al^{3+} (cmol$_c$ kg^{-1})	H^++Al^{3+} (cmol$_c$ kg^{-1})	CEC_{ef}[1] (cmol$_c$ kg^{-1})	CEC_{pot}[2] (cmol$_c$ kg^{-1})	*OMC*[3] (%)	pH
0.046	1.23	0.11	0.026	0.0	0.7	1.37	2.07	0.0	6.01

[1]CEC_{ef} - Effective Cation Exchange Capacity for natural soil pH; [2]CEC_{pot} - Potential Cation Exchange Capacity for pH = 7; [3]*OMC* - organic matter content.

ple types allowed definition of the soil clay fraction composition as kaolinite, goethite and a very small amount of hematite (Nascentes, 2006).

The amount of iron was determined using the dithionite-citrate extraction method (Coffin, 1963) to quantify the presence of iron oxides. Iron oxides content was 13.3% in mass which was entirely allocated to goethite. It is important to determine the amount of iron oxides in the clay fraction of the soil since these mineral constituents exhibit a high energy retention capacity for heavy metals.

2.2. Heavy metals contaminant solution

An artificial contaminant solution (synthetic landfill leachate) consisting of six heavy metals was used in the column tests. This solution was prepared by addition of nitrate salts, available at the laboratory, which are water soluble, of manganese, zinc, cadmium, copper, lead and chromium, metals commonly encountered in landfill leachates (Azevedo *et al.*, 2006). The pH and heavy metal concentrations used (Table 4) are within the range of values for Brazilian landfill leachate (Oliveira & Jucá, 1999).

2.3. Column tests

The flexible-walled permeameter used in the column tests is similar to a triaxial cell and capable of simultaneously testing four soil samples of 0.05 m in diameter by 0.10 m in height. Each sample cell has an inlet for the percolating fluid and an outlet for effluent collection. Fluid flows upward through the soil samples. Each inlet is connected, by a latex hose, to a Mariotte bottle containing the contaminant fluid. The equipment also has an inlet for applying confining pressure that allows reproduction of *in situ* horizontal stresses (Azevedo *et al.*, 2003).

The tests were performed under controlled temperature conditions (17 to 21 °C). A confining pressure of 50 kPa was applied to the samples to simulate a 10 m deep urban solid waste layer over the liner.

Tests were performed on two groups of samples, with different compaction energies. Three samples from group I and eight from group II were dynamically compacted in a 0.05 m diameter metallic cylinder at 21.9% (group I) and 22.5% (group II) water content, corresponding to 95% of optimum specific dry density (15.63 kN m^{-3}). The compaction energy was such that all samples were compacted until they reached 0.10 m in height and 0.05 m in diameter. As the water content varied slightly, the compaction energy also varied, as shown in Fig. 2.

Tables 5 and 6 present a summary of molding and testing conditions for groups I and II, respectively.

Table 4 - Chemical characteristics of the contaminant solution.

pH	Cr^{3+} (mg L^{-1})	Cd^{2+} (mg L^{-1})	Pb^{2+} (mg L^{-1})	Cu^{2+} (mg L^{-1})	Mn^{2+} (mg L^{-1})	Zn^{2+} (mg L^{-1})
5.2	0.7	1.6	1.6	5.0	36.0	62.0

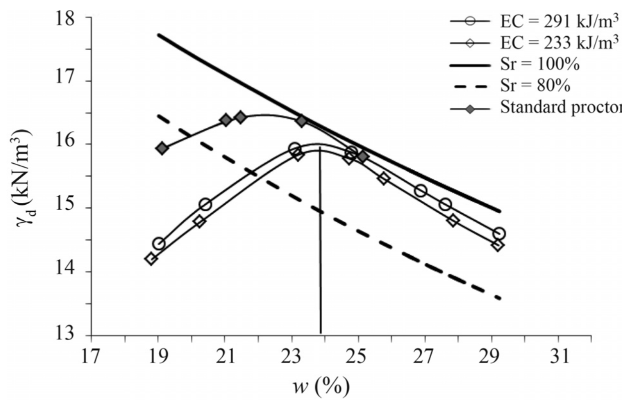

Figure 2 - Soil compaction curves.

The different gradients and, consequently, different percolation velocities, adopted for CP06, CP07, CP010 CP011 samples of group II, were adopted with the purpose of evaluating the diffusion coefficient, which was not possible.

The procedure used in this type of test is similar to that used in constant head permeability tests. The main differences are the need for measuring the effluent chemical concentration (C_e) and the generation of several pore volumes of chemical solution.

During the tests, both affluent and effluent chemical concentrations were determined at regular intervals. The relationship C_e/C_0 was calculated considering the value of C_0 read at the instant preceding the collection of the effluent.

The hydraulic gradient was maintained constant during the tests. Soil samples were initially saturated by upward percolation of distilled water, without applying counter pressure, prior to the percolation of the contaminant solution. Soil columns were considered saturated when constancy of flow was observed. The soil hydraulic conductivity coefficient was determined using Darcy's law (Lambe and Whitman, 1979).

Samples CP04 and CP09 from group II were percolated with distilled water to serve as reference for the other group II samples which were saturated with distilled water and then percolated with the contaminant solution.

Table 5 - Compaction tests - Sample characteristics: Group I - water content = 21.9% and compaction energy of 291 kJ/m^3.

	CP01	CP02	CP03
GC (%)	98.7	99.0	98.4
Gradient	13.4	13.4	13.4
Void ratio	0.713	0.706	0.718
Porosity	0.416	0.414	0,418
Void volume (mL)	80.0	79.7	80.4
Saturation degree (%)	82.9	83.7	82.3
Water content deviation (%)	-2.0	-2,0	-2.0

Table 6 - Compaction tests - Sample characteristics: Group II - water content = 22.5% and compaction energy of 233 kJ/m^3.

	CP04	CP05	CP06	CP07
GC (%)	98.7	98.6	98.9	98.3
Gradient	13.4	13.4	7.3	7.3
Void ratio	0.729	0.731	0.726	0.737
Porosity	0.422	0.422	0.421	0.424
Void volume (mL)	81.4	81.4	80.7	82.0
Saturation degree (%)	83.2	83.0	83.6	82.4
Water content deviation (%)	-1.6	-1.6	-1.6	-1.6
	CP08	CP09	CP10	CP11
GC (%)	98.3	98.7	98.9	98.6
Gradient	13.4	13.4	7.3	7.3
Void ratio	0.737	0.729	0.726	0.731
Porosity	0.424	0.422	0.421	0.422
Void volume (mL)	81.7	81.5	81.0	81.3
Saturation degree (%)	82.4	83.3	83.6	83.0
Water content deviation (%)	-1.6	-1.6	-1.6	-1.6

Column effluents were collected daily from 50 mL burettes fixed to the base of the equipment and stored in bottles, previously washed with a solution of nitric acid, for subsequent determination of metal concentrations in an atomic absorption spectrophotometer. After measuring effluent concentrations of each metal (C_e), for each percolated pore volume (T), breakthrough curves (C_e/C_0 *vs.* T) were elaborated for manganese.

Two methods can be used for data analysis of the effluent concentration from column tests (traditional method and the cumulative mass method). The traditional method consists in measuring instantaneous concentrations *vs.* time, determining the breakthrough curve and applying an analytical model to determine the retardation factor and hydrodynamic dispersion coefficient. The concentration of solutes in any point of the column is calculated using Eq. (1) (Ogata & Banks, 1961), for the initial and boundary conditions given in Eq. (2), as follow:

$$C_r(x,t) = \frac{C_0}{2}\left\{ erfc\left[\left(\frac{R_d x - V_x t}{2\sqrt{D_h R_d t}}\right) + \exp\left(\frac{V_x x}{D_h}\right)\times erfc\left[\left(\frac{R_d x + V_x t}{2\sqrt{D_h R_d t}}\right)\right]\right\}\right] \tag{1}$$

$$\begin{aligned} &C_r(x,0) = 0 \quad \text{for} \quad x \geq 0 \\ &C_r(x,t) = C_0 \quad \text{for} \quad t \geq 0 \\ &\frac{\partial C_r(\propto,t)}{\partial x} = 0 \quad \text{for} \quad x \geq 0 \end{aligned} \tag{2}$$

where C_r is the solute resident concentration [ML^{-3}]; C_0 is the initial concentration [ML^{-3}]; R_d is the retardation factor; x is the direction coordinate; t is the time [T]; D_h is the hydrodynamic dispersion coefficient [L^{2}T^{-1}]; V_x is the percolation velocity in x direction [LT^{-1}] and *erfc* is the complementary error function.

When the length of the column is sufficiently long, the second term in the right side of Eq. (1) is negligible compared to the first, so that the effluent concentration at $x = L$ is given by (Shackelford, 1993):

$$C_e(L,t) = \frac{C_0}{2}\left\{ erfc\left(\frac{R_d L - V_x t}{2\sqrt{D_h R_d t}}\right)\right\} \tag{3}$$

or,

$$C_e(L,t) = \frac{C_0}{2}\left\{ erfc\left((R_d - T)\left(\frac{P_L}{4\,T\,R_d}\right)^{1/2}\right)\right\} \tag{4}$$

$$T = \frac{V_x t}{L} \tag{5a}$$

$$P_L = \frac{V_x L}{D_h} \tag{5b}$$

where C_e [ML^{-3}] is the effluent concentration at $x = L$; T is the number of pore volume; P_L is the column Peclet number; and L [L] is the soil column height.

The derivative of Eq. (4) with relation to T, at the point $T = R_d$, gives the value $b = \sqrt{P_L / 4\pi R_d^2}$. If the tangent to the experimental curve C_e/C_0 *vs.* T at the point $C_e/C_0 = 0.5$ is known and substituting P_L by the value given in Eq. (5), then the hydrodynamic dispersion coefficient, D_h, is determined from Eq. (6) as:

$$D_h = \frac{V_x L}{b^2 \ 4\pi \ R_d^2} \tag{6}$$

3. Results and Discussion

3.1. Percolation of distilled water

Soil hydraulic conductivity (k) *vs.* number of pore volumes (T) curves obtained from distilled water percolation through groups I and II sample columns are presented in Fig. 3. A significant variation in the hydraulic conductivity values for group II samples with time is evident, as shown in Fig. 3b. Since these samples were compacted with greater water content than those of group I, their structure was slightly more dispersed. Therefore, saturation with distilled water promoted greater variations in hydraulic conductivity of group II samples, which reached constant flow after percolation of almost ten times more number of pore volumes, compared to samples of group I. For these last samples, however, constant flow was reached more quickly (for a smaller number of pore volumes) because of a more flocculated soil structure after compaction, as compared to samples of group II. More flocculated soil structures facilitate the exit of air which in turn allows constant flow values to be reached for a smaller number of percolated pore volumes.

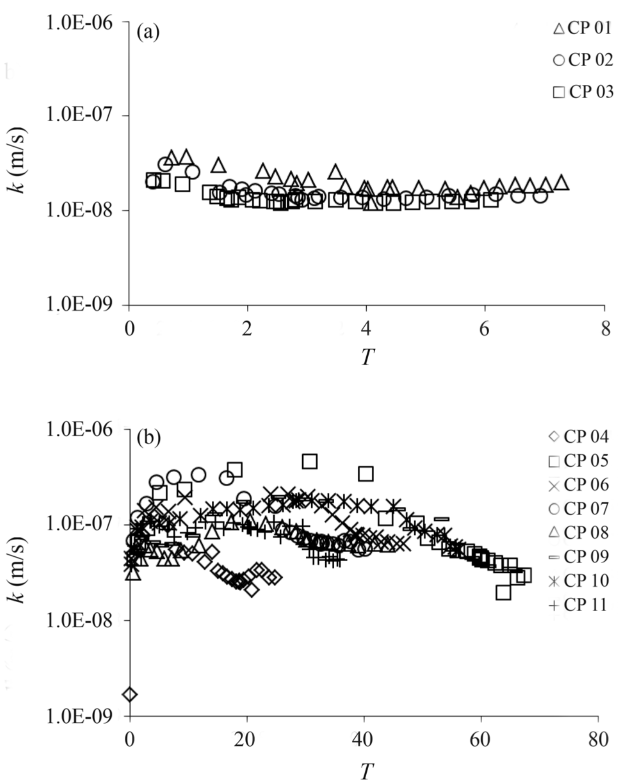

Figure 3 - Hydraulic conductivity for distilled water percolation in samples: (a) Group I and (b) Group II.

Percolation of group II samples with distilled water, associated with colloidal dispersion and double layer expansion, lead to a decrease in soil solution ionic concentration (Na^+, Ca^{2+}, Mg^{2+}), as shown in Fig. 4. An expansion of this layer results in a narrower and more tortuous solution percolation path and, consequently, in lower soil hydraulic conductivity. In other words, there was more salt leaching and as a consequence, a larger double layer thickness, for a

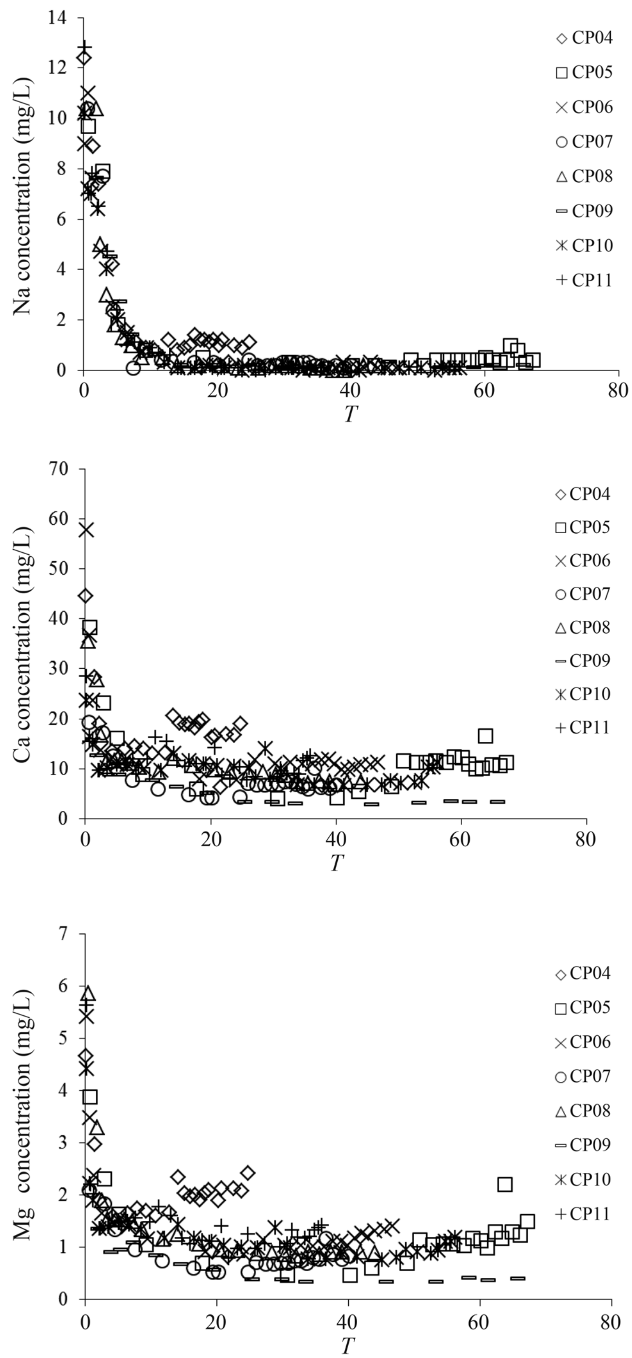

Figure 4 - Group II: Cation concentrations in effluent after distilled water percolation through soil columns. (a) Sodium, (b) Calcium, and (c) Magnesium.

greater number of distilled water pore volumes percolated through the samples.

The average final values of hydraulic conductivity were 1.5 x 10^{-8} m/s for group I and 5.0 x 10^{-9} m/s for group II. The heterogeneity of the soil samples tested and something in this particular testing procedure probably contributed to a slight difference in the final values of k between the two groups.

3.2. Percolation of contaminant solution

Soil hydraulic conductivity *vs.* number of pore volume curves for percolation of the contaminant solution through the two soil sample groups are shown in Figs. 5 and 6. The significant difference observed in hydraulic conductivity behavior for the two groups is attributed to the distinct double layer thicknesses attained by each after the saturation process. In other words, the soil hydraulic conductivity for contaminant solution percolation depended mainly on the compacted soil structure and the previous percolation with distilled water.

Group I samples exhibited an initial great increase in hydraulic conductivity followed by a pronounced decrease, while a monotonic significant decrease was observed for all group II samples. However, this decrease occurred in a distinct way for each sample, possibly as a result of the different structures formed after the saturation process. The large difference in number of distilled water pore volumes directly influenced the behavior of the hydraulic conductivity by the time the contaminant solution was percolated.

The small difference in the numbers of percolated distilled water pore volumes in samples CP07 and CP08 from group II (40.1 and 44.1, respectively), the approximate amount of leached cations and the same Standard Proctor compaction degree of 94.5% led to similar behaviors in hydraulic conductivity, when the contaminant solution was percolated through these samples.

The introduction of chemical substances to soil generally produces variations in its hydraulic conductivity. The contact between these substances and the soil may lead to redistribution of pore spaces as a result of clay particle rearrangement (flocculation or dispersion) and chemical reac-

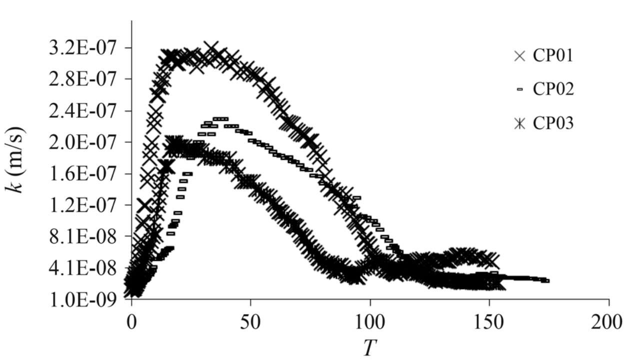

Figure 5 - Hydraulic conductivity for percolation of the contaminant solution through samples: Group I.

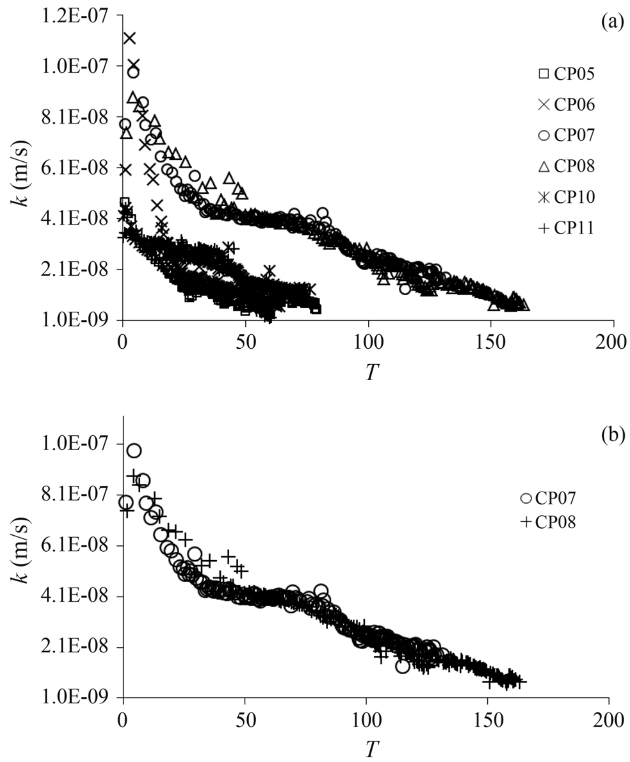

Figure 6 - Hydraulic conductivity for percolation of the contaminant solution through samples: (a) Group II and (b) Samples CP07 and CP08.

tions, such as dissolution or precipitation of solids, between these substances and clay minerals. As a result of this contact, ionic changes may occur that can cause double layer contraction or expansion. The thickness of the double layer and the magnitude of acting forces depend mainly on the dielectric constant, temperature, electrolytic concentration in the interstitial fluid and cation valence, and to a lesser extent on cation size, fluid pH and anion adsorption on clay particle surfaces (Boscov, 1997).

The samples in group I showed more flocculated structures (thinner double layer) than those in group II after percolation with distilled water. Thus, the initial increase in hydraulic conductivity probably occurred as a result of exchange of monovalent ions, naturally found in the soil, with divalent and trivalent cations present in the contaminant solution, leading to flocculation. Hydraulic conductivity started to decrease when the soil exhausted its capacity to retain zinc and manganese, precisely the metals present in high concentrations in the contaminant solution.

In group II samples, the increase in pH could have been a factor favouring metal precipitation and leading to a decrease in hydraulic conductivity, as a consequence of the obstruction of soil pores by metal precipitates. In this case the soil structure was more dispersed and the duration of contact between the contaminant solution and samples was greater, which also favours precipitation.

Effluent pH was measured for all samples and curves of pH *vs.* T are shown in Fig. 7a. In Fig. 7b, for the sake of clarity, only pH *vs.* T curves for soil columns CP10 and CP11 (group II) are presented.

When heavy metal solutions percolate through the soil columns, variations in the pH of the effluent, due to sorption and desorption reactions, are common. In these reactions, the cations naturally present in the soil are liberated and leached, usually associated to the hydroxyl (OH^-). In this way, the pH of the effluent varies according to the type and the leached amount of the cation, which could explain the oscillation of the pH value around the one that would be reached when reactions of sorption and desorption cease.

According to Fig. 6b, the hydraulic conductivity in sample CP10 was lower than that of CP11 for values of T between 13 and 50, approximately. In this range, effluent pH in CP10 was greater than in CP11, indicating a possible higher precipitation in the former sample. Both samples showed similar pH values as well as hydraulic conductivities between $T = 50$ and $T = 104$. From $T = 104$ on, effluent pH in sample CP11 increased in relation to that in sample CP10 and hydraulic conductivity in CP11 consequently decreased more than in CP10.

3.3. Determination of transport parameters

Breakthrough curves (curves of relative concentration (C_e/C_0) *vs.* number of percolated pore volumes) were constructed for manganese for both sample groups and are presented in Figs. 8 and 9.

Manganese is a metal that happens naturally in great amount in tropical soils. The easily exchangeable concentration of this element in the studied soil is approximately 0.046 $cmol_c\ kg^{-1}$, obtained by sequential extraction method with $CaCl_2$, which accounts for the total amount of Mn^{2+} released into solution when in competition with other ions for adsorption sites. The largest Mn^{2+} desorption in CP03 of group I and in all samples of group II, as shown in Figs. 8c and 9, may be explained by the greater time of contact between the solution and the soil particles, as indicated by the hydraulic conductivity variations observed during the tests. According to Azevedo *et al.* (2006) and Nascentes (2006), manganese (Mn^{2+}) was least sorbed by soil when compared to the other metals (Zn^{2+}, Cd^{2+}, Pb^{2+}, Cu^{2+} and Cr^{3+}) present in the contaminant solution. The mobility sequence obtained from test column and soil sequential extraction was $Mn^{2+} > Zn^{2+} > Cd^{2+} > Cu^{2+} > Cr^{3+} > Pb^{2+}$.

The behavior of Zn^{2+}, Cd^{2+}, Cu^{2+}, Pb^{2+} and Cr^{3+} was also studied and published in Nascentes *et al.* (2008). Their

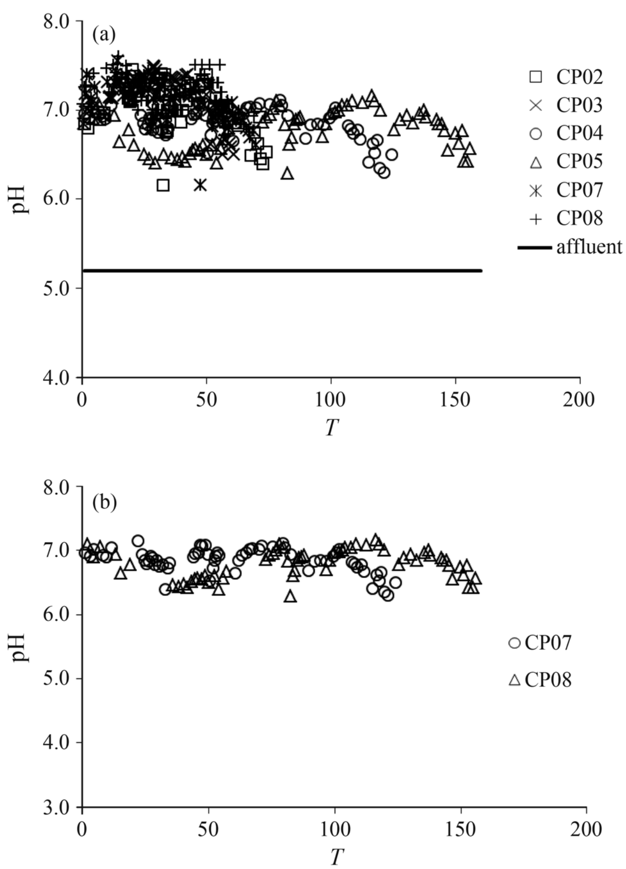

Figure 7 - Effluent pH *vs.* number of pore volumes - Group II (a) For all samples and (b) CP07 and CP08.

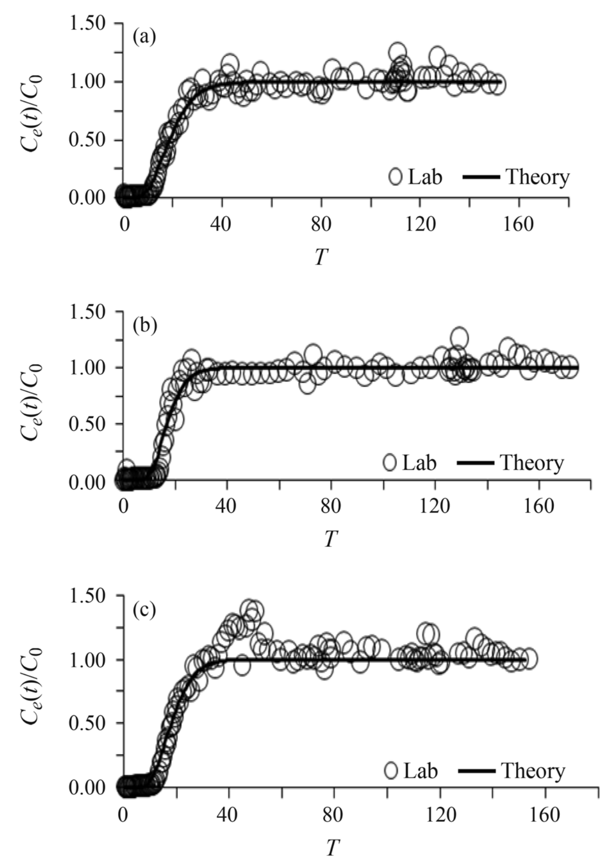

Figure 8 - Breakthrough curves for manganese - Group I (a) CP01; (b) CP02 and (c) CP03.

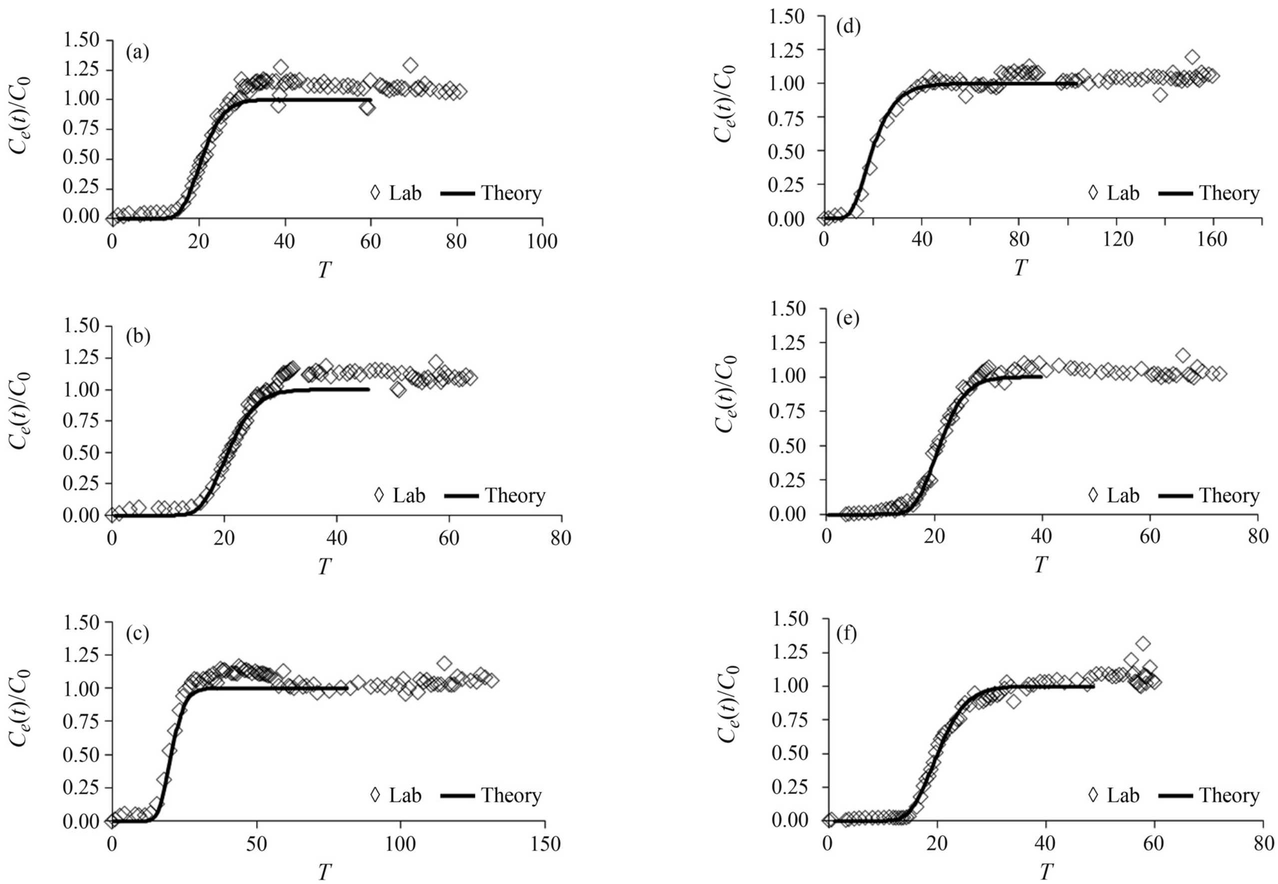

Figure 9 - Breakthrough curves for manganese - Group II (a) CP05; (b) CP06; (c) CP07; (d) CP08; (e) CP10 and (f) CP11.

mobility differed from that of manganese and was shown to depend on soil hydraulic conductivity.

The Peclet number is a parameter that helps in determining the predominant type of transport. This number for each column was calculated using Eq. (5b), considering the average percolation velocity of each test, up to $C_e/C_0 = 1$, as shown in Table 7. A mean value of 54.2 was determined for group II samples implying, according to the classification proposed by Sun (1995), that the predominant transport processes in column tests were advection and mechanical dispersion, since P_L was higher than 10 and less than 100, which depend on hydraulic conductivity.

Table 7 - Peclet numbers for each column.

Sample	V_{xm} (cm/min)	L (cm)	D_h (cm^2/min)	V/D_h (1/cm)	P_L
CP05	3.63E-03	10.00	6.55E-04	5.54	55.42
CP06	2.88E-03	10.00	5.21E-04	5.52	55.42
CP07	5.97E-03	10.00	1.08E-03	5.53	55.46
CP08	9.89E-03	10.20	2.10E-03	4.71	48.03
CP10	2.92E-03	10.00	5.27E-04	5.54	55.43
CP11	3.04E-03	10.00	5.49E-04	5.54	55.37

V_{xm} - average percolation velocity; L - column length; D_h - hydrodynamic dispersion coefficient.

The retardation factor (R_d) values shown in Table 8 were determined using the traditional method (Rowe *et al.*, 1995) with R_d given by the value of T for C_e/C_0 equal to 0.5.

Korf *et al.* (2008) conducted column tests in an undisturbed clayey soil, which was percolated by a synthetic multispecies solution composed of Cu^{2+} (20 mg/L), Cr^{3+} (20 mg/L), Mn^{2+} (1 mg/L), and Zn^{2+} (10 mg/L), and obtained an average value of 10.1 for the retardation factor.

It can be noted that the breakthrough curves for the two sample groups shown in Figs. 7 and 8 are quite similar as are the R_d values presented in Table 8. These similarities indicate that the mobility of manganese (Mn^{2+}) did not depend on hydraulic conductivity, for the range of k values of this investigation, which was markedly different for the two

Table 8 - Retardation factor for manganese.

	Group I*			Group II					
Test	01	02	03	04	06	07	08	10	11
R_d	19.5	18.0	18.5	20.0	20.0	18.0	20.0	20.5	20.4

*Azevedo *et al.* (2006).

groups when the contaminant solution was percolated through the soil columns.

The importance of test duration must be emphasized since the reactions between the soil and the contaminant solution did not occur in the same way for the manganese and the remaining heavy metals. Long term tests allow the development of chemical interactions of each heavy metal in competition with soil particles since a great number of pore volumes of contaminant solution are allowed to percolate through the soil column. In both sample groups, more than 60 pore volumes of the multi-species solution percolated through the soil columns, but in spite of significant differences in the values of hydraulic conductivities, the mobility of manganese in the soil was nearly the same in both groups.

4. Conclusion

The main conclusions drawn from this study can be summarized as follows.

Hydraulic conductivity behavior of a compacted clay layer saturated with distilled water and subsequently leached with a heavy metal solution is sensitive to the number of percolated pore volumes in the saturation process as well as to the compaction energy which can promote significant alterations in the structure of the material.

A mean value of 54.2 for Peclet number was determined for group II samples implying that the predominant transport processes in the column tests were advection and mechanical dispersion.

The mobility of manganese in test columns was not influenced by the compaction water content varying in the range of $\pm 0.5\%$ around the optimum value, indicating the potential of this metal to contaminate soil and groundwater, even for low values of saturated hydraulic conductivity.

Acknowledgments

The authors would like to acknowledge the National Council of Technological and Scientific Development (CNPq), the Support Research Foundation of the State of Minas Gerais (FAPEMIG), the Superior Level Personnel Improvement Coordination (CAPES) for financial support, and the Civil Engineering, Agricultural Engineering and Soil Departments of the Federal University of Viçosa, MG, Brazil, for carrying out tests.

References

ABNT (1984) Specific Gravity Determination, NBR 6508.

ABNT (1986) Soil Sample - Preparation for Test Compression and Characterization Testing, NBR 6457.

ABNT (1984) Soil - Determination of Liquid Limit, NBR 6459.

ABNT (1984) Soil - Determination of Plasticity Limit, NBR 7180.

ABNT (1984) Grain Size Analysis, NBR 7181.

Alleoni, L.R.F.; Borba, R.P. & Camargo, O.A. (2005) Heavy metals: from cosmogenesis to Brazilian soils. Topics in Soil Science v. 4, p. 2-42.

Azevedo, I.C.D.A.D.; Nascentes, R.; Azevedo, R.F.; Matos, A.T. & Guimarães, L.M. (2003) Hydrodynamic dispersion coefficient and retardation factor of heavy metals in residual compacted soil. Solos e Rochas, v. 26:3, p. 229-249.

Azevedo, I.C.D.A.D.; Nascentes, C.R.; Matos, A.T. & Azevedo, R.F. (2006) Determination of transport parameters for heavy metal in residual compacted soil using two methodologies. Canadian Journal of Civil Engineering, v. 33:7, p. 912-917.

Barceloux, D.G. (1999) Manganese. Journal of Toxicology - Clinical Toxicology, v. 37:2, p. 293-307.

Boscov, M.E.G. (1997) A contribution to the project of containment systems of hazardous waste using lateritic soils. PhD. Dissertation, Universidade de São Paulo, Escola Politécnica, São Paulo, SP, Brazil, 259 pp.

Coffin, D.E. (1963) A method for the determination of free iron in soils and clays. Canadian Journal of Soil Science, v. 43:1, p. 9-17.

EMBRAPA, National Center for Research in Soils - CNPS (1987) Manual methods of soil analysis. Rio de Janeiro, RJ, Brazil, 211 pp.

Korf, E.P.; Melo, E.F.R.Q.; Thomé, A. & Escosteguy, P.A.V.E. (2008) Retention of metals in soil from former disposal area of urban solid waste in Passo Fundo - RS. Journal of Environmental Sciences, v. 2:2, p. 43-60.

Lambe, T.W. & Whitman, R.V. (1979) Soil mechanics, SI version. New York: John Wiley & Sons, 533 pp.

Nascentes, R. (2006) Study of the Mobility of Heavy Metals in a Residual Compacted Soil. PhD. Dissertation, Universidade Federal de Viçosa, Viçosa, 153 pp.

Nascentes, R.; Azevedo, I.C.; Matos, A.T.; Fontes, M.P.F.; Azevedo, R.F. & Guimarães, L.M. (2008) Laboratory study of mobility of heavy metals in residual compacted soil. Solos e Rochas, v. 31:1, p. 29-44.

Ogata, A. & Banks, R. (1961) A solution of the differential equation of longitudinal dispersion in porous media. U.S. Geol. Surv. Prof. Paper 411-A.

Oliveira, F.J.S. & Jucá, J.F.T. (1999) Study of contamination of the subsoil in the region of solid waste landfill of Muribeca, PE. Proc. Brazilian Congress on Environmental Geotechnics, REGEO'99, São José dos Campos, pp. 456-461.

Rowe, R.K.; Quigley, R.M. & Booker, J.R. (1995) Clayey Barrier Systems for Waste Disposal Facilities. E&FN Spon, London, 390 pp.

Shackelford, C.D. (1993) Contaminant transport. Daniel, D.E. (ed) Geotechnical Practice for Waste Disposal. Chapman & Hall, London, pp. 33-65.

Shackelford, C.D. (1995) Cumulative mass approach for column testing. Journal of Geotechnical Engineering, ASCE, v. 121:10, p. 696-703.

Theisen, A.A. & Harward, M.E. (1962) A paste method for preparation of slides for clay mineral identification by X-ray diffraction. Soil Science Society of American Proceedings, v. 26, p. 90-91.

Wills, B.A. (1992) Mineral Processing Technology. 5 ed. Pergamon Press, Oxford, 855 pp.

Passive Earth Pressure on a Vertical Retaining Wall with Horizontal Cohesionless Backfill

G.S. Kame, D.M. Dewaikar, D. Choudhury

Abstract. A method based on the application of Kötter's equation is proposed for the complete analysis of passive earth pressure on a vertical wall retaining horizontal cohesionless backfill. The unique failure surface consisting of log spiral and its tangent is identified on the basis of force equilibrium conditions. One distinguishing feature of the proposed method is its ability to compute the point of application of passive thrust using moment equilibrium. Another distinguishing feature is the prediction of distribution of soil reaction on the failure surface. The results show a close agreement with some of the available solutions.

Keywords: Kötter's equation, passive earth pressure coefficient, cohesionless soil, log spiral, point of application, horizontal backfill.

1. Introduction

Earth retaining structures such as sheet piles, retaining walls, wing walls, abutments and bulkheads are very common in engineering practices. While retaining earth, these structures are subjected to lateral earth pressures. Anchors of the bulkhead and vertical plate anchors are some of the structures which are located very near to ground level and subjected to passive earth pressure of the retained cohesionless soil.

Coulomb (1776) and Rankine (1857) proposed methods for the estimation of earth pressure on retaining walls based on the assumption of a plane failure surface. For the limit equilibrium analysis of passive thrust on retaining wall, Terzaghi (1943) proposed a failure mechanism, in which, the failure surface consisted of a log spiral originating from the wall base, followed by a tangent, that met the ground surface at an angle corresponding to Rankine's passive state. Several other research workers have adopted this failure mechanism.

Caquot & Kerisel (1948) and Kerisel & Absi (1990) proposed a log spiral mechanism and presented their results in the form of charts. Janbu (1957), Sheilds & Tolunay (1973), Basudhar & Madhav (1980), and Kumar & Subba Rao (1997) used method of slices for computing passive pressure coefficients in respect of a cohesionless soil by considering soil mass in a state of limit equilibrium.

Morgenstern & Eisenstein (1970) compared the values of passive earth pressure coefficient K_p calculated with the theories proposed by Caquot & Kerisel (1948), Brinch-Hansen (1953), Janbu (1957) and Sokolovski (1965). They concluded that with the assumption of a plane failure surface, Coulomb's (1776) theory overestimated the passive resistance.

Lancellotta (2002) provided an analytical solution for the passive earth pressure coefficients, based on the lower bound theorem of plasticity. Soubra & Macuh (2002) used an approach based on rotational log-spiral failure mechanism with the upper-bound theorem of limit analysis for the analysis of passive earth pressures.

In the recent past, Shiau *et al.* (2008) have reported the values of passive earth pressure coefficient using upper and lower bound theorems of limit analysis coupled with finite element formulation and nonlinear programming techniques.

From the review of literature, it is observed that, Kötter's (1903) equation has been employed (Balla, 1961 and Matsuo, 1967) to evaluate soil shearing resistance on a curved failure surface. Dewaikar & Mohapatro (2003) used Kötter's (1903) equation for computation of bearing capacity factor, N_γ for shallow foundations.

In the proposed investigations, a method is developed using Kötter's (1903) equation for the computation of passive thrust and its point of application for a vertical wall retaining horizontal cohesionless backfill, using the failure mechanism suggested by Terzaghi (1943). The distribution of soil reaction on the failure surface is also evaluated.

2. Proposed Method

The proposed method is an attempt to analyse the capacity of vertical plate anchors which are shallow or deep laid in cohesionless soil. The basic case refers to the situation where the plate anchor is flushing with the ground surface and involves estimation of the passive thrust. The same is analysed here.

Figure 1 shows a vertical retaining wall DE, with a horizontal cohesionless backfill. The failure surface con-

G.S.Kame, Research Scholar, Department of Civil Engineering, Indian Institute of Technology, 400076 Bombay, Powai, Mumbai, India. e-mail: gskame@iitb.ac.in.
D.M. Dewaikar, PhD, Professor, Department of Civil Engineering, Indian Institute of Technology, 400076 Bombay, Powai, Mumbai, India. e-mail: dmde@civil.iitb.ac.in.
D. Choudhury, PhD, Associate Professor, Department of Civil Engineering, Indian Institute of Technology, 400076 Bombay, Powai, Mumbai, India. e-mail: dc@civil.iitb.ac.in.
Submitted on October 1, 2010; Final Acceptance on February 14, 2011; Discussion open until April 30, 2012.

sists of log spiral EA, that originates from wall base, with tangent, AB meeting the ground surface at an angle, (45° - ϕ/2), where, ϕ is the angle of soil internal friction. At A, there is a conjugate failure plane AD, passing through the wall top. Thus, as seen from the figure, ABD is a passive Rankine zone and pole of the log spiral lies on the line AD or its extension and this is also shown in Figs. 2(a) and 2(b).

From Fig. 1, the following information is generated:

H = height of the retaining wall,

α = inclination of the tangent to the log spiral at point G with the horizontal,

θ = spiral angle measured from the starting radius,

r_0 = starting radius of the log spiral at the wall base (at $\theta = 0$),

r = radius of log spiral at point G corresponding to the spiral angle θ,

θ_m = maximum spiral angle,

r_1 = radius of the maximum spiral angle at $\theta = \theta_m$,

θ_v = angle between vertical face of the wall and the starting radius r_0.

Figures 2(a) and 2(b) show the location of pole of the log spiral when it is located above and below the wall top respectively. From Fig. 2(b), the following additional information is generated.

θ_A = angle between vertical face of the wall and line OD when pole is located below the wall top.

θ_S = angle between the radius r_0 and line OD when pole is located below the* wall top.

From Figs. 3(a) and 3(b), which show free body diagrams of failure wedge EABCD, the following information is generated.

P_{pH}, P_{pV} = horizontal and vertical components of resultant passive thrust, P_p,

R_H, R_V = horizontal and vertical components of resultant soil reaction acting on the curved part of the failure surface,

H_1 = active thrust exerted by the backfill on the Rankine wall AC,

W_{ACD} = weight of soil in the failure wedge, forming a part of the Rankine zone,

W_{ADE} = weight of soil in the zone, EAD of the failure wedge, EABCD.

In Fig 3(a), line AC represents the Rankine wall and force, H_1 as described above, is the force exerted on this wall by the backfill it retains. With this consideration and also considering that pole of the log spiral lies above the wall top on line AD, the dispositions of various forces are shown in the same figure.

In Fig. 3(b), which refers to location of pole, O below the wall top, in addition to forces mentioned earlier, forces, W_{ODE} and W_{OEA} together represent the weight of portion EAD of the failure wedge, EACD, as shown in the same figure.

2.1. Geometry of failure surface

This is dependent upon the location of pole of the log spiral.

2.1.1. Pole above wall top

Referring to Fig. 2(a) and considering triangle, ODE,

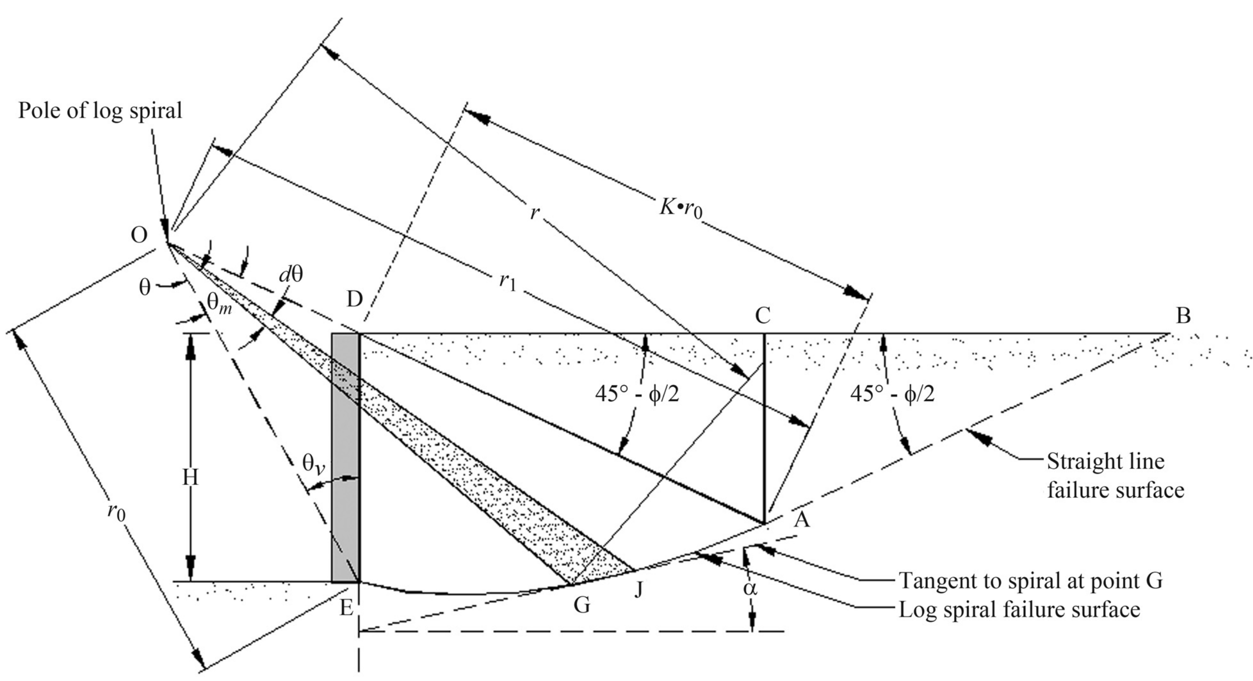

Figure 1 - Retaining wall with a horizontal cohesionless backfill - failure mechanism.

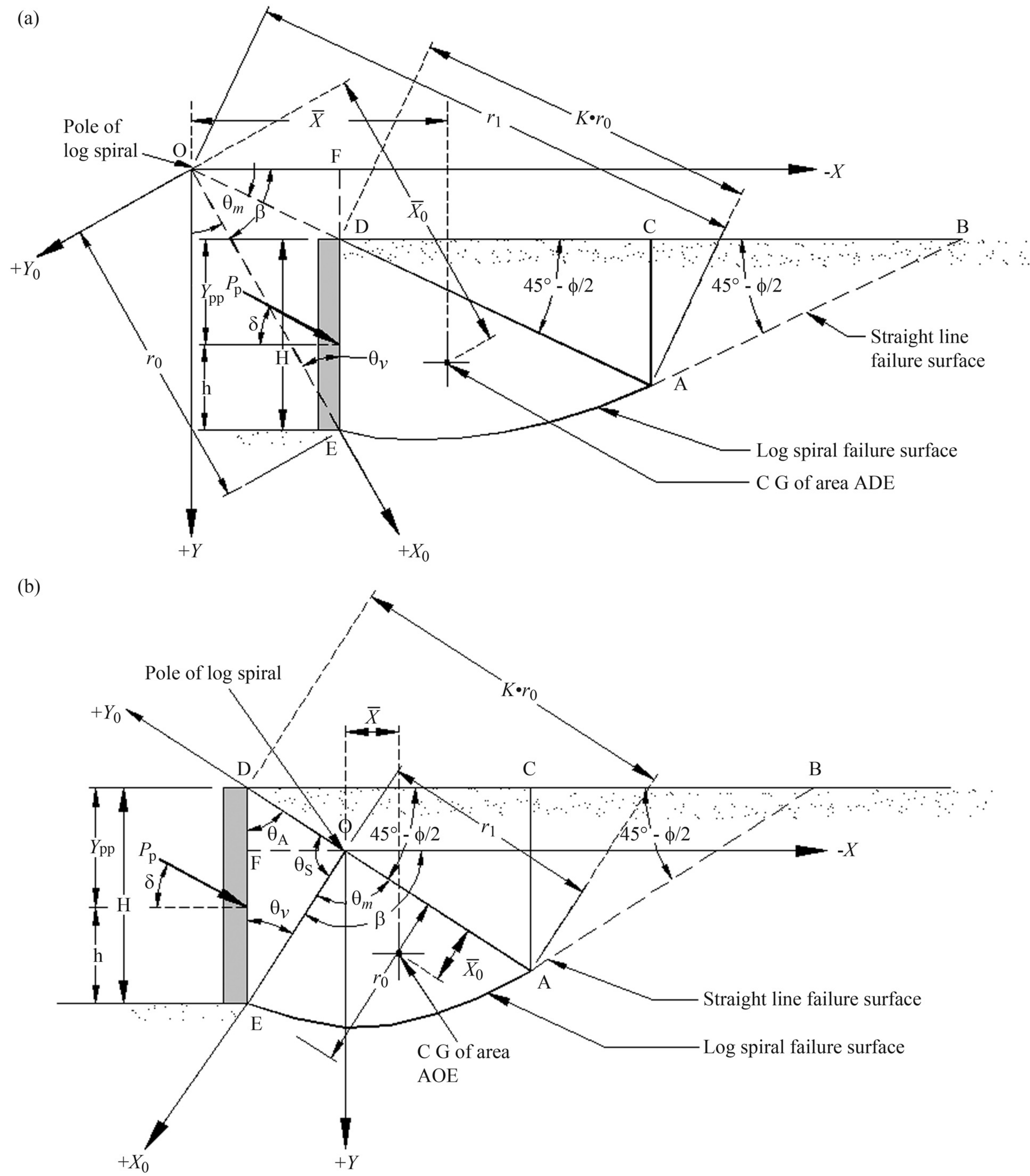

Figure 2 - (a) Failure surface adopted in the proposed analysis with pole located above the wall top. (b) Failure surface adopted in the proposed analysis with pole located below the wall top.

$$\frac{\mathrm{OD}}{\sin\theta_v} = \frac{\mathrm{OE}}{\sin\left\{135-\frac{\phi}{2}\right\}} = \frac{\mathrm{DE}}{\sin\theta_m} = \frac{\mathrm{H}}{\sin\theta_m} \qquad (1)$$

In which, angles, θ_m and θ_v are as shown in the same figure.

From the above expression,

$$\mathrm{OD} = \frac{\mathrm{H}\sin\theta_v}{\sin\theta_m}$$

The initial radius, $\mathrm{OE} = r_0$ of the log spiral is given as

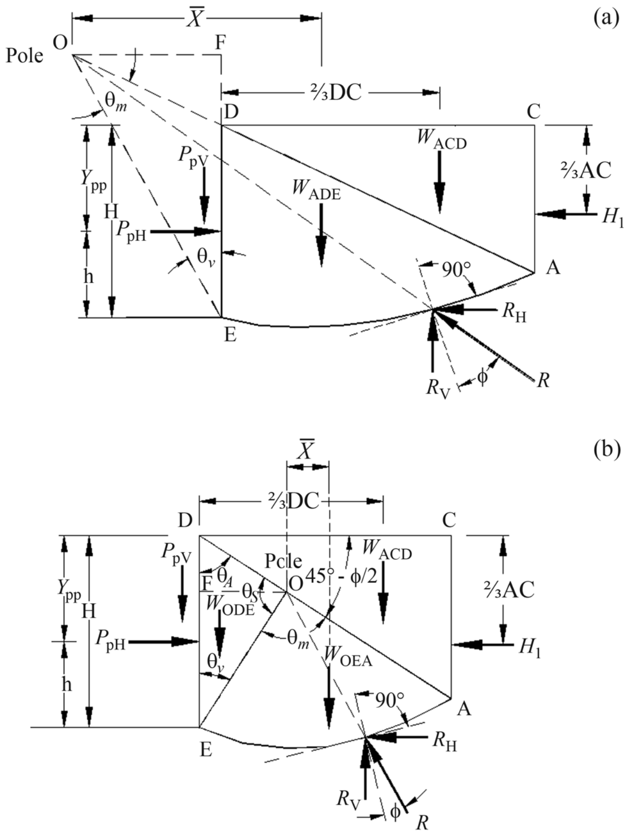

Figure 3 - (a) Free body diagram of failure wedge EACD with pole above the wall top. (b) Free body diagram of failure wedge EACD with pole below the wall top.

$$\mathrm{OE} = r_0 = \frac{\mathrm{H}\sin\left\{135 - \frac{\phi}{2}\right\}}{\sin\theta_m}$$

Also, from the equation of the log spiral,

$$\mathrm{OA} = r_0 \cdot e^{\theta_m \tan\phi}$$

and

$$\mathrm{AD} = \mathrm{OA} - \mathrm{OD}$$

2.1.2. Pole below wall top

Referring to Fig. 2(b) and considering triangle ODE,

$$\frac{\mathrm{OD}}{\sin\theta_v} = \frac{\mathrm{OE}}{\sin\theta_A} = \frac{\mathrm{DE}}{\sin\theta_S} = \frac{\mathrm{H}}{\sin\theta_S} \tag{2}$$

From which, the initial radius, OE = r_0, of the log spiral is given as

$$\mathrm{OE} = r_0 = \frac{\mathrm{H}\sin\theta_A}{\sin\theta_S}$$

and

$$\mathrm{OD} = \frac{\mathrm{H}\sin\theta_v}{\sin\theta_S}$$

Also, from the equation of the log spiral,

$$\mathrm{OA} = r_0 \cdot e^{\theta_m \tan\phi}$$

and

$$\mathrm{AD} = \mathrm{OA} + \mathrm{OD}$$

2.2. Computation of soil reaction on the failure surface

Kötter's (1903) equation basically refers to the distribution of reactive pressure on the failure surface, in a cohesionless soil medium and for the passive state of equilibrium (Fig. 4), it is as given below:

$$\frac{dp}{ds} + 2p\tan\phi\frac{d\alpha}{ds} = \gamma\sin(\alpha + \phi) \tag{3}$$

in which dp = differential reactive pressure on the failure surface, ds = differential length of arc of failure surface, ϕ = angle of soil internal friction, $d\alpha$ = differential angle, γ = unit weight of soil and, and α = inclination of the tangent at the point of interest with the horizontal.

The failure surface as shown in Fig.1 has two parts; EA, which is curved and AB, which is a straight line. Kötter's (1903) equation is used to obtain the distribution of reactive pressure on both these parts.

2.2.1. Computation of soil reaction on plane failure surface AB

For a plane failure surface, $d\alpha/ds = 0$ and Eq. (3) takes the following form:

$$\frac{dp}{ds} = \gamma\sin(\alpha + \phi) \tag{4}$$

Integration of the above equation gives

$$p = \gamma\sin(\alpha + \phi) + C_1 \tag{5}$$

Equation (5) gives distribution of reaction on the plane failure surface, AB. The distance, s is measured from

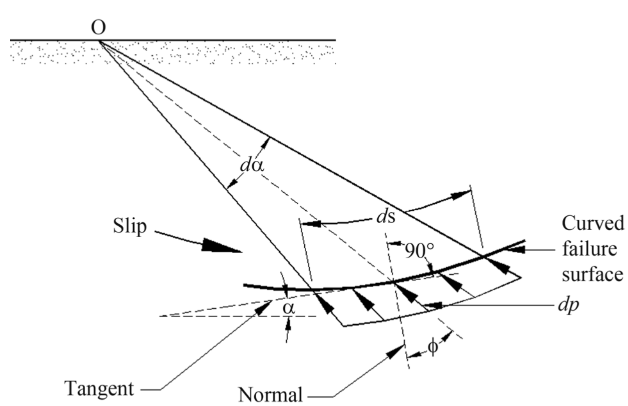

Figure 4 - Reactive pressure distribution on the failure surface for passive case.

point B (Fig. 1). The integration constant, C_1 is evaluated from the boundary condition that, pressure, p is zero at point B, which corresponds to $s = 0$. With this condition, C_1 is zero and Eq. (5) becomes

$$p = \gamma \sin(\alpha + \phi)s \tag{6}$$

In the above equation, $\alpha = 45 - \phi/2$ and with this substitution one obtains

$$p = \gamma \sin(45 + \phi/2)s \tag{7}$$

At point A (Fig. 1), p is given as

$$p = \gamma \sin(\alpha + \phi)\mathrm{AB} \tag{8}$$

The distance, AB depends upon the location of pole of log spiral, *i.e.*, whether it lies below or above the wall top.

2.2.2. Computation of vertical and horizontal components of reaction on curved failure surface EA

Multiplying Eq. (3) throughout by $ds/d\alpha$ and rearranging, the following equation is obtained:

$$\frac{dp}{d\alpha} + 2p\tan\phi = \gamma \sin t \frac{ds}{d\alpha} \tag{9}$$

In which

$$t = (\alpha + \phi), \text{ with } d\alpha = dt \tag{10}$$

From the geometry of log spiral,

$$\frac{ds}{d\theta} = r\sec\phi \tag{11}$$

From Fig. 1, the angle, α is evaluated in terms of log spiral angle, θ as given below:

$$\alpha = \theta - (90 - \theta_V)$$

with $(90 - \theta_V) = \theta_L$, α is written as

$$\alpha = \theta - \theta_L \text{ and } d\alpha = d\theta \tag{12}$$

From Eqs. (10) and (12), θ is obtained as

$$\theta = t + \theta_L - \phi \tag{13}$$

After making necessary substitutions in Eq. (9) the following equation is obtained.

$$\frac{dp}{dt} + 2p\tan\phi = \gamma \sin t \frac{ds}{d\theta} \tag{14}$$

Using Eq. (11), the above equation is written as

$$\frac{dp}{dt} + 2p\tan\phi = \gamma \sin t r \sec\phi \tag{15}$$

With $r = r_0 e^{\theta\tan\phi}$ the above equation is transformed to

$$\frac{dp}{dt} + 2p\tan\phi = \gamma \sin t r_0 e^{\theta\tan\phi} \sec\phi \tag{16}$$

Substitution of the value of θ from Eq. (13), in Eq. (16) gives the following equation.

$$\frac{dp}{dt} + 2p\tan\phi = \gamma\sec\phi r_0 e^{(t+\theta_L-\phi)\tan\phi} \sin t \tag{17}$$

The solution of above differential equation is obtained as

$$p = \gamma \cdot r_0 \sec\phi e^{(3\theta_L - 2\theta - 3\phi)\tan\phi}[p_1 + C_2] \tag{18}$$

where

$$p_1 = \left[\frac{e^{(3\tan\phi)(\theta-\theta_L+\phi)}[3\tan\phi(\theta-\theta_L+\phi) - \cos(\theta-\theta_L+\phi)]}{(1+9\tan^2\phi)}\right] \tag{19}$$

C_2 is the constant of integration and it is obtained from the boundary condition that, at Point A (Fig. 1) with , reaction is as calculated from Eq. (8).

$$C_2 = \frac{e^{(3\tan\phi)(\theta_m-\theta_L+\phi)}}{(1+9\tan^2\phi)}\left\{K\cos\phi\sin\left(\frac{\pi}{4}+\frac{\phi}{2}\right)(1+9\tan^2\phi) - [3\tan\phi\sin(\theta_m-\theta_L+\phi) - \cos(\theta_m-\theta_L+\phi)]\right\} \tag{20}$$

With the above value of C_2, pressure distribution on the curved surface is given as

$$p = \left[\gamma r_0 K \sin\left(\frac{\pi}{4}+\frac{\phi}{2}\right)e^{\tan\phi(3\theta_m - 2\theta)} + \frac{\gamma r_0 \sec\phi e^{\theta\tan\phi}}{(1+9\tan^2\phi)}(3\tan\phi\sin(\theta-\theta_L+\phi) - \cos(\theta-\theta_L+\phi)) - \frac{\gamma r_0 \sec\phi e^{\tan\phi(3\theta_m-2\theta)}}{(1+9\tan^2\phi)} \times (3\tan\phi\sin(\theta_m-\theta_L+\phi) - \cos(\theta_m-\theta_L+\phi))\right] \tag{21}$$

where K is the parameter indicating location of the pole of the log spiral along line AO in terms of radius r_0 measured from point D (Fig. 1).

The expression for K is given as

$$K = \left[1 - \frac{\mathrm{OD}/r_0}{e^{\theta_m\tan\phi}}\right], \text{ for pole above wall top (Fig.2 (a))}$$

and

$$K = \left[1 + \frac{\mathrm{OD}/r_0}{e^{\theta_m\tan\phi}}\right], \text{ for pole below wall top (Fig.2 (b))}$$

2.3. Components of resultant soil reaction on the failure surface

The resultant soil reaction, R on the failure surface is given as

$$R = \int p \cdot ds \tag{22}$$

The vertical component, R_V (Fig. 3) of resultant soil reaction is obtained as

$$R_V = \int_0^{\theta_m} p\cos(\theta - \theta_L + \phi) ds \tag{23}$$

Using Eq. (11),

$$R_V = \int_0^{\theta_m} p r_0 e^{\theta \tan\phi} \cos(\theta - \theta_L + \phi) \sec\phi d\theta \tag{24}$$

After substituting the value of p from Eq. (21), R_V is obtained in the following form after carrying out integrations.

$$R_V = R_{V1} + R_{V2} + R_{V3} \tag{25a}$$

where

$$R_{V1} = \gamma r_0^2 K\left[\left\{e^{3\tan\phi\theta_m} \sin\left(\frac{\pi}{4} + \frac{\phi}{2}\right)\right\} \times \left\{e^{-\tan\phi_m} \sin\left(\frac{\pi}{4} - \frac{\phi}{2}\right) - \sin\sin\left(\frac{\pi}{4} - \theta_m - \frac{\phi}{2}\right)\right\}\right] \tag{25b}$$

$$R_{V2} = \frac{\gamma r_0^2 \sec^2\phi}{4(1 + 9\tan^2\phi)}\left[\left\{\frac{3\tan\phi}{\sec\phi}\left[e^{2\tan\phi\theta_m} \sin 2\phi + \sin 2(\theta_m - \phi)\right]\right\} - \left\{\frac{1}{\tan\phi}\left[e^{2\phi_m \tan\phi} - 1\right] + \frac{1}{\sec\phi}\left[e^{2\theta_m \tan\phi} \cos 2\phi - \cos\left(2\phi - 2^{\theta_m}\right)\right]\right\}\right] \tag{25c}$$

and

$$R_{V3} = -\frac{\gamma r_0^2 \sec^2\phi e^{3\tan\phi\theta_m}}{(1 + 9\tan^2\phi)}\left[\left\{e^{-\theta_m \tan\phi} \sin\left(\frac{\pi}{4} - \frac{\phi}{2}\right) - \sin\left(\frac{\pi}{4} - \theta_m - \frac{\phi}{2}\right)\right\} \times \left\{3\tan\phi\sin\left(\frac{\pi}{4} + \frac{\phi}{2}\right) - \cos\left(\frac{\pi}{4} + \frac{\phi}{2}\right)\right\}\right] \tag{25d}$$

Similarly, the horizontal component, R_H (Fig. 3) of soil reaction is given as

$$R_H = \int_0^{\theta_m} p r_0 e^{\theta\tan\phi} \sin(\theta - \theta_L + \phi) \sec\phi d\theta \tag{26}$$

After substituting the value of p from Eq. (21), R_H is obtained in the following form after carrying out integrations.

$$R_H = R_{H1} + R_{H2} + R_{H3} \tag{27a}$$

where

$$R_{H1} = \gamma r_0^2 K\left[\left\{e^{3\tan\phi\theta_m} \sin\left(\frac{\pi}{4} + \frac{\phi}{2}\right)\right\} \times \left\{\cos\left(\frac{\pi}{4} - \theta_m - \frac{\phi}{2}\right)\right\} - e^{-\tan\phi\theta_m} \cos\left(\frac{\pi}{4} - \frac{\phi}{2}\right)\right] \tag{27b}$$

$$R_{H2} = \frac{\gamma r_0^2 \sec^2\phi}{4(1 + 9\tan^2\phi)}\left\{3\tan\phi\left[\frac{1}{\tan\phi}(e^{2\theta_m \tan\phi} - 1) - \frac{1}{\sec\phi}[e^{2\theta_m \tan\phi} \cos(2\phi) - \cos(2\phi - 2\theta_m)]\right] - \frac{1}{\sec\phi}\left(e^{2\tan\phi_m} \sin(2\phi) + \sin(2\theta_m - 2\phi)\right)\right\} \tag{27c}$$

and

$$R_{H3} = \frac{\gamma r_0^2 \sec^2\phi e^{3\tan\phi\theta_m}}{(1 + 9\tan^2\phi)}\left\{\left[3\tan\phi\sin\left(\frac{\pi}{4} + \frac{\phi}{2}\right) - \cos\left(\frac{\pi}{4} + \frac{\phi}{2}\right)\right] \times \left[\cos\left(\frac{\pi}{4} - \theta_m - \frac{\phi}{2}\right) - e^{-\tan\phi\theta_m} \cos\left(\frac{\pi}{4} - \frac{\phi}{2}\right)\right]\right\} \tag{27d}$$

2.4. Magnitude of passive thrust

In Fig. 3, the active Rankine thrust H_1 acts at a distance 2/3 AC from point, C. Static equilibrium of wedge, EACD is then considered.

Vertical force equilibrium condition gives

$$P_{pV} = P_p \sin\delta = R_v - W_{ACD} - W_{ADE} \tag{28}$$

From which, P_p is obtained as

$$P_p = \frac{R_v - W_{ACD} - W_{ADE}}{\sin\delta} \tag{29}$$

Horizontal force equilibrium condition gives

$$P_{pH} = P_p \cos\delta = R_H + H_1 \tag{30}$$

From which, P_p is obtained as

$$P_p = \frac{R_H + H_1}{\cos\delta} \tag{31}$$

It may be noted that, both Eqs. (29) and (31) give the magnitude of unknown thrust, P_p. These two equations will yield the same and unique value of P_p only when the equilibrium conditions correspond to those at failure, which are uniquely defined by a characteristic value of θ_V and this value can be determined by trial and error procedure.

2.5. Trial and error procedure

In this procedure, first a trial value of θ_V is assumed and corresponding weight of trial failure wedge, EACD (Fig. 3) is computed. Using Eqs. (25) and (27), magnitudes of vertical and horizontal components of soil reaction (R_v

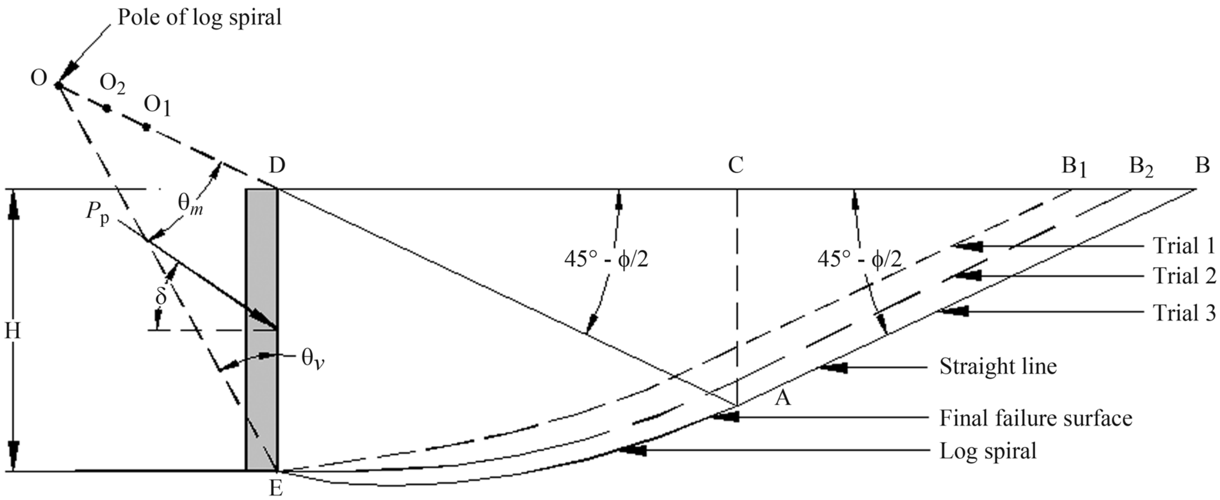

Figure 5 - Trial procedure for locating pole of the log spiral.

and R_H) are computed and from Eqs. (29) and (31), values of P_p are determined. If the trial value of θ_v is equal to its characteristic value corresponding to the failure condition, the two computed values of P_p will be the same; otherwise, they will be different.

For various trial values of θ_v, computations are carried out till the convergence is reached to a specified (third) decimal accuracy.

Thus, in this method of analysis, the unique failure surface (Fig. 5) is identified by locating the pole of log spiral in such a manner that, force equilibrium condition of failure wedge, EACD is satisfied. This approach is different from other analyses in which, P_p is obtained from the consideration of its minimum value.

The passive earth pressure coefficient, K_p is expressed as

$$K_p = \frac{2P_p}{\gamma H^2} \tag{32}$$

Values of passive earth pressure coefficient, K_p are obtained for different values of angles of soil internal friction, ϕ and wall friction, δ.

2.6. Centroid of log spiral

These calculation are performed with reference to Fig. 2(a) (for pole of the log spiral above the wall top) and Fig. 2(b) (for pole of the log spiral below the wall top) respectively. Axis, X_0 is taken along the line that joins pole, O of the log spiral to the wall base. Axis, Y_0 is perpendicular to the axis, X_0 and passes through pole of the log spiral. With respect to these axes, coordinates of the centroid of area inscribed in the log spiral are given as,

$$\bar{X}_0 = \frac{-4r_0}{3}\frac{\tan\phi}{(1+9\tan^2\phi)}\times \left[\frac{e^{3\tan\phi\theta_m}(\sin\theta_m + 3\tan\phi\cos\theta_m) - 3\tan\phi}{e^{2\tan\phi\theta_m} - 1}\right] \tag{33}$$

$$\bar{Y}_0 = \frac{-4r_0}{3}\frac{\tan\phi}{(1+9\tan^2\phi)}\times \left[\frac{e^{3\tan\phi\theta_m}(3\tan\phi\sin\theta_m - \cos\theta_m) - 1}{e^{2\tan\phi\theta_m} - 1}\right] \tag{34}$$

where, r_0 is radius of arc of log spiral at the base of retaining wall, *i.e.* at $\theta = 0°$.

Axes, X and Y are another set of coordinate axes. Axis, X passes through the pole of log spiral and is horizontal. Axis, Y is perpendicular to X axis and passes through the pole, O. With reference to these axes, the coordinates, of centroid of log spiral are given as

$$\bar{X} = \bar{Y}_0 \sin\beta + \bar{X}_0 \cos\beta \tag{35}$$

$$\bar{Y} = \bar{Y}_0 \cos\beta - \bar{X}_0 \sin\beta \tag{36}$$

where, β is the angle made by the axis, X_0 with horizontal.

2.7. Point of application of passive thrust

Moment equilibrium condition is now used to compute the point of application of passive thrust by considering moments of forces and reactions about the pole of the log spiral.

2.7.1. Pole above wall top

Referring to Fig. 3(a), the following moment equilibrium equation is obtained.

$$P_{pH}(Y_{pp} + \text{FD}) = \left[\left(W_{ACD}\cdot(\text{OF} + \tfrac{2}{3}\cdot\text{DC}) + W_{ADE}\cdot\bar{X}\right) + H_1(\tfrac{2}{3}\cdot\text{AC} + \text{FD}) + P_{pV}\cdot\text{OF}\right] \tag{37}$$

In which, the terms on the right hand side of the above expression represent moment of weight of soil in the failure wedge, EACD, moment of the force H_1 and moment due to vertical component of the resultant passive thrust, P_{pV} about the pole, O. The term on the left hand side of the above expression is the moment due to horizontal component of the resultant passive thrust, P_{aH} about the pole, O. From the above equation, Y_{pp} (which is the distance of point of application of P_p from the wall top), is obtained as

$$Y_{PP} = \frac{1}{P_{pH}}\Big[\Big(W_{ACD}\cdot(\text{OF}+\tfrac{2}{3}\cdot\text{DC})+W_{ADE}\cdot\overline{X}\Big)+ H_1(\tfrac{2}{3}\cdot\text{AC}+\text{FD})+P_{vP}\cdot\text{OF}-P_{pH}\cdot\text{FD}\Big] \quad (38)$$

2.7.2. Pole below wall top

Referring to Fig. 3(b), by taking moments of forces and reactions about the pole, O the following equation is obtained.

$$P_{pH}(Y_{PP}-\text{DF}) = \Big[\Big(W_{ACD}\cdot(\tfrac{2}{3}\cdot\text{DC}-\text{OF})-W_{ODE}\cdot\tfrac{2}{3}\cdot\text{OF} +W_{OEA}\overline{X}\Big)+H_1(\tfrac{2}{3}\cdot\text{AC}-\text{DF})-P_{pV}\cdot\text{OF}\Big] \quad (39)$$

In which, the terms on the right hand side of the above expression represent moment of weight of soil in the failure wedge, EACD, moment of the force H_1 and moment due to vertical component of the resultant passive thrust, P_{pV} about the pole, O. The term on the left hand side of the above expression is the moment due to horizontal component of the resultant passive thrust, P_{pH} about the pole, O. From Eq. (39), Y_{PP} (which is the distance of point of application of P_P from the wall top), is obtained as

$$Y_{PP} = \frac{1}{P_{pH}}\Big[(W_{ACD}\cdot(\tfrac{2}{3}\cdot\text{DC}-\text{OF})-W_{ODE}\cdot\tfrac{2}{3}\cdot\text{OF}+ +W_{OEA}\cdot\overline{X})+H_1(\tfrac{2}{3}\cdot\text{AC}-\text{DF})-P_{PV}\cdot\text{OF}+P_{pH}\cdot\text{DF}\Big] \quad (40)$$

The height, h of the passive thrust, P_p from the wall base is obtained as

$$h = H - Y_{PP} \quad (41)$$

3. Discussion

The basic purpose of this analysis was to compute passive pressure coefficient, K_p, location of point of application of passive thrust and study their variation with respect to the parameters involved in the analysis. It was found convenient to express the height, h of point of application of passive thrust from the wall base in terms of its ratio with respect to height, H of the retaining wall, in a non-dimensional form ($H_r = h/H$).

In Table 1, values of passive earth pressure coefficient, K_p along with angle θv (angle defining position of the pole of the log spiral on line AD) are shown for various combinations of soil friction angle, ϕ and angle of wall friction, δ. For ϕ = 20°, pole of the log spiral is located below the wall top for all the values of δ. For ϕ = 25° it goes below the wall top for higher value of δ.

3.1. Point of application of passive thrust

One distinguishing feature of the proposed method is its ability to compute the point of application of passive thrust using moment equilibrium. This has not been possible with other existing methods. In Table 2, computed values of *H*r are shown. They vary over a very narrow range, from 0.225 (for ϕ = 20° and δ = 5°) to 0.275 (for ϕ = 40° and δ = 40°).

Table 1 - Passive earth pressure coefficients and location of pole of the log spiral.

Angle of soil friction ϕ° (degrees)		Angle of wall friction δ° (degrees)							
		5	10	15	20	25	30	35	40
20	K_p	2.780	2.967	3.142	3.298				
	ϕv°	-3.880	-9.264	-14.320	-19.065				
25	K_p	3.404	3.705	4.001	4.287	4.560			
	ϕv°	6.568	1.254	-3.800	-8.622	-13.243			
30	K_p	4.196	4.655	5.126	5.606	6.090	6.572		
	ϕv°	15.405	10.167	5.132	0.276	-4.427	-9.000		
35	K_p	5.231	5.921	6.658	7.439	8.264	9.126	10.018	
	ϕv°	23.174	18.001	12.990	8.117	3.358	-1.303	-5.888	
40	K_p	6.624	7.668	8.823	10.098	11.499	13.030	14.689	16.464
	ϕv°	30.199	25.08	20.089	15.204	10.406	5.676	0.999	-3.639

Note: Negative sign of angle θ*v* refers to pole location below the wall top (Fig. 2 (b)).

Table 2 - Variation of Hr with ϕ and δ.

Angle of soil internal friction, ϕ (degrees)	Angle of wall friction, δ (degrees)							
	5	10	15	20	25	30	35	40
	Hr = h/H							
20	0.225	0.226	0.229	0.234				
25	0.235	0.235	0.237	0.241	0.248			
30	.241	0.240	0.241	0.244	0.250	0.259		
35	0.246	0.243	0.243	0.245	0.249	0.257	0.268	
40	0.249	0.245	0.243	0.244	0.247	0.253	0.262	0.275

3.2. Distribution of reactive pressure over failure surface

Another distinguishing feature of the proposed analysis is its ability to predict the distribution of reactive pressure on the failure surface using Kötter's (1903) equation. This is shown in Fig. 6 for ϕ = 40° and δ = 30°. The pressure distribution varies linearly over the straight part of the failure surface followed by curvilinear variation over the log spiral part with a maximum ordinate at the wall base.

3.3. Comparison with other solutions

In Table 3, computed values of K_p for ϕ = 20°, 30° and 40° and δ = ϕ/2 and ϕ are compared with other available solutions and in Table 4 percentage variations in the results obtained by the proposed method in comparison with other solutions are reported.

The values computed by Coulomb's (1776) theory up to ϕ = 30° and δ = ϕ/2 are lower than the proposed values in the range 2.69 to 2.92%, and up to ϕ = 30° and δ = ϕ, they are higher than the proposed values in the range 7.29 to 53.73%. For ϕ = 40° and δ = 40°, they tend to be very high with no possible comparison.

The values reported by Chen (1975) are based on limit analysis. Up to ϕ = 40° and δ = 20°, they are lower than the proposed values in the range 0 to 13.13%, and for ϕ = 40° and δ = 40°, they are higher than the proposed values by 26.97%.

Comparison with the values, which are based on rotational log spiral failure mechanism with the upper-bound theorem of limit analysis reported by Soubra & Macuh (2002) shows that, these values are lower than the proposed values in the range 2.85 to 13.5% and higher in the range 5.48 to 22.11%.

The values reported by Caquot & Kerisel (1948) are based on limit equilibrium of a log spiral mechanism. Up to ϕ = 40° and δ = 20°, they are lower than the proposed values

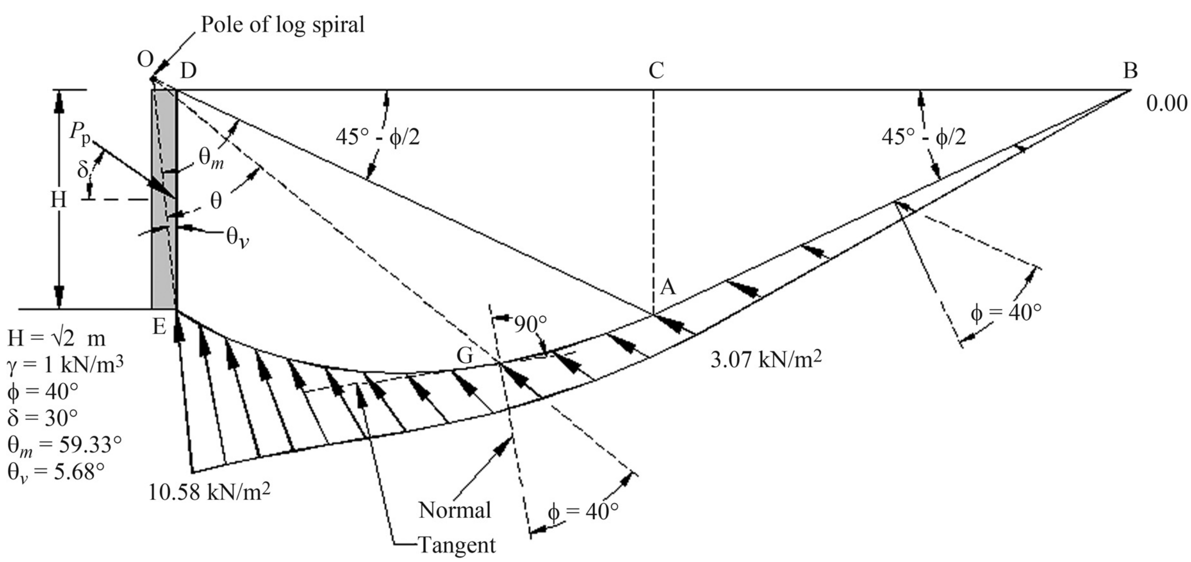

θ (degrees)	0	5	10	15	20	25	30	35	40	45	50	55	59.32
Ordinate (kN/m²)	10.58	9.16	7.96	6.93	6.07	5.35	4.75	4.26	3.87	3.56	3.33	3.16	3.07

Figure 6 - Reactive pressure distribution on the failure surface.

Table 3 - Comparison of *K*p values.

Parameters	Passive earth pressure coefficient, K_p					
Angle of soil friction, ϕ (degrees)	20		30		40	
Angle of wall friction, δ (degrees)	1/2ϕ	ϕ	1/2ϕ	ϕ	1/2ϕ	ϕ
Proposed Method	2.97	3.29	5.13	6.57	10.098	16.46
Coulomb (1776)	2.89	3.53	4.98	10.1	11.77	92.57
Caquot & Kerisel (1948)	2.60	3.01	4.50	6.42	10.36	17.5
Janbu (1957)	2.60	3.00	4.50	6.00	9.00	14.0
Sokolovski (1965)	2.55	3.04	4.62	6.55	9.69	18.2
Shield & Tolunay (1974)	2.43	2.70	4.13	5.02	7.86	11.00
Chen (1975)	2.58	3.14	4.71	7.11	10.07	20.90
Basudhar & Madhav (1980)	2.56	3.12	4.64	6.93	9.56	19.35
Kumar & Subba Rao (1997)	2.5	3.07	4.6	6.68	9.8	18.86
Soubra & Macuh (2002)	2.57	3.13	4.65	6.93	9.81	20.1
Lancellotta (2002)	2.48	2.70	4.29	5.03	8.38	11.03
Shiau *et al.* (2008) lower bound	2.50	3.02	4.38	6.58	8.79	18.64
Shiau *et al.* (2008) upper bound	2.62	3.21	4.46	7.14	10.03	20.10

in the range 2.28 to 12.45%, and for ϕ = 40° and δ = 40°, they are higher than the proposed values by 6.32%.

The values reported by Kumar & Subba Rao (1997) are based on the method of slices. Up to ϕ = 40° and δ = 20°, they are lower than the proposed values in the range 2.95 to 15.83%, and for ϕ = 40° and δ = 40°, they are higher than the proposed values by 14.58%.

The values reported by Sokolovski (1965) are based on the method of characteristics. Up to ϕ = 40° and δ = 20°, they are lower than the proposed values in the range 0.3 to 14.1% and for ϕ = 40° and δ = 40°, they are higher than the proposed values 10.57%.

Comparison with the values, which are based on limit equilibrium analysis and reported by Basudhar & Madhav (1980) shows that, these values are lower than the proposed values in the range 5.3 to 13.8% and higher in the range 5.4 to 17.5%.

With the analytical solution based on the lower bound theorem of plasticity, the K_p values as reported by Lancellotta (2002) are lower than the proposed values in the range 16.37 to 32.98%.

The K_p values reported by Shiau *et al.* (2008) using lower bound theorem coupled with finite element formulations of limit analysis and nonlinear programming techniques, are lower than the proposed values in the range 0.15 to 35.35% .The values obtained using upper bound theorem are lower than the proposed values in the range, 0.67 to 13.06% up to ϕ = 40° and δ = 20°. For ϕ and δ = 30° and ϕ and δ values of 40° and 40°, they are higher than the proposed values in the range, 8.67 to 22.11%. The possible reason for the proposed values being higher than the upper and lower bound values reported by Shiau *et al.* (2008) can be explained with the observation that, the failure surface changes from nearly a straight one to the one consisting of curved part followed by a straight line in Shiau's *et al.* (2008) method whereas, it is always a log-spiral followed by a tangent in the proposed analysis. Considering practical situations with wall friction angle in the range of one half to two third of the soil friction angle, the proposed value of K_p for δ = 1/2ϕ (ϕ = 40°) is higher by only 0.67% than the upper bound solution of Shiau *et al.* (2008). For for δ = 2/3ϕ, the proposed K_p value is higher by 6.15% than the lower bound solution and lower by 6.79% than the upper bound solution of Shiau *et al.* (2008).

Similarly, the K_p values as reported by Janbu (1957) which are based on limit equilibrium analysis are lower than the proposed values in the range 8.7 to 14.95%.

The values of K_p as reported by Shields & Tolunay (1973) are also based on limit equilibrium analysis. These values are lower than the proposed values in the range, 17.93 to 33%.

The above comparison shows that proposed values are fairly close to some of the available solutions, except those of Shields & Tolunay (1973) and Lancellotta (2002).

In Table 4, more data giving K_p values computed by Coulomb's theory (1776), Caquot & Kerisel (1948), Kumar & Subba Rao (1997), Soubra & Macuh (2002), Lancellotta (2002) and by the proposed method is reported.

It may be noted that, for the failure mechanism consisting of log spiral and its tangent, which is adopted in the proposed analysis, the K_p values are unique; since they are evaluated from the identification of a unique failure surface that satisfies force equilibrium conditions. This may be the

Table 4 - Comparison of K_p values.

Angle of friction (degrees)		Passive earth pressure coefficient *Kp*										
		Coulomb (1776)		Caquot & Kerisel (1948)		Kumar & Subba Rao (1997)		Soubra & Macuh (2002)		Lancellotta (2002)		Proposed method
Soil ϕ	Wall δ	K_p	% diff.	K_p	% diff.	K_p	% diff.	K_p	% diff.	K_p	% diff.	K_p
20	0	2.04	-21.5	2.04	-21.5	2.04	-21.5	2.04	-21.5	2.04	-21.5	2.60
25		2.46	-20.5	2.46	-20.6	2.46	-20.6	2.46	-20.6	2.46	-20.5	3.10
30		3.00	-18.9	3.03	-18.1	3	-18.9	3.00	-18.9	3.00	-18.9	3.70
35		3.69	-19.8	3.69	-19.8	3.69	-19.8	3.69	-19.8	3.69	-19.8	4.60
40		4.60	-19.3	4.59	-19.5	4.6	-19.3	4.60	-19.3	4.60	-19.3	5.70
20	1/3ϕ	2.41	-15.1	2.35	-17.4	2.38	-16.3	2.39	-16.0	2.35	-17.4	2.84
25		3.12	-13.3	3.03	-16.0	3.06	-15.1	3.07	-14.8	2.99	-17.0	3.61
30		4.14	-11.0	4.00	-14.1	4.02	-13.6	4.03	-13.4	3.89	-16.5	4.66
35		5.68	-7.8	5.28	-14.3	5.42	-12.0	5.44	-11.7	5.17	-16.1	6.16
40		8.15	-3.3	7.25	-13.9	7.58	-10.0	7.62	-9.6	7.09	-15.9	8.43
20	1/2ϕ	2.64	-11.2	2.60	-12.4	2.5	-15.7	2.57	-13.4	2.48	-16.5	2.97
25		3.55	-7.8	3.40	-11.8	3.4	-11.8	3.41	-11.5	3.22	-16.4	3.85
30		4.98	-2.9	4.50	-12.2	4.6	-10.3	4.65	-9.3	4.29	-16.3	5.13
35		7.36	4.5	6.00	-14.8	6.6	-6.3	6.59	-6.4	5.88	-16.5	7.04
40		11.8	16.6	9.00	-10.9	9.8	-3.0	9.81	-2.9	8.38	-17.0	10.10
20	2/3ϕ	2.89	-6.4	2.65	-14.1	2.73	-11.5	2.75	-10.9	2.58	-16.3	3.09
25		4.08	-0.4	3.56	-13.1	3.72	-9.2	3.76	-8.2	3.41	-16.7	4.10
30		6.11	8.9	5.00	-10.8	5.26	-6.2	5.34	-4.7	4.63	-17.4	5.61
35		9.96	24.8	7.10	-11.1	7.78	-2.5	7.95	-0.4	6.51	-18.5	7.98
40		18.7	56.0	10.7	-10.6	12.24	2.0	12.6	5.0	9.57	-20.2	12.00
20	ϕ	3.53	7.1	3.01	-8.5	3.07	-6.7	3.13	-4.9	2.70	-18.0	3.29
25		5.60	22.8	4.29	-5.9	4.42	-3.1	4.54	-0.4	3.63	-20.5	4.56
30		10.1	53.6	6.42	-2.3	6.68	1.6	6.93	5.4	5.03	-23.5	6.57
35		22.9	129	10.2	1.8	10.76	7.4	11.3	12.8	7.25	-27.6	10.02
40		92.6	462	17.5	6.3	18.86	14.6	20.1	22.1	11.03	-33.0	16.46

Percentage difference = (100 x (value obtained by other solution-value obtained by proposed method)/value obtained by proposed method).

possible reason for the variation in results obtained by the proposed method when compared to the other available solutions. The proposed method also enables the computation of point of application of passive thrust using moment equilibrium and reactive pressure distribution on the failure surface.

4. Conclusion

A method based on the application of Kötter's (1903) equation is proposed for the complete analysis of passive earth pressure on a vertical wall retaining horizontal cohesionless backfill. Kötter's (1903) equation lends itself as a powerful tool in the analysis and the results show a close agreement with some of the available solutions.

Kötter's (1903) equation facilitates identification of the unique and only possible failure surface (log-spiral followed by its tangent) using the force equilibrium conditions. The value of computed passive pressure co-efficient is therefore a unique one that can be obtained using limit equilibrium method. Another advantage of the proposed method is its ability to compute the point of application of the passive thrust using moment equilibrium which. Thus all the equations of equilibrium are effectively used in the proposed method. The distribution of soil reactions on the failure surface is also computed.

References

Balla, A. (1961) The resistance to breaking out of mushroom foundations for pylons. Proc of the 5th Int. Conf. on Soil Mechanics and Foundation Engineering, Paris, France, v. 1, pp. 569-576.

Basudhar, P.K. & Madhav, M.R. (1980) Simplified passive earth pressure analysis. Journal of the Geotechnical Engineering Division, ASCE, v. 10:GT4, p. 470-474.

Brinch Hansen, J. (1953) Earth pressure calculation. The Danish Technical Press. The Institution of Danish Civil Engineers, Copenhagen, 271 pp.

Caquot, A.I. & Kerisel, J. (1948) Tables for the Calculation of Passive Pressure, Active Pressure, and Bearing Capacity of Foundations. Libraire du Bureau des Longitudes, de L'ecole Polytechnique. Gauthier-Villars, Paris, 120 pp.

Chen, W.F. (1975) Limit Analysis and Soil Plasticity. Elsevier Science publishers, BV, Amsterdam, The Netherlands, pp. 111-146

Coulomb, C.A. (1776) Essais sur une application des regles des maximis et minimis a quelques problems de statique relatits a architecture. Mem. Acad. Roy. Pres. Divers, Sav., Paris, v. 7, p. 343-382.

Dewaikar, D.M. & Mohapatro B.G. (2003) Computation of bearing capacity factor N_γ- Terzaghi's mechanism. Int. J. Geomech., ASCE, v. 3:1, p. 123-128.

Janbu, N. (1957) Earth pressure and bearing capacity calculations by generalized procedures of slices. Proc. 4th Int. Conf. on Soil Mechanics and Foundation Engineering, London, v. 2, p. 207-212.

Kumar, J. & Subba Rao (1997) Passive pressure coefficients, critical failure surface and its kinematic admissibility. Geotechnique, v. 47:1, p. 185-192.

Kerisel, J. & Absi, E. (1990) Active and Passive Earth Pressure Tables. Balkema, Rotterdam, 220 pp.

Kötter, F. (1903) Die Bestimmung des Drucks an gekrümmten Gleitflächen, eine Aufgabe aus der Lehre vom Erddruck Sitzungsberichte der Akademie der Wissenschaften. Berlin, p. 229-233.

Lancellotta, R. (2002) Analytical solution of passive earth pressure. Géotechnique, v. 52:8, p. 617-619.

Matsuo, M. (1967) Study of uplift resistance of footings: I. Soils and Foundations, v. 7:4, p. 1-37.

Morgenstern, N.R. & Eisenstein, Z. (1970) Methods of estimating lateral loads and deformations. Proc. ASCE Speciality Conf. on Lateral Stresses in the Ground and Design of Earth-Retaining Structures, Ithaca, pp. 51-102.

Rankine, W. (1857) On the stability of loose earth. Philosophical Transactions of the Royal Society of London, v. 147, p. 9-27

Shiau, J.S.; Charles, E.A.; Andrei, V.I. and Sloan, S.W. (2008) Finite element limit analysis of passive earth resistance in cohesionless soils. Japanese Geotechnical Society, Soils and Foundations, v. 48:6, p. 843-850.

Shields, D.H. & Tolunay, A.Z. (1973) Passive pressure coefficients by method of slices. Journal of the Soil Mechanics and Foundations Division, ASCE, v. 99:SM12, Proc. Paper 10221, p. 1043-1053.

Sokolovski, V.V. (1965) Statics of Granular Media. Pergamon, Oxford, 270 pp.

Soubra, A.H. & Macuh, B. (2002) Active and passive earth pressure coefficients by a kinematical approach, Proc. of the Institution of Civil Engineers and Geotechnical Engineering., v. 155:2, p. 119-131.

Terzaghi, K. (1943) Theoretical Soil Mechanics. Wiley and Sons, New York, 510 pp.

Technical Note

Soils and Rocks
v. 34, n. 3

The Use of Hydrophobic and Hydrophilic Tensiometers in the Measurement of Water and NAPL Suctions and Determination of SLRC

R.P. Sousa, I.B. Oliveira, S.L. Machado

Abstract. This technical note presents some preliminary results obtained with the use of hydrophobic and hydrophilic tensiometers to measure liquid pressures in three-phase systems (air-NAPL-water). The porous tips of the hydrophobic tensiometers underwent a surface treatment known as silanization. The silanized tensiometers demonstrated little influence of the interstitial water in the measured values of NAPL suctions, the contrary occurring in the case of the standard ones. Due to water preferential wetability, the water tensiometers with standard porous stone tips presented adequate hydrophilic behavior, measuring water suctions satisfactorily. These tensiometers were also used to determine the soil-liquid retention curves (SLRC) of an eolian sand by vaporization. Water and diesel were used in the performed tests. The performance of the vaporization technique was satisfactory, reducing the time required for test accomplishment and presenting repeatable results. In the case of diesel, due its low vapor pressure and the selective nature of its vaporization process, the use of this technique was shown to be limited. Sample heating was used to accelerate the vaporization process.

Keywords: vaporization technique, soil-liquid retention curves, NAPL, multiphase flow.

1. Introduction

Multiphase flow normally involves several processes that occur simultaneously in the soil during the transport of a non aqueous phase liquid (NAPL) from the soil surface to the water table. NAPLs are divided into two groups: Those denser than water (DNAPL) and those lighter than water (LNAPL). During LNAPL migration when the water table is reached, there in an accumulation and posterior spreading of the liquid in the contact between the two phases. Contrarily, DNAPL moves continuously down (below the water table) until an impervious layer is found. The main phenomena occurring during NAPL transport through the subsoil are: free phase flow (NAPL flow as a separate liquid phase), NAPL free phase adsorption/desorption by the soil solid particles, dissolution and transport of the NAPL soluble part (which in its turn involves adsorption, advection and diffusion) and volatilization and transport of the NAPL vapor involving the same phenomena cited above.

One of the most important aspects of NAPL transport is the NAPL free phase flow from soil surface to water table across the vadose zone or the unsaturated layer of soil. This layer acts naturally protecting the water table from NAPL contamination and the adoption of remediation techniques before NAPL reaches the saturated zone always leads to less expensive remediation procedures.

On the other hand, unfortunately, the simultaneous transport of three or more liquid phases in unsaturated soils is a complex matter. Liquid distribution inside soil pores will be a function of their wettability order which in turn can vary with the amount of organic matter in the soil as it is a function of the ranking of the superficial tension values of the liquids involved in the process. Water usually presents the highest values of superficial tension when in contact with most mineral surfaces whereas NAPL presents higher values of superficial tension when in contact with organic surfaces. In the case of unsaturated soils with a negligible organic content, wettability order is water-NAPL-air (more to less wettable). In the case of soils presenting high amounts of organic matter the wettability order changes and we have NAPL-water-air. As the water has the highest wettability in most cases involving multiphase flow, it tends to occupy the smaller pores of the soil. NAPL tends to occupy the remaining spaces and the interstitial air fills only the larger voids in the soil. As a consequence, the concept of suction must be extended in comparison to traditional unsaturated soil mechanics. At least two values of suction can be adopted: one calculated as the difference between the pressures of NAPL and water and the other considering the pressures of air and NAPL.

As regards the suctions of water and NAPL due to capillarity effects, not only is the water superficial tension important but also the NAPL superficial tension and the

R.P. Sousa, PhD Student, Programa de Engenharia Industrial, Universidade Federal da Bahia, 2 Aristides Novis St. 40210-630 Salvador, BA, Brazil. e-mail: riseuda.sousa@gmail.com.
I.B. Oliveira, PhD, Associate Professor III, Departamento de Engenharia Ambiental, Universidade Federal da Bahia, 02 Aristides Novis St. 40210-630 Salvador, BA, Brazil. e-mail: oliveira@ufba.br.
S.L. Machado, PhD, Associate Professor III, Departamento de Tecnologia e Ciência de Materiais, Universidade Federal da Bahia, 2 Aristides Novis St. 40210-630 Salvador, BA, Brazil. e-mail: smachado@ufba.br.
Submitted on September 29, 2010; Final Acceptance on February 14, 2011; Discussion open until April 30, 2012.

tension in the interface NAPL-Water. Besides this, NAPL normally presents a low dielectric constant (ε_r) or low polarity compared to water (ε_{rw} = 80 and ε_{rnapl} ~ 2). In this case, the thickness of the NAPL double layer is smaller due to a less pronounced electrical attraction between the solid particle surface in the NAPL molecules. Therefore it can be said that the adsorption phenomena will be much more pronounced in the case of water than NAPL.

In order to model water unsaturated flow the hydraulic conductivity and soil-water retention curves of the soil must be known. The model proposed by Van Genuchten (1980) is most commonly used model to represent the soil-water retention curve. Despite the fact that this model does not address the possibility of completely dry soil, as in the model of Fredlund & Xing (1994), it is simple and can be used for the values of suction normally found in the field. In the case of problems involving shallow depths in dry and hot climates and/or very low water content values, however, the use of the Fredlund & Xing (1994) equation becomes more attractive.

$$\theta = \theta_r + \frac{\theta_s - \theta_r}{\left[1+(\alpha\psi)^n\right]^m} \tag{1}$$

where θ is the soil volumetric water content; θ_r (-) is the soil residual volumetric water content; θ_s (-) is the soil saturated volumetric water content, ψ is the water suction (kPa) and n (-), m (-), and α (kPa^{-1}) are soil parameters.

From a historical perspective, the physics of three phase flow on porous media has appeared in the petroleum reservoir literature. These models are used to model oil and natural gas recovery from petroleum reservoirs (Collins, 1961; Corey, 1986, Aziz & Settari, 1979 and Marle, 1981). Due to the arduous experimental procedures to determine truly multiphase soil-liquid retention curves (SLRC), several attempts have been made to transform one curve obtained for a pair of liquids (mostly air-water) to a multiphase curve or to one of the possible two phase systems (air-NAPL or NAPL-water). In many cases in such situations the Van Genuchten (1980) equation is employed.

Capillary scaling is the most common idea used to transform one soil-liquid retention curves into another one. Lenhard & Parker (1988) and USEPA (1997) present some scaling rules to transform soil-liquid curves from one pair of fluids to multiphase curves. In the case of USEPA (1997), the main assumptions are listed below. Equations (2) and (3) define the suctions involving the immiscible phases of the system

$$\psi_{nw} = \psi_{nw}(\theta_w) = u_n - u_w \tag{2}$$

$$\psi_{an} = \psi_{an}(\theta_{tw}) = u_a - u_n \tag{3}$$

In these equations, the subscripts *a, w* and *n* stand for the phases air, water and NAPL, respectively. θ_{tw} (-) means the total volumetric content of liquids (water and NAPL) in the system. u_a, u_w and u_n (kPa) are the interstitial pressures of air, water and NAPL, respectively. It can be noted from Eq. (3) that the suction between the phases air and NAPL is a function of θ_{tw}. This equation brings implicitly the idea of wettability of the phases. As NAPL has intermediate wettability, in soil pores with water and NAPL, NAPL will be in contact with the interstitial air. Water will preferentially occupy the inner part of the pore and/or the the smaller pores of the soil. In this case, the radius of the air-NAPL meniscus will be a function of the total amount of liquids, which is represented by θ_{tw}.

The suction air-water is calculated using Eq. (4). Besides this, the values of suction between the immiscible phases are scaled using the values of interfacial tensions along the interfaces between the air and water phases (σ_{aw}), the NAPL and water phases (σ_{nw}) and the air and NAPL phases (σ_{an}), according to Eq. (5) (Leverett, 1941).

$$\psi_{aw} = \psi_{an} + \psi_{nw} \tag{4}$$

$$\frac{\psi_{aw}}{\sigma_{aw}} = \frac{\psi_{an}}{\sigma_{an}} + \frac{\psi_{nw}}{\sigma_{nw}} \tag{5}$$

In order for Eqs. (4) and (5) to be compatible, another assumption must be made which is represented by Eq. (6). As can be seen, the interfacial tension air-water (or the water superficial tension) is assumed to be equal to the sum of the interfacial tensions NAPL-water and air-NAPL.

$$\sigma_{aw} = \sigma_{an} + \sigma_{nw} \tag{6}$$

The wettability order used in this paper is controversial among some authors such as Bradford & Leij (1995 and 1996), mainly due to the fact that NAPL is a mixture of many different chemicals and/or when the soil is mineralogically heterogeneous and contains a significant amount of organic matter. In this case of the experiments performed by the authors a 5% solution of octadecyltrichlorosilane, OTS, in ethanol was added to a sand (25% fine, 50% medium and 25% coarse) to form a totally hydrophobic medium, which was mixed in different proportions with pure sand in order to form a medium with fractional wettability. The constraints of the Eqs. (4) to (7) are also questioned by authors such as Wilson *et al.* (1990) and McBride *et al.* (1992).

Using the aforementioned assumptions the equations below summarize some of the possibilities of the use of the capillary scaling to enable Eq. (1) to be used in the case of multiphase flow.

$$\theta_w = f(\psi_{nw}) = \theta_{wr} + \frac{\theta_s - \theta_{wr}}{\left[1+(\alpha\psi_{nw})^n\right]^m} \tag{7}$$

$$\theta_{tw} = f(\psi_{an}) = \theta_{twr} + \frac{\theta_s - \theta_{twr}}{\left[1+(\alpha\psi_{an})^n\right]^m} \tag{8}$$

where θ_w (-) is the volumetric content of water (the same of θ in Eq. (1)); θ_{nw} (-) is the volumetric content of NAPL; θ_{tw} (-) is the volumetric content of liquids (water + NAPL); θ_{wr} (-) is the residual volumetric content of water; and θ_{twr} (-) is the residual volumetric content of liquids (water + NAPL).

The value of the volumetric water content of air, θ_a (-) is obtained using the equation below:

$$\theta_a = n - \theta_{tw} \tag{9}$$

where n (-) is the soil porosity.

Table 1 presents the values of interfacial tension of some liquids. As can be noted the interfacial tension air-liquid (also called superficial tension) of the NAPLS are about one third of the value obtained for water. On the other hand, comparing the values of interfacial tensions air-liquid and NAPL-water the assumption embodied in Eq. (6) is only fairly fulfilled in the case of benzene and toluene. In the case of diesel which is a mixture of different chemicals Eq. (6) can not be applied.

Several experimental methods have been proposed and reported to determine the soil-water retention curves in bi-phase systems (Machado & Dourado, 2001, Lenhard & Parker, 1988; Mahler & Oliveira, 1998; Feuerharmel *et al.* 2004, Oliveira & Marinho, 2008, Fredlund & Rahardjo, 1993, etc.). Axis translation and its variations is still the most widely spread technique used to determine the soil-water retention curve, however, some other techniques such as osmotic devices, air relative humidity and temperature control, paper filter and vaporization techniques have gained attention in recent years. Vaporization (or evaporation) are techniques where soil is left to evaporate its liquid content in a controlled way. The attention of many researchers has focused on the case of the determination of SLRC using materials with a high vapor pressure. According to Oliveira (1995), in sandy soils, the combination of the vaporization technique and the use of contact tensiometers for soil suction measurements resulted in similar results to those obtained using *tempe cells*. In this case, only bi-phase systems (air-NAPL and air-water) were used. The interstitial liquids were water, ethylene glycol, 4-clorotoluene and n-hexanol. With the use of the vaporization technique the time required to finish the tests was reduced substantially.

In the case of multiphase systems, however, using the axis translation technique or otherwise, there is the need for an additional medium to separate the interstitial pressures of water and NAPL. This is normally achieved transforming a standard (hydrophilic) porous medium, such as a high entry value ceramic disk, into a hydrophobic one. The silanization technique is one of the alternatives to perform this conversion, as described by Lenhard & Parker (1988).

Table 1 - Values of interfacial tension of some liquids.

Liquid	Air-liquid interfacial tension (dynes/cm)	NAPL-water interfacial tension (dynes/cm)
Benzene	28.9 (20 °C)	35.0(25 °C)
Toluene	29.0 (20 °C)	36.1(25 °C)
Diesel	26.9 (25 °C)	22.3 (25 °C)
Water	71.97 (25 °C)	-

This paper presents the performance of hydrophilic and hydrophobic contact tensiometers of small dimensions, developed by the authors, used to measure interstitial pressures of water and NAPL (Diesel) in a multiphase flow system. Contact tensiometers, saturated with oil and water, were also used in the vaporization technique in order to obtain SLRC in an eolian sand. The obtained results are compared with the results provided by Eqs. (4) to (8).

2. Materials and Methods

The soil used was a uniform eolian sand, typical of the dunes found around Salvador, Bahia (coast material, quaternary age). The physical properties of the dune were obtained using the following Brazilian Standards: NBR 6457/1986, NBR 6502/1995, NBR 6508/1984, NBR 13292/1995 and NBR 7181/1984. Samples presented average values of porosity n = 0.37, 100% of sand fraction (mainly fine to medium sand) and unit weight of solid particles ρ_s = 2.68 g/cm^3. Soil samples were classified as SP (poor graded in the USCS). Liquids used in the performed tests were water and diesel. Table 2 summarizes the main properties of interest of the liquids used. Interfacial tensions are given in Table 1.

Average values of fluid conductivity (k) were k = 1.2 x 10^{-2} cm/s (water) and k = 4.34 x 10^{-3} cm/s (Diesel). These values are compatible with the concept of intrinsic permeability of Nutting (1930).

$$k = \frac{K \cdot \rho \cdot g}{\mu} \tag{10}$$

where K is the soil intrinsic permeability [L^2], ρ is the fluid density [ML^{-3}], μ is the fluid dynamic viscosity [$ML^{-1}T^{-1}$] and g is the gravity acceleration [LT^{-2}].

Table 2 - Main liquid properties.

Liquid	ρ (g/cm^3)	μ (cp)	Vapor pressure, 20 °C (mmHg)	ε (-)	Water solubility (mL/L)
Water	1.00	1.00	17.535	80.0	∞
Diesel	0.83	3.75	< 5	2,31	298

Vaporization tests used two different types of vaporization cells. In the first set of tests a stainless vaporization cell was used similar to that used by Oliveira (1995), with nominal internal dimensions of 50 x 20 mm. Standard tensiometers, saturated with oil or water, were employed. The pressure transducers used had a pressure range of 0-100 kPa (absolute pressure) and the porous stone tips of the tensiometers had an air entry value of 100 kPa (Model 0604D04-B01M1, Soilmoisture Equipment Corp.). Tensiometers had an internal chamber of about 200 mm^3. Due to their relatively large inner chamber they are able to sustain suctions only up to 70 kPa. Figure 1 presents the cell and tensiometers used in the first set of tests. The maximum time interval for suction measurement stabilization was about 10 min (suctions of 8 and 16 kPa were applied to the water reservoir containing the tensiometer porous tip). The obtained time-response curves were considered satisfactory taking into account the vaporization rate of the experiments. All the tensiometers were saturated (with water or Diesel) under vacuum before tests in a vacuum chamber designed specially for this purpose. Figure 2 presents details of the developed tensiometers. The picture below shows the coupling of the pressure transducer to the tensiometer tip and its cross section, the ceramic tips used and the coupling of the tensiometers to the flow channel (not used in this technical note).

Soil samples were statically compacted in thin layers of 2 mm in the vaporization chamber until desired dry density was reached (ρ_d = 1.69 g/cm^3). Sample saturation was carried out by the use of vacuum pressure and a drip of the desired liquid. This procedure was adopted to fully saturate

Figure 1 - Vaporization chamber used in the first set of tests, tensiometer and porous tip.

the samples before the tests. During the performed tests samples were exposed to the atmosphere in a chapel with exhaustion, allowed to evaporate its liquid content for some period, weighed and then closed using the cell cover. The tensiometer was then placed in contact with the sample until the suction measurement stabilized. This process was repeated until the evaporation rate became negligible. As the evaporation rate decreased during the test, the periodicity of the readings at the beginning of the tests was higher. Similar procedures were used for both water and diesel.

In the case of the diesel however, the evaporation rate became negligible even with the sample clearly presenting high values of saturation. A process of selective evapora-

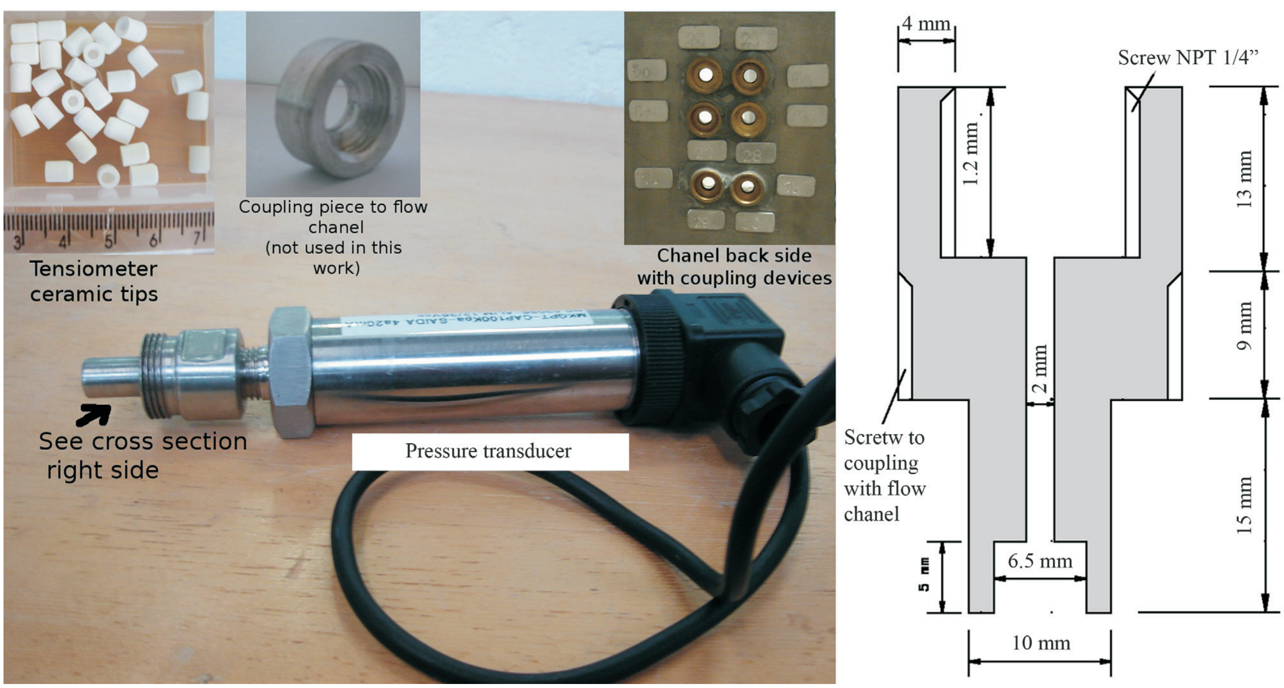

Figure 2 - Details of the tensiometer tip and couplings with pressure transducer and flow channel.

tion of the diesel components was observed in such a way that this product changed its characteristics during the evaporation process, decreasing its vapor pressure drastically and almost ceasing the evaporation process. In order to increase the vapor pressure of the remaining diesel components, soil samples were submitted to progressive heating up to 220 °C. During this process, for each heating step, samples were cooled and weighed and the suction measured as described above.

A second set of tests used the apparatus illustrated in Fig. 3. In this case both standard and silanized tensiometers were used. The silanization process modifies the surface of silica and metal oxides with the introduction of a layer chemically bonded to the substrate. There are many silanization techniques, however, the organic silanization in anhydrous conditions is the most commonly used for silica modification. Although there is the possibility that some parts of the porous stone surface are not accessible to the silanization agent, this process is considered irreversible and the hydrophobic nature of the transformed porous stone is considered permanent (Lenhard & Parker, 1988 and Kecharvazi *et al.* 2005)

In this paper, the silanization process was similar to that proposed by Lenhard & Parker (1988). After heating the porous stones for water removal (100 °C, 24 h), they were cooled to environment temperature in a dissector and then immersed in chloretrimetilsilane (PA; 98%), in an hermetic chamber for two hours. After this samples were washed with toluene (PA; 99.5%) and methanol (PA; 99,9%).

The apparatus used to perform the multiphase tests is composed of a Nylon cell with internal nominal dimensions of 50 mm x 6 mm, a balance and a pair of tensiometers, one saturated with water and the other with oil, which was installed to measure the interstitial pressures. Two types of tensiometers saturated with oil were used, with silanized and standard tips. The idea was to observe the benefits of the silanization technique in the tensiometers performance. The compaction process was similar to that used in the first set of tests, however, in the case of the second set of tests the evaporation process was carried out continuously as well as the suction and mass measurements.

Figure 3 - Multiphase system suction measurement.

Samples were first saturated by water and then submitted to vaporization. One experiment of the second set of tests was performed keeping the room closed while the other was performed with all the windows of the room open (better ventilation conditions).

After the desired water suction was reached, samples were saturated with oil and the changes in the interstitial pressures were recorded. The water suction measurements made during the water vaporization stage were also used to obtain the soil-water retention curve of the samples.

3. Results and Discussion

Figure 4 presents the soil-water retention curves obtained using the two vaporization cells used in the tests. As can be observed, all the samples presented similar results, showing the equivalence of the techniques used. Figure 4 also shows the fitting of Eq. (1) to experimental results. Minimum square method was used in the fitting process. The obtained soil parameters were $\theta_s = 0.37$, $\theta = 0.25$ kPa^{-1}, $\theta_r = 0.0004$, $m = 0.77$ and $n = 4.38$ ($R^2 = 0{,}99$). Figure 5 presents soil-liquid retention curves obtained for water and diesel.

As can be observed, diesel experimental points are located to the left of the average water curve. This had been expected since according to Eq. (5) and data presented in Table 1, due to the smaller air-diesel superficial tension compared to water, smaller suction values are expected for the same liquid content. Due to the nature of the soil used

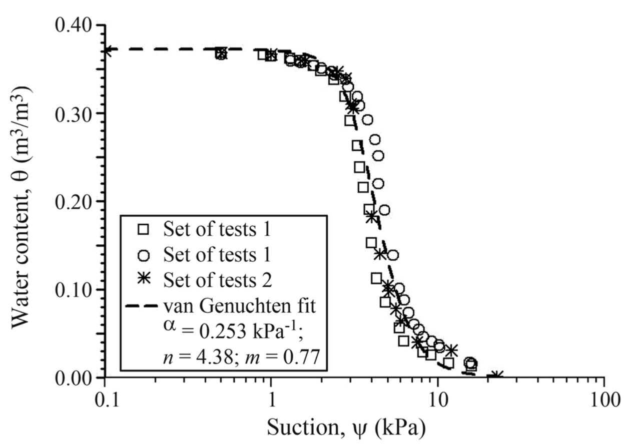

Figure 4 - Soil water retention curves using the two vaporization cells.

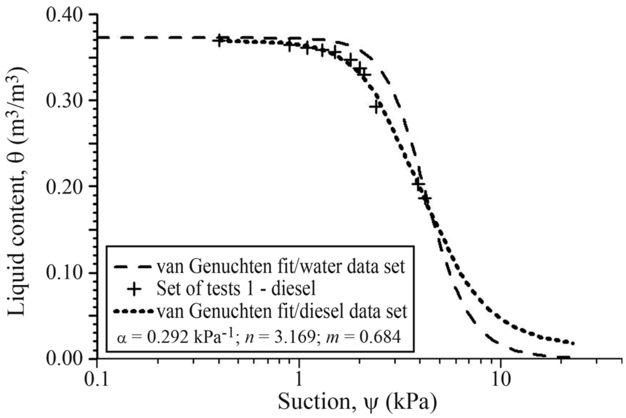

Figure 5 - Soil-liquid retention curves for water and Diesel.

(an eolian medium to fine sand) the influence of the adsorption phenomena in the soil suction values is considered negligible. Figure 5 also shows the fitting of Eq. (1) to experimental results. The obtained soil parameters were $\theta_s = 0.37$, $\theta = 0.29$ kPa^{-1}, $\theta_r = 0.012$, $m = 0.684$ and $n = 3.17$ (R^2 = 0,99). Figure 6 presents the fitted SLRC (diesel and water) and the soil-diesel curve estimated using Eq. (5) (capillary scaling).

As can be observed, the use of the capillary scaling concept did not expected reasonable results. The observed reduction in the interstitial suction was much less than previewed by the use of Eq. (5). It must be noted that the capillarity scaling technique assumes suction as proportional to fluid superficial tension (air-liquid interfacial tension values shown in Table 1).

As the tested samples presented similar physical indexes and the soil structure is not a matter of concern because of the soil texture, other reasons must be found to justify the observed experimental results. One possible explanation for such behavior is that diesel is a mixture of compounds with varying vapor pressures. Therefore the evaporation process is selective and only the compounds with very low vapor pressures remain in the soil. After about a 30% reduction in the initial degree of saturation, the interstitial fluid of the soil becomes much more viscous than the original diesel used for sample saturation and its color is clearly changed. These findings are in accordance with previous observations made by Bradford & Leij (1995 and 1996) concerning the use of capillary scaling.

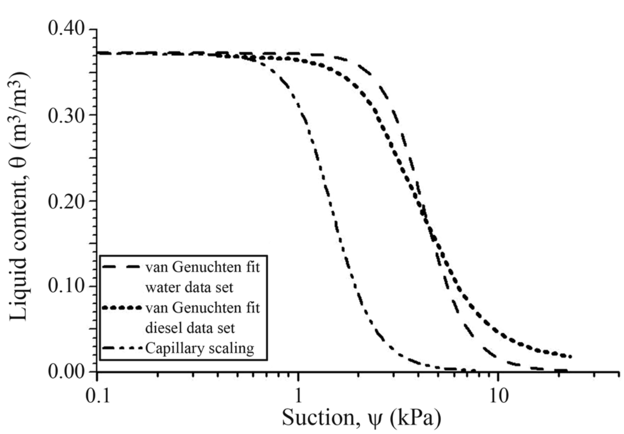

Figure 6 - Fitted soil-liquid retention curves and soil-Diesel capillary scaling curve (use of Eq. (5)).

Table 3 illustrates how the diesel interfacial tension changes as a function of the amount of liquid already evaporated (ESTC, 1997). All the presented values refer to a temperature of 25 °C. As can be observed from Table 3, air-liquid interfacial tension tends to increase with the evaporation process, the opposite occurring with the NAPL-water interfacial tension. Furthermore, according to (ESTC, 1997), diesel viscosity remained almost constant for 25 °C. For values of temperature of 0 °C and 15 °C however, viscosity increased with the evaporation process. Volatile Organic Compounds decreased from 17793 ppm (about 1.8%) to 272 ppm when the diesel evaporated 14%.

The data presented in Tables 1 and 3 help to understand why capillary scaling seems to fail in the case of diesel. Not only is Eq. (6) not satisfied, considering the fluid with its original characteristics, but the liquid also changes its interfacial tensions as the evaporation process progresses.

Despite these experimental aspects the evaporation technique proved to be very useful and repeatable and reduced the time required to carry out the experiment accomplishment. This is particularly true in the case of fluids having high vapor pressures. In the first set of tests, the average time required to carry out the tests was about 5 days (soil water retention curve). In the second set of tests, the experiment performed keeping the room closed lasted about 90 h while the experiment performed with better ventilation conditions required about 24 h to complete. In the case of clayey soils, however, due its lower fluid conductivity, the time required to finish the tests must be higher and the replacement of the used tensiometers for micro-tensiometers, which are able to sustain values of suction higher than 70 kPa without cavitation is mandatory. Figures 7 and 8 present the performance of the tensiometers used in the second set of tests. As mentioned before, in this case samples were first saturated with water and then submitted to continuous vaporization until the desired value of suction was reached. After that, samples were saturated with diesel.

Table 3 - Changes in some diesel properties in function of the progress of the evaporation process.

Diesel evaporation (%)	Air-liquid interfacial tension (dynes/cm)	NAPL-water interfacial tension (dynes/cm)
0	26.9	22.3
8	27.2	20.9
14	27.4	19.8

Source: ESTC (1997).

In the case of Fig. 7, the tensiometer used had a standard porous tip. As can be observed, in the first phase of the test (water evaporation), the oil tensiometer measured similar results of suction compared with the tensiometer saturated with water (the observed differences in the first part of the experiment can be credited to the fact that tensiometers are located in different parts of the samples and that the vaporization and sample compaction are not completely uniform). In other words, the tensiometer tip behaved hydrophilically. After oil injection in the system, the suction values in the oil tensiometer drop immediately while the suction recorded in the water tensiometer presented a decrease over time.

When the tensiometer with the silanized tip (saturated with diesel) is used (Fig. 8), it is almost insensitive to water suction, presenting only a slight increase in the suction (less than 10% of the water suction) as the water evaporation process progressed. This indicates that the silanization process used was not 100% efficient.

After diesel injection the suction in the silanized tensiometer reduced to zero, while the water suction reduced from 47.2 kPa to 7 kPa. This reduction was higher than predicted by the use of Eq. (5) (NAPL-water interfacial tension is about 22.3 dynes/cm, which should produce a NAPL-water suction of about 14.64 kPa after sample saturation with oil).

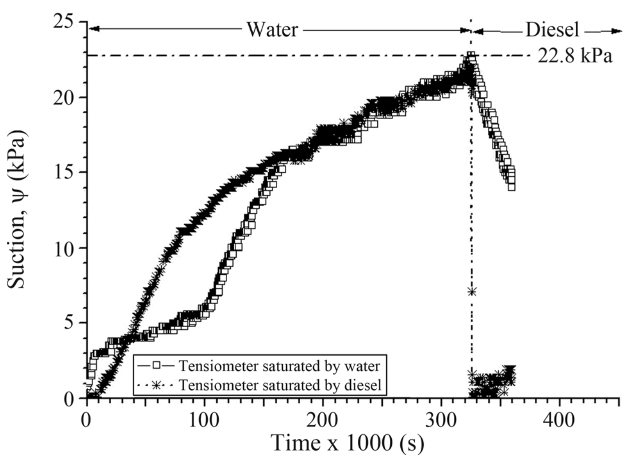

Figure 7 - Performance of the tensiometers with standard porous tip.

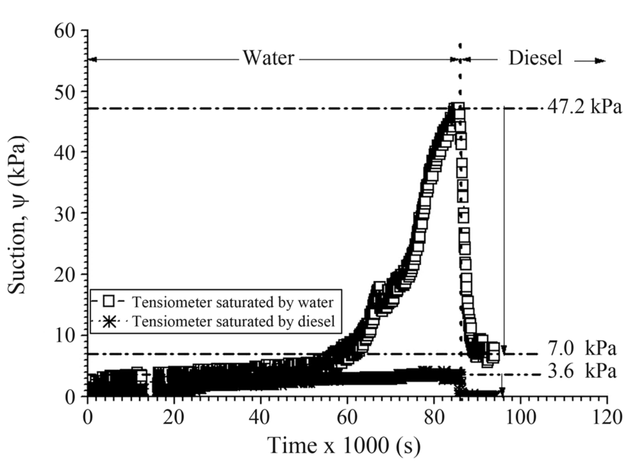

Figure 8 - Performance of the tensiometers with the silanized tip.

Analyzing the results presented in Figs. 5, 6 and 8 and considering the capillary scaling rule valid for this soil, the diesel used in the tests behaves as if it has a higher superficial tension (air-diesel interfacial tension) and a lower diesel-water interfacial tension than values presented in Table 3. These differences can be related to the selective nature of the diesel vaporization process which changes its interfacial tensions over time or simply to a different characteristic of Brazilian diesel.

4. Final Remarks

This technical note presents some preliminary results obtained with the use of the vaporization technique to obtain soil-liquid retention curves. Despite some problems due to the diesel selective evaporation process, the evaporation technique proved to be very useful and repeatable and reduced the required time for SLRC determination. This technique can be easily adapted for use in clayey soils, replacing the used tensiometers for micro-tensiometers, which are able to sustain values of suction higher than 70 kPa without cavitation.

In the second set of tests, the silanized tensiometers suffer little influence of the water suction, the contrary occurring in the case of the standard tips. Due to the water preferential wettability, water tensiometers presented satisfactory hydrophilic behavior in measuring water suction.

References

ABNT (1984) Solo - Determinação de Limite de Plasticidade, NBR 7180. Associação Brasileira de Normas Técnicas, Rio de Janeiro, Brasil, 3 pp.

ABNT (1984) Solo - Análise Granulométrica, NBR 7181. Associação Brasileira de Normas Técnicas, Rio de Janeiro, Brasil, 13 pp.

ABNT (1984) Grãos de Solos que Passam na Peneira 4,8 mm - Determinação da Massa Específica, NBR 6508. Associação Brasileira de Normas Técnicas, Rio de Janeiro, Brasil, 8 pp.

ABNT (1986) Amostra de Solo - Preparação para Ensaios de Compactação e Ensaios de Caracterização, NBR 6457. Associação Brasileira de Normas Técnicas, Rio de Janeiro, Brasil, 9 pp.

ABNT (1995) Solos e Rochas, NBR 6502. Associação Brasileira de Normas Técnicas, Rio de Janeiro, Brasil, 18 pp.

ABNT (1995) Determinação do Coeficiente de Permeabilidade dos Solos Granulares a Carga Constante, NBR 13292. Associação Brasileira de Normas Técnicas, Rio de Janeiro, Brasil, 8 pp.

Aziz, K. & Settari, A. (1979) Petroleum reservoir simulation. Applied Science Publishers, London, 476 pp.

Bradford, S.A. & Leij, F.J. (1995) Fractional wettability effects on two and three fluid capillary pressure-saturation relations. J. Contaminant Hydrology, v. 20:1-2, p. 89-109.

Bradford, S.A. & Leij, F.J. (1996) Predicting two and three fluid capillary pressure-saturation relationships of porous media with fractional wettability. Water Resource Researchers, v. 32:2, p. 251-260.

Collins, R.E. (1961) Flow of Fluids Through Porous Materials. Reinhold Publishing Corporation, New York, 270 pp.

Corey, A.T. (1986) Mechanics of Immiscible Fluids in Porous Media. Water Resources Publications, Littleton, 253 pp.

ESTC – Environmental Science and Technology Centre (1997) Diesel Fuel Oil (Southern U.S.A., 1997). Available at http://www.etc-cte.ec.gc.ca/databases/Oilproperties/oil_D_e.html, 28/9/2010.

Feuerharmel, C.; Gehling, W.Y.Y.; Bica, A.V.D. & Pereira, A. (2004) Determinação das curvas características de solos coluvionais pelo uso combinado da placa de sucção e método do papel de filtro. Proc. V Simpósio Brasileiro de Solos Não Saturados, São Carlos, v. 1, pp. 243–247.

Fredlund, D.G. & Rahardjo, H. (1993) Soil Mechanics for Unsaturated Soils. John Wiley & Sons, New York, online version available at http://knovel.com/web/portal/browse/display?_ext_knovel_display_bookid=1725&VerticalID = 0.

Fredlund D.G. & Xing, A. (1994) Equations for the soil water characteristic curve. Can. Geotechnical Journal, v. 31:3, p. 521-532.

Lenhard, R.J. & Parker, J.C. (1988) Experimental validation of theory of extending two-phase saturation-pressure relations to three-fluid phase systems for monotonic drainage paths. Water Resource Research, v. 4:3, p. 373-380.

Leverett, M.C. (1941) Capillary behavior in porous media solids. Trans. AIME, v. 142, p. 341-358.

Machado, S.L. & Dourado, K.A. (2001) Novas técnicas para obtenção da curva característica de sucção do solo. Proc. 4° Simpósio Brasileiro de Solos Não Saturados, Porto Alegre. v. 1, pp. 325-336.

Mahler, C.F. & Oliveira L.C.D. (1998) Measurement of matrix and total in situ suction of porous soils of São Paulo using the filter-paper method. Proc. of the 2st Int. Conf. on Unsaturated Soils, pp. 402-409.

Marle, C.M. (1981) Multiphase Flow in Porous Media. Gulf Publishing Corporation, Huston, 257 pp.

Mcbride, J.F.; Simmons C.S. & Cary, J.W. (1992) Interfacial spreading effects on one dimensional organic liquid imbibition in water-wetted porous media, J. Contaminant Hydrology, v. 11:1-2, p. 1-25.

Nutting, P.G. (1930) Physical analysis of oil sands. Am. Assoc. Petroleum Geologists Bull., v. 14, p. 1337-1349.

Oliveira, I.B. (1995) Infiltration of Organic Liquids in Unsaturated Sands: Comparison of Experimental Measurements with Scaled and Unscaled Analytical Solutions. Doctoral Thesis, University of Michigan, 335 pp.

Oliveira, O.M. & Marinho, F.A.M. (2008) Suction equilibration time for a high capacity tensiometer. ASTM. Geotechnical Testing Journal, v. 31:1, p. 61-66.

United States Environmental Protection Agency-USEPA (1997) Ground Water and Ecosystems Restoration Research-GWERD. Software NAPL Simulator Documentation. Available in http://www.epa.gov/ada/csmos/models/napl.html.

van Genuchten, M.T. (1980) A closed form equations for predicting the hydraulic conductivity of unsaturated soils. Soil Science Society of America Journal, v. 44:5, p. 892-898.

Wilson, J.L.; Conrad, S.H.; Mason W.R.; Peplinski W. & Hagan, E. (1990) Laboratory investigation of residual liquid organics from spills, leaks and the disposal of hazardous waste in groundwater, PB-90-235797/XAB, OSTI ID: 6702517. New Mexico Inst. of Mining and Technology, Socorro, 285 pp.

SOILS and ROCKS
An International Journal of Geotechnical and Geoenvironmental Engineering

Publication of
ABMS - Brazilian Association for Soil Mechanics and Geotechnical Engineering
SPG - Portuguese Geotechnical Society
Volume 34, N. 3, September-December 2011

Author index

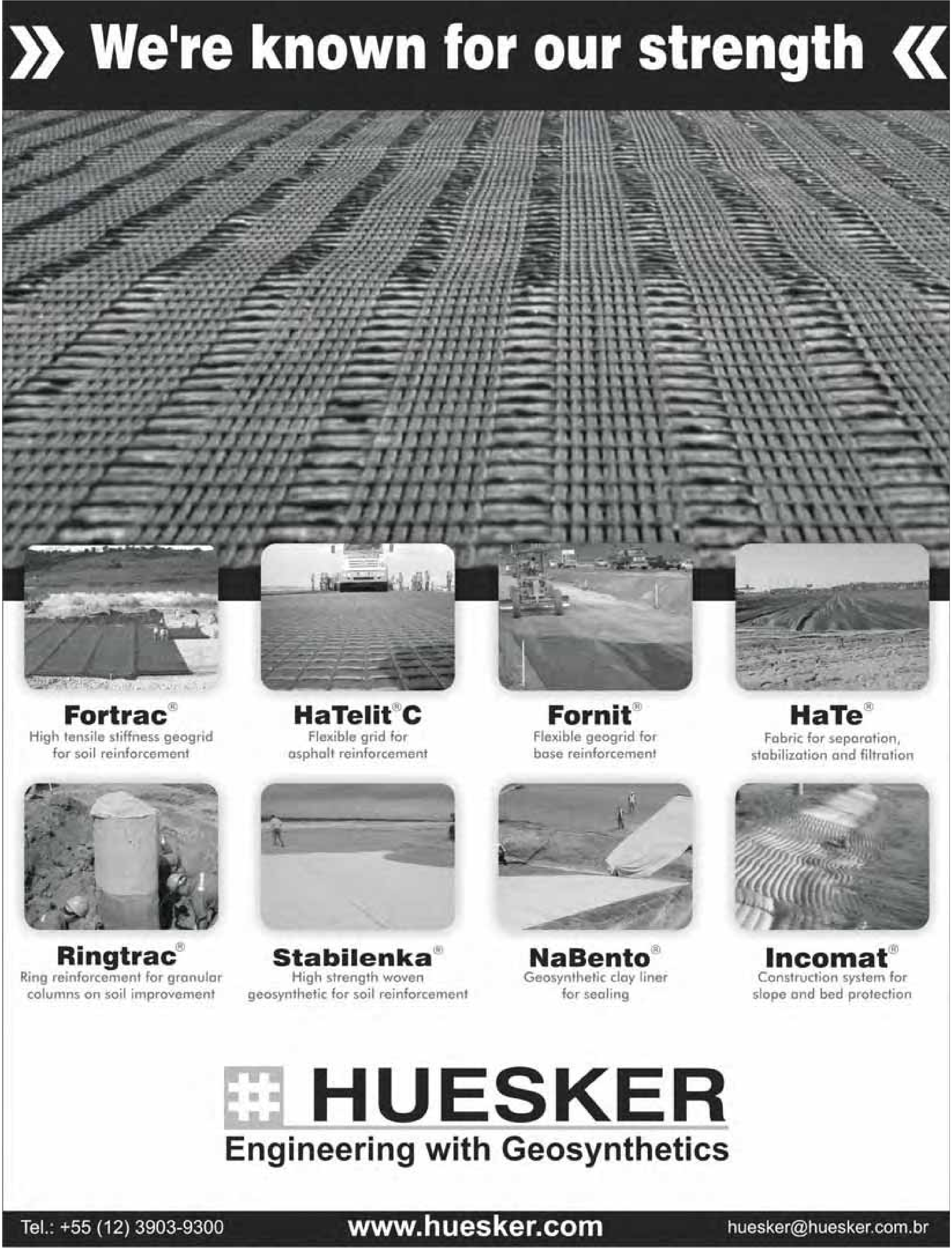
We're known for our strength
Fortrac®
High tensile stiffness geogrid for soil reinforcement
HaTelit® C
Flexible grid for asphalt reinforcement
Fornit®
Flexible geogrid for base reinforcement
HaTe®
Fabric for separation, stabilization and filtration
Ringtrac®
Ring reinforcement for granular columns on soil improvement
Stabilenka®
High strength woven geosynthetic for soil reinforcement
NaBento®
Geosynthetic clay liner for sealing
Incomat®
Construction system for slope and bed protection
HUESKER
Engineering with Geosynthetics
Tel.: +55 (12) 3903-9300
www.huesker.com
huesker@huesker.com.br

Instructions to Authors

Category of the Papers

Soils and Rocks is the scientific journal edited by the Brazilian Association for Soil Mechanics and Geotechnical Engineering (ABMS) and the Portuguese Geotechnical Society (SPG). The journal is intended to the divulgation of original research works from all geotechnical branches.

The accepted papers are classified either as an Article paper, a Technical Note, a Case Study, or a Discussion according to its content. An article paper is an extensive and conclusive dissertation about a geotechnical topic. A paper is considered as a technical note if it gives a short description of ongoing studies, comprising partial results and/or particular aspects of the investigation. A case study is a report of unusual problems found during the design, construction or the performance of geotechnical projects. A case study is also considered as the report of an unusual solution given to an ordinary problem. The discussions about published papers, case studies and technical notes are made in the Discussions Section.

When submitting a manuscript for review, the authors should indicate the category of the manuscript, and is also understood that they:

a) assume full responsibility for the contents and accuracy of the information in the paper;

b) assure that the paper has not been previously published, and is not being submitted to any other periodical for publication.

Manuscript Instructions

Manuscripts must be written in English. The text is to be typed in a word processor (MS Word or equivalent), using ISO A4 page size, left, right, top, and bottom margins of 25 mm, Times New Roman 12 font, and line spacing of 1.5. All lines and pages should be numbered. The text should be written in the third person.

The fist page of the manuscript is to include the title of the paper in English, followed by the names of the authors with the abbreviation of the most relevant academic title. The affiliation, address and e-mail is to be indicated below each author's name. An abstract of 200 words is to be written in English after the author's names. A list with up to six keywords at the end of the abstract is required.

Although alteration of the sequence and the title of each section may be required, it is suggested that the text contains the following sections: Introduction, Material and Methods, Results, Discussions, Conclusion, Acknowledgements, References and List of Symbols. A brief description of each section is given next.

Introduction: This section should indicate the state of the art of the problem under evaluation, a description of the problem and the methods undertaken. The objective of the work is to be clearly presented at the end of the section.

Materials and Methods: This section should include all information needed to the reproduction of the presented work by other researchers.

Results: In this section the data of the investigation should be presented in a clear and concise way. Figures and tables should not repeat the same information.

Discussion: The analyses of the results should be described in this section. **Conclusions**: The text of this section should be based on the presented data and in the discussions.

Acknowledgements: If necessary, concise acknowledgements should be written in this section.

References: References to other published sources are to be made in the text by the last name(s) of the author(s), followed by the year of publication, similarly to one of the two possibilities below:

"*while Silva & Pereira (1987) observed that resistance depended on soil density*" or "*It was observed that resistance depended on soil density (Silva & Pereira, 1987).*"

In the case of three or more authors, the reduced format must be used, *e.g.*: Silva *et al.* (1982) or (Silva *et al.*, 1982). Two or more citations belonging to the same author(s) and published in the same year are to be distinguished with small letters, *e.g.*: (Silva, 1975a, b, c.). Standards must be cited in the text by the initials of the entity and the year of publication, *e.g.*: ABNT (1996), ASTM (2003).

Full references shall be listed alphabetically at the end of the text by the first author's last name. Several references belonging to the same author shall be cited chronologically. Some examples are listed next:

Papers: Bishop, A.W. & Blight, G.E. (1963) Some aspects of effective stress in saturated and unsaturated soils. Géotechnique, v. 13:2, p. 177-197.

Books: Lambe, T.W & Whitman, R.V. (1979) Soil Mechanics, SI Version, 2nd ed. John Wiley & Sons, New York, p. 553.

Book with editors: Sharma, H.D.; Dukes, M.T. & Olsen, D.M. (1990) Field measurements of dynamic moduli and Poisson's ratios of refuse and underlying soils at a landfill site. Landva A. & Knowles, G.D. (eds) Geotechnics of Waste Fills - Theory and Practice, American Society for Testing and Materials - STP 1070, Philadelphia, p. 57-70.

Proceedings (printed matter or CD-ROM): Jamiolkowski, M.; Ladd, C.C.; Germaine, J.T & Lancellotta, R. (1985) New developments in field and laboratory testing of soils. Proc. 11th Int. Conf. on Soil Mech. and Found. Engn., ISSMFE, San Francisco, v. 1, pp. 57-153.(specify if CD – ROM)

Thesis and dissertations: Lee, K.L. (1965) Triaxial Compressive Strength of Saturated Sands Under Seismic Loading Conditions. PhD Dissertation, Department of Civil Engineering, University of California, Berkeley, 521 p.

Standards: ASTM (2003) Standard Test Method for Particle Size Analysis of Soils - D 422-63. ASTM International, West Conshohocken, Pennsylvania, USA, 8 p.

Internet references: Soils and Rocks available at http://www.abms.com.br.

On line first publications must also bring the digital object identifier (DOI) at the end.

Figures shall be either computer generated or drawn with India ink on tracing paper. Computer generated figures must be accompanied by the corresponding digital file (.tif, .jpg, .pcx, etc.). All figures (graphs, line drawings, photographs, etc.) shall be numbered consecutively and have a caption consisting of the figure number and a brief title or description of the figure. This number should be used when referring to the figure in text. Photographs should be black and white, sharp, high contrasted and printed on glossy paper.

Tables shall be numbered consecutively in Arabic and have a caption consisting of the table number and a brief title. This number should be used when referring to the table in text. Units should be indicated in the first line of the table, below the title of each column. Abbreviations should be avoided. Column headings should not be abbreviated. When applicable, the units should come right below the corresponding column heading. Any necessary explanation can be placed as footnotes.

Equations shall appear isolated in a single line of the text. Numbers identifying equations must be flush with the right margin. International System (SI) units are to be used. The symbols used in the equations shall be listed in the List of Symbols. It is recommended that the used symbols be in accordance with Lexicon in 8 Languages, ISSMFE (1981) and the ISRM List of Symbols.

The text of the submitted manuscript (including figures, tables and references) intended to be published as an article paper or a case history should not contain more than 30 pages formatted according to the instructions mentioned above. Technical notes and discussions should have no more than 15 and 8 pages, respectively. Longer manuscripts may be exceptionally accepted if the authors provide proper explanation for the need of the required extra space in the cover letter.

Discussion

Discussions must be written in English. The first page of a discussion paper should contain:

• The title of the paper under discussion in the language chosen for publication;

• Name of the author(s) of the discussion, followed by the position, affiliation, address and e-mail. The discusser(s) should refer himself (herself, themselves) as "the discusser(s)" and to the author(s) of the paper as "the author(s)".

Figures, tables and equations should be numbered following the same sequence of the original paper. All instructions previously mentioned for the preparation of article papers, case studies and technical notes also apply to the preparation of discussions.

Editorial Review

Each paper will be evaluated by reviewers selected by the editors according to the subject of the paper. The authors will be informed about the results of the review process. If the paper is accepted, the authors will be required to submit a version of the revised manuscript with the suggested modifications. If the manuscript is refused for publication, the authors will be informed about the reasons for rejection. In any situation comprising modification of the original text, classification of the manuscript in a category different from that proposed by the authors, or refusal for publication, the authors can reply presenting their reasons for disagreeing with the reviewers' comments

Submission

The author(s) must submit for review:

1. A hard copy of the manuscript to Editors - Soils and Rocks, Av. Prof. Almeida Prado, 532 – IPT, Prédio 54 – DEC/ABMS, 05508-901 - São Paulo, SP, Brazil. The first page of the manuscript should contain the identification of the author(s), or

2. The digital file of the manuscript, omitting the authors' name and any information that eventually could identify them, should be sent to **abms@ipt.br**. The following must be written in the subject of the e-mail message: "*Paper submitted to Soils and Rocks"*. The authors' names, academic degrees and affiliations should be mentioned in the e-mail message. The e-mail address from which the digital file of the paper was sent will be the only one used by the editors for communication with the corresponding author.

Follow Up

Authors of manuscripts can assess the status of the review process at the journal website (www.soilsandrocks.com.br) or by contacting the ABMS secretariat.

Volume 34, N. 3, September-December 2011

Table of Contents